For Reference

NOT TO BE TAKEN FROM THIS ROOM

For Reference

NOT TO BE TAKEN FROM THIS ROOM

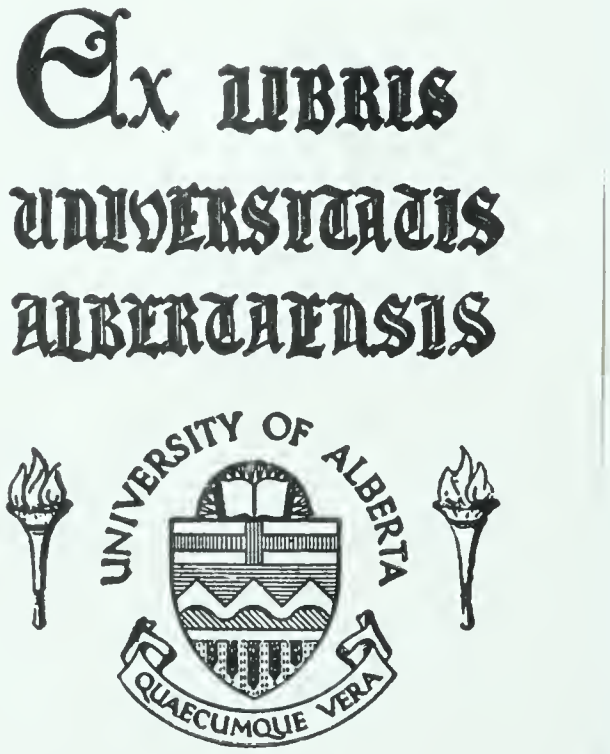

University of Alberta
Printing Department

Digitized by the Internet Archive
in 2019 with funding from
University of Alberta Libraries

https://archive.org/details/mechanicsoflarge00rasb

Thesis
1963(F)
#3D

THE UNIVERSITY OF ALBERTA

THE MECHANICS OF LARGE GAS BUBBLES IN TUBES

by

R.A.S. BROWN

A THESIS

SUBMITTED TO THE FACULTY OF GRADUATE STUDIES

IN PARTIAL FULFILMENT OF THE REQUIREMENTS FOR THE DEGREE

OF DOCTOR OF PHILOSOPHY

IN CHEMICAL ENGINEERING

DEPARTMENT OF CHEMICAL AND PETROLEUM ENGINEERING

EDMONTON, ALBERTA

MAY, 1963

UNIVERSITY OF ALBERTA

FACULTY OF GRADUATE STUDIES

The undersigned certify that they have read, and recommend to the Faculty of Graduate Studies for acceptance, a thesis entitled "The Mechanics of Large Gas Bubbles in Tubes" submitted by R.A.S. Brown, M.S. in partial fulfilment of the requirements for the degree of Doctor of Philosophy in Chemical Engineering.

ABSTRACT

The effect of liquid viscosity on the rise of large bubbles of gas through liquids in tubes is shown to be limited to the film flow past the bubble on the wall of the tube. The frontal flow is described quite well by potential flow theory even for liquids of relatively high viscosity. On the basis of an assumed equilibrium laminar film on the tube wall and an observed similarity between the geometries of gas bubbles rising through different liquids, a general correlation for the velocities of rise is obtained which gives good agreement with existing experimental values. The limit of applicability of the correlating equation is the initiation of control by surface tension and this limit is defined through semi-empirical means. The minimum size of bubble in a given tube which is described by the proposed model is also considered.

The applicability of the model to single bubbles in moving streams of liquids in tubes and to bubbles in slug flow is considered. In these cases, it is not possible to solve the frontal flow; however, from consideration of the material balance relation for the flow in the film, a form

is developed for empirical correlation of the gas content. In application, this form proves equally useful for the correlation of the gas content in gas-liquid flow for all flow patterns except bubble flow and is not restricted to slug flow.

From consideration of the force-momentum balance for a single bubble, a method is developed for the empirical correlation of pressure drops in gas-liquid slug flow. The form of correlation developed effectively systematizes the results for all the flow patterns encountered in gas-liquid flow; however, its applicability for correlating pressure drops is limited to gas contents below about 0.8 for low viscosity liquids and to somewhat lower values for high viscosity liquids.

ACKNOWLEDGEMENTS

The author would like to express his sincere appreciation of the able guidance of Dr. G. W. Govier throughout the course of the investigation.

For financial support of the project, the author is indebted to the National Research Council of Canada. Thanks are also due to the Government of the Province of Alberta for a Province of Alberta Graduate Scholarship which was received for two years.

The assistance of the staff of the Department of Chemical Engineering Workshop in modifying the equipment for this study is gratefully acknowledged as are the efforts of Miss D. Lockard and Mr. F. Moens in the preparation of the manuscript.

The author also acknowledges the assistance obtained through personal communications with Dr. D. J. Nicklin and Mr. E. T. White.

TABLE OF CONTENTS

	Page
List of Tables	
List of Figures	
Introduction	1
Fundamental Relations	5
Large Bubbles in Infinite Media	8a
Large Bubbles in Tubes I - Stagnant Media	16
1. Bubble Characteristics in Inviscid Liquids	17
2. Macroscopic Balances - Stagnant Media	30
3. Bubble Characteristics in Actual Liquids	38
a. The Film Region	38
b. The Nose Region	43
c. General Correlation	51
d. Limit of Applicability	52
e. Comparison with Literature Results	55
f. Minimum Size of Taylor Bubbles	62
g. Summary	65
Large Bubbles in Tubes II - Moving Media	67
1. Macroscopic Balances - Moving Media	67
a. Single Bubble	67

		Page
2.	The Effect of Liquid Velocity on Bubble Velocity	74
3.	Macroscopic Balances - Moving Media	93
	b. Slug Flow	93
4.	Bubble Motion in Slug Flow	98
5.	Pressure Drop in Slug Flow	123
6.	Summary	145
Conclusions		148
Nomenclature		151
List of References		155
Appendices		
I.	Experimental Equipment and Procedure	159
II.	Laminar Film Analysis	175
III.	Calculation of Momentum Flux	182

LIST OF TABLES

Table		Page
I	Liquid Properties	27
II	Experimental Bubble Velocities	29
III	Experimental Bubble Velocities	49
IV	Bubbles in Stagnant Media - Comparison with Experimental Results	58
V	Minimum Sizes for Taylor Bubbles	64
VI	Force-Momentum Balance Results	87
VII	System Characteristics - Air-Liquid Flow Tests	105
VIII	Correlation of Gas Content - Coordinates of Average Curve	117
I-1	Experimental Bubble Velocities - Air-Water System	167
I-2	Experimental Bubble Velocities - Air-Varsol System	168
I-3	Experimental Bubble Velocities - Air-Marcol System	169
I-4	Experimental Bubble Velocities - Air-Primol System	170

LIST OF FIGURES

Figure		Page
1	Spherical-Cap Bubble	13
2	A Taylor Bubble	18
3	A Taylor Bubble	19
4	Proposed Model of Taylor Bubble	31
5	Bubble Shapes	45
6	Normalized Bubble Shapes	47
7	Bubbles in Stagnant Media - Comparison with Experimental Results	56
8	A Taylor Bubble in Moving Liquid	68
9	Change of C_4 with Liquid Velocity	80
10	Change in Film Thickness with Water Velocity	84
11	Force-Momentum Balance	88
12	Bubble Velocities in Moving Liquid Streams	92
13	Schematic Representation of Slug Flow	94
14	Model for Pressure Drop Calculations	99
15	Correlation of In Situ Gas Content System: Air-Water; 0.630-inch Tube	106
16	Correlation of In Situ Gas Content System: Air-Water; 1.025-inch Tube	107
17	Correlation of In Situ Gas Content System: Air-Water; 1.50-inch Tube	108

LIST OF FIGURES (continued)

Figure		Page
18	Correlation of In Situ Gas Content System: Air-Water; 2.50-inch Tube	109
19	Correlation of In Situ Gas Content System: Air-Trichlorethylene; 1.049-inch Pipe	110
20	Correlation of In Situ Gas Content System: Air-Water; 1.049-inch Pipe	111
21	Correlation of In Situ Gas Content System: Air-Varsol; 1.049-inch Pipe	112
22	Correlation of In Situ Gas Content System: Air-Sodium Carbonate Solution; 1.049-inch Pipe	113
23	Correlation of In Situ Gas Content System: Air-Oil Blend No. 1; 1.049-inch Pipe	114
24	Correlation of In Situ Gas Content System: Air-Oil Blend No. 2; 1.049-inch Pipe	115
25	Correlation of In Situ Gas Content Experimental Data for Slug Flow	121
26	Relation of Pressure Drop to Gas Content Experimental Data for Slug Flow System: Air-Water; 0.630-inch Tube	128
27	Relation of Pressure Drop to Gas Content Experimental Data for Slug Flow System: Air-Water; 1.025-inch Tube	129
28	Relation of Pressure Drop to Gas Content System: Air-Water; 0.630-inch Tube	131

LIST OF FIGURES (continued)

Figure		Page
29	Relation of Pressure Drop to Gas Content System: Air-Water; 1.025-inch Tube	132
30	Relation of Pressure Drop to Gas Content System: Air-Water; 1.50-inch Tube	133
31	Relation of Pressure Drop to Gas Content System: Air-Water; 2.50-inch Tube	134
32	Relation of Pressure Drop to Gas Content System: Air-Trichlorethylene; 1.049-inch Pipe	135
33	Relation of Pressure Drop to Gas Content System: Air-Water; 1.049-inch Pipe	136
34	Relation of Pressure Drop to Gas Content System: Air Varsol; 1.049-inch Pipe	137
35	Relation of Pressure Drop to Gas Content System: Air-Sodium Carbonate Solution; 1.049-inch Pipe	138
36	Relation of Pressure Drop to Gas Content System: Air-Oil Blend No. 1; 1.049-inch Pipe	139
37	Relation of Pressure Drop to Gas Content System: Air-Oil Blend No. 2; 1.049-inch Pipe	140
I-I	Schematic Diagram of Bubble Introduction System	161
I-2	Schematic Diagram of Tube	163
I-3	Bubble Shape - Air-Water System	171

LIST OF FIGURES (continued)

Figure		Page
I-4	Bubble Shape - Air-Varsol System	172
I-5	Bubble Shape - Air-Marcol System	173
I-6	Bubble Shape - Air-Primol System	174
II-1	The Equilibrium Film	176
II-2	Forces Acting on an Element of a Bubble	180

INTRODUCTION

The upward flow of gas-liquid mixtures in a vertical cylindrical tube can be characterized by a number of 'flow patterns' or modes of dispersion of the gas and liquid phases. While the flow patterns occurring are a function of the system properties (liquid, gas and tube) to some extent, they are dependent primarily on the flow rates of the gas and the liquid. The greatest variety of flow patterns occurs at low liquid flow rates and, considering successively larger flow rates of gas at a low liquid flow rate, the flow patterns occurring are:

1. bubble flow - in which the gas is dispersed in the liquid in the form of bubbles small in size relative to the tube diameter;
2. slug flow - in which the gas rises in the form of bullet-shaped bubbles, large relative to the diameter of the tube, separated by 'slugs' of liquid which may or may not contain gas entrained in the form of small bubbles;
3. froth flow - in which the gas and liquid appear to flow as a highly turbulent mixture;

4. annular flow - in which the liquid moves up the wall of the tube as a film (not necessarily a film of constant thickness) and the gas flows in the core within this annular film; and

5. annular-mist or mist flow - in which the liquid is dispersed in the gas stream (to some extent, at least) in the form of fine droplets.

At high liquid flow rates, froth flow does not occur, the flow changing directly to annular flow from slug flow. The type of behavior described above has been observed in a number of investigations including those of Cromer and Huntington (5), Govier, Radford and Dunn (9), and Kozlov (19).

The analysis of vertically-flowing gas-liquid systems to obtain the pressure drop has been discussed in several review articles, for example those of Bennett (2) and Isbin, Moen and Mosher (18), and involves, in general, the assumption of some physical model to describe the dispersion of the phases. The applicability of the predictions then depends upon two factors - the accuracy of analysis of pressure drop for the model and the accuracy with which the model describes the two-phase flow. By the second factor

is meant the accuracy of description of the pressure drop and not necessarily the physical description of the flow. More success has been attained recently with analyses limited to specific flow patterns and based on physical models of the flow patterns occurring. The slug flow analyses of Griffith and Wallis (12) and of Nicklin (24) and the annular flow analyses of Anderson and Mantzouranis (1) and Hewitt (16) are examples of this type of approach. These methods seem especially appropriate for the analysis of vertical gas-liquid flow where the liquid content of the tube introduces a 'static' component of the pressure drop in addition to the 'dynamic' or frictional component due to the resistance to flow. In the prediction of pressure drops by these methods, the accuracy of description of the two-phase flow can be considered from two separate aspects - the prediction of the distribution of phases (i.e. the fraction of liquid or gas in the tube) and the prediction of the pressure drop from the model when the distribution of phases is known.

In the present investigation, a detailed study was made of the mechanism of liquid flow associated with the rise of single large bubbles through stagnant liquids with a view to the application of the results to pressure drop prediction

in slug flow. While this flow pattern has been studied quite intensively in previous investigations (12, 24), the results obtained appeared to be limited to systems in which the liquid has a low viscosity.

The analysis fell naturally into three sections - single bubble movement in stagnant liquids; the distribution of phases in slug flow; and the pressure drop in slug flow.

As the main purpose of the study of single bubble movement was to obtain knowledge about the mechanism of flow which could be used eventually in the analysis of slug flow, consideration was limited to relatively large bubbles. In addition, the movement of bubbles in small diameter tubes for which the surface tension of the liquid was important in determining the shape of the bubble was not considered. This necessitated, however, the definition of the region of applicability of the relations developed.

The rate of rise of single bubbles in infinite media is considered briefly before treatment of the more complicated case of the rise of single bubbles in tubes, both to provide background and to indicate the qualitative similarity between the movement of large bubbles in infinite media and in tubes.

FUNDAMENTAL RELATIONS

For the solution of problems or situations in fluid mechanics, there are three general relations:

1. the material balance expressing the law of conservation of matter;
2. the force-momentum balance expressing Newton's second law of motion - rate of change of momentum of a body is equal to the sum of the forces producing the acceleration; and
3. the energy balance expressing the law of conservation of energy.

In addition to these general relations, there are usually available two relations describing the fluid being considered - the equation of state and stress-rate of strain relationship.

The material balance can be written using standard vector notation as

$$\frac{D\rho}{Dt} = -\rho(\nabla\cdot\bar{V}) \qquad (1)$$

where ρ is the fluid density, t denotes time and $\bar{V}$ is the velocity vector in the coordinate system being used.

Similarly, the force-momentum balance for an element, assuming

the only body force to be gravity, can be written as

$$\rho \frac{D\overline{V}}{Dt} = -\nabla P - (\nabla \cdot \overline{\tau}) + \rho \overline{g} \qquad (2)$$

In Equation (2), P denotes pressure, $\overline{\tau}$ is the stress tensor and $\overline{g}$ the gravity vector in the coordinate system. If the fluid is Newtonian, the force-momentum equations for the element become the well-known Navier-Stokes equations. For a non-diffusing system, the energy balance can be written as

$$\rho \frac{DE}{Dt} = - (\nabla \cdot \overline{q}) - (\nabla \cdot P\overline{V}) - (\nabla \cdot (\overline{\tau} \cdot \overline{V})) \qquad (3)$$

where E is the total energy and $\overline{q}$ is the heat flux. For flow in an isothermal system and assuming that surface energy effects are negligible, no additional information can be obtained from the energy balance relation and it will not be considered further.

For the flow of inviscid fluids (i.e. for friction-less flow) the shear term in Equation (2) is zero and Eulers' equation of motion is obtained.

$$\rho \frac{D\overline{V}}{Dt} = - \nabla P + \rho \overline{g} \qquad (4)$$

This assumption of frictionless flow is frequently made to approximate the flow behavior in actual systems when the flow in the 'free stream' outside the field of influence of

bounding surfaces is being considered. In frictionless flow, the motion is irrotational since no tangential surface forces are present to cause the rotation of a fluid element. In mathematical terms, this can be expressed as

$$\text{curl } \bar{V} = \nabla \times \bar{V} = 0 \qquad (5)$$

Substitution of Equation (5) into Euler's equation (Equation (4)) yields

$$\rho \frac{\partial \bar{V}}{\partial t} + \frac{1}{2}\rho\nabla(\bar{V}\cdot\bar{V}) = -\nabla P + \rho\bar{g}$$

or

$$\rho \frac{\partial \bar{V}}{\partial t} + \frac{1}{2}\rho\nabla(V^2) = -\nabla P + \rho\bar{g} \qquad (6)$$

where V is the magnitude of the velocity vector. Equation (6) is the differential form of Bernoulli's equation for unsteady-state conditions.

Equation (5) implies the existence of a scalar function which satisfies the relation

$$\nabla\Phi = \bar{V} \qquad (7)$$

The scalar function, Φ, is known as the potential function for the flow. Substitution of Equation (7) into the material balance or continuity equation, Equation (1), gives

$$\frac{D\rho}{Dt} = -\rho(\nabla^2\Phi) \qquad (8)$$

Associated with the potential function of Equation (7), there is another scalar function, Ψ, defined by the equation

$$\nabla\Psi\cdot\nabla\Phi = 0 \tag{9}$$

Considering three-dimensional flow, then, the surfaces Ψ = constant are everywhere orthogonal to the surfaces Φ = constant. From this visualization, the surfaces Ψ = constant are seen to be formed by the traces of individual fluid particles and the function Ψ is known, therefore, as the stream function. The importance of the stream function to the study of irrotational or potential flow arises from the fact that any continuous boundary of the flow is a surface of constant Ψ.

For incompressible and steady state flow, Equations (6) and (8) become

$$\frac{1}{2}\rho\nabla(V^2) = -\nabla P + \rho\bar{g} \tag{10}$$

and

$$\nabla^2\Phi = 0 \tag{11}$$

BUBBLES IN INFINITE MEDIA

Theoretical studies of the movement of gas bubbles through liquids are complicated by the fact that the shape of the bubble is usually a result of the dynamics of the flow and hence is unknown. The solution, therefore, must determine not only the bubble velocity but the bubble shape as well. The general approach to the determination of bubble velocity, however, is well established and involves the application of Newtons' second law of motion which takes the form

$$F = \mathcal{V}_b(\rho-\rho')\frac{g}{g_c} \qquad (12)$$

where F is the resistance to motion or the drag force, $\mathcal{V}_b$ is the volume of the bubble and ρ and ρ' are the densities of the liquid and gas, respectively. Generally, the bubble volume is expressed through definition of an equivalent spherical radius, r_e, where

$$\mathcal{V}_b = \frac{4}{3}\pi r_e^3 \qquad (13)$$

Introducing Equation (13) into Equation (12) and recognizing that the gas density will be negligible with respect to the liquid density leads to the relation

$$F = \frac{4}{3}\pi r_e^3 \rho\frac{g}{g_c} \qquad (14)$$

The problem, then, is to use the material balance and force-momentum balance relations, Equations (1) and (2), to solve the flow field external to the bubble and determine the drag force.

One of the few cases for which a rigorous solution of these relations has been successful is the movement of very small spherical bubbles in viscous liquids. The restriction of the solution to spherical bubbles is a realistic one in this case since the surface tension forces are large and constrain the bubble to a spherical shape. For sufficiently small bubbles this surface tension force is much greater than the tangential shear forces at the surface of the bubble which prevents internal circulation and causes the bubble to behave as a solid sphere. As can be seen from Equation (12), the net buoyant force will be very small for a small bubble and the bubble velocity will also be small. Under these conditions, the acceleration and gravitational terms in Equation (2) can be neglected and, with the introduction of Newton's law of viscosity, the Navier-Stokes equations for the case being considered are obtained for steady-state conditions as

$$\nabla P = -\frac{\mu}{g_c}(\nabla^2 \overline{V}) \tag{15}$$

where μ is the viscosity of the liquid. The material balance is given by

$$(\nabla \cdot \overline{V}) = 0 \tag{16}$$

Equations (15) and (16) were solved by Stokes (21) for the movement of a small sphere at low velocity (often referred to as the creeping motion of a sphere) and gave for the drag force,

$$F = 6\pi \frac{\mu}{g_c} r_o V_b^\circ \tag{17}$$

where r_o is the radius of the spherical bubble and V_b° is the bubble velocity. Substitution of Equation (17) into Equation (14) gives for the bubble velocity,

$$V_b^\circ = \frac{2}{9} \frac{r_o^2 \rho g}{\mu} \tag{18}$$

where the equivalent spherical radius, r_e, has been replaced by the radius of the sphere, r_o, since the two are identical for a spherical bubble. In the case of air bubbles rising in water, Equation (18) applies quite accurately to bubbles smaller than 0.0019 inches in radius.

For liquids with lower surface tensions than that of water, the tangential shear stress becomes sufficiently

large to overcome the surface tension force before the normal pressure forces due to the flow around the bubble become sufficient to deform the bubble. When this occurs, the bubble no longer behaves as a rigid or solid sphere and shear stress is transmitted across the gas-liquid interface, causing circulation of the gas within the bubble. This case has also been solved for the hypothesis of creeping motion (21) and leads to the relation

$$V_b^\circ = \frac{1}{3} \frac{r_o^2 \rho g}{\mu} \qquad (19)$$

As would be expected, greater bubble velocities occur when internal circulation occurs than when the bubble behaves as a rigid sphere.

The other limiting case of bubble motion in infinite media is the case of very large bubbles. These have been found experimentally to assume a lens shape with the frontal surface being very nearly a segment of a spherical surface and the rear surface approximately flat. For these very large bubbles, the inertial forces should be larger than the viscous forces and the potential flow solution would be expected to approximate the actual flow. As the complete solution is not possible due to the difficulties involved in

calculating the flow in the wake region, approximate methods must be used.

Since the frontal radius is large, surface tension forces will be insignificant and there will be circulation of the gas within the bubble. Also, since the gas density is small relative to the liquid density, the bubble surface can be assumed to be a surface of constant pressure. A schematic representation of a spherical cap bubble is shown in Figure 1 on which have been indicated the coordinates being used. From Equation (10), the condition that the gas-liquid interface be a surface of constant pressure results in

$$V_i^2 = 2g(-x_i) \tag{20}$$

where V_i is the magnitude of the velocity vector at the interface and $-x_i$ is the vertical distance from the stagnation point. Since inertial forces predominate, the flow external to the spherical front should be approximated by the potential solution for the flow around a sphere. This solution can be obtained, for convenience, in the transformed coordinate system with the bubble at rest and the liquid at infinity moving with a velocity $-V_b^\circ$ parallel to the x-axis. The potential function for the flow around a sphere in these coordinates is (22, 26)

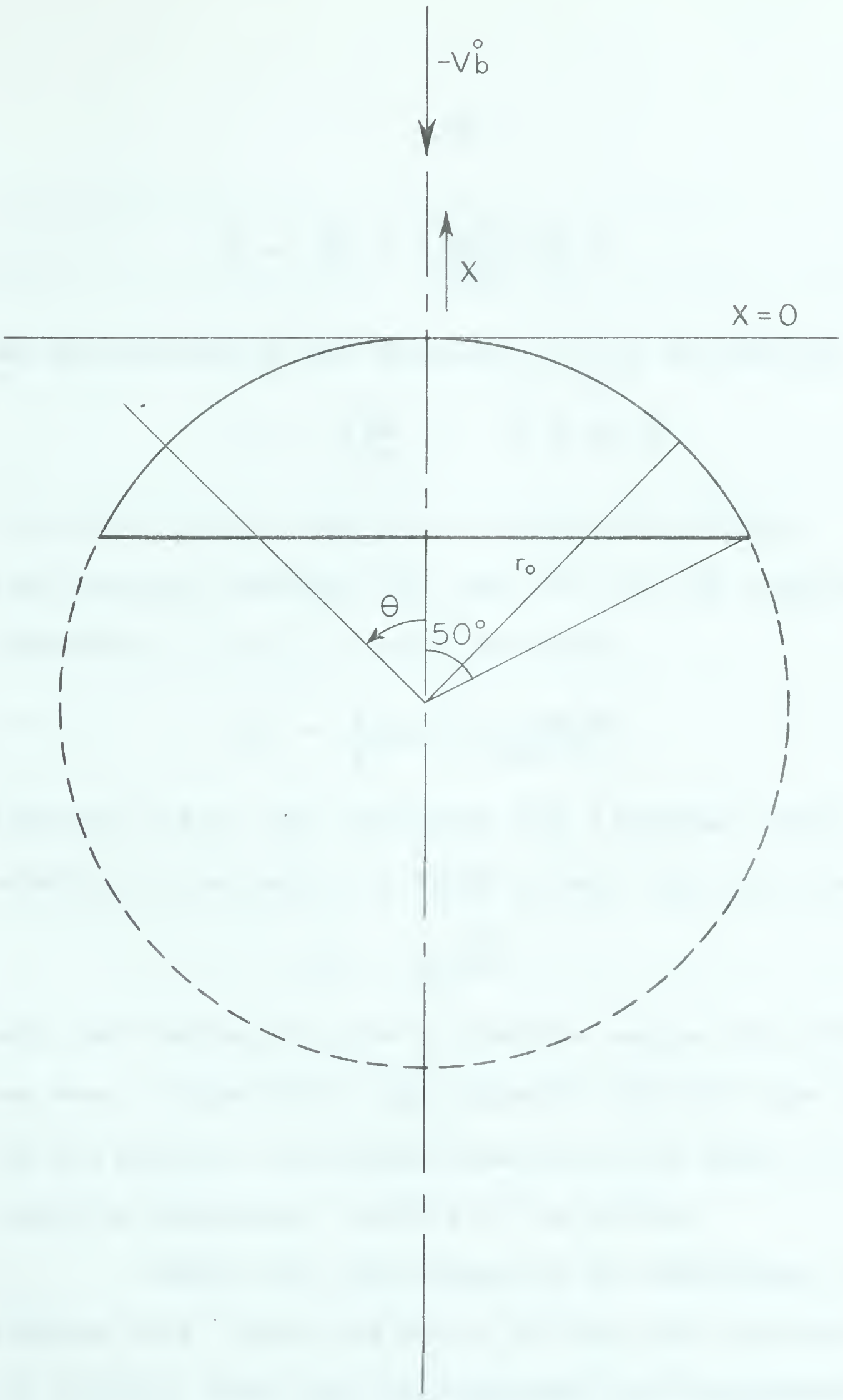

FIGURE 1

SPHERICAL-CAP BUBBLE

$$\Phi = V_b^\circ \left(r + \frac{r_o^3}{2r^2}\right) \cos \theta \tag{21}$$

and the velocity at the interface, $r = r_o$, is given by

$$V_i = \frac{1}{r} \frac{\partial \Phi}{\partial \theta} = -\frac{3}{2} V_b^\circ \sin \theta \tag{22}$$

The bubble velocity can then be obtained by solving simultaneously Equations (20) and (22) with the coordinate conversion $-x = r_o (1 - \cos \theta)$ to obtain

$$V_b^{\circ 2} = \frac{8}{9} g r_o \frac{(1 - \cos \theta)}{\sin^2 \theta} \tag{23}$$

Equation (23) is only consistent with a constant bubble velocity in the limit as θ tends to zero, for which results

$$V_b^\circ = \frac{2}{3}\sqrt{g r_o} \tag{24}$$

Only the limiting solution is possible because the problem has been overspecified - once potential flow has been assumed and the pressure distribution specified, the shape is no longer an independent variable of the problem.

Despite the shortcomings of the development of Equation (24), Davies and Taylor (6) who first developed the relation, found very good agreement with experimental results. Later experimental investigations at the Taylor

Model Basin (27, 13) have confirmed that the form of Equation (24) applies over a wide range of liquid properties but have modified the numerical coefficient slightly to give

$$V_b^\circ = 0.645\sqrt{gr_o} \qquad (25)$$

These experiments, the results of which have been given by Haberman and Morton, showed that Equation (25) applies to liquids ranging in viscosity to 58.0 centipoise. Davies and Taylor's observation that the spherical-cap bubbles were geometrically similar regardless of the size of the bubble was confirmed by Rosenberg and the angle, Θ, (see Figure 1) subtended by the spherical surface was found to be about 50 degrees. The transition to spherical-cap bubbles was found (13) to be relatively independent of the liquid properties and occurs at a bubble volume of about 4.2 cubic centimeters.

As was noted above, the specification of the bubble shape as spherical at the nose, while convenient, led to overspecification of the problem and, hence, to the limiting solution finally obtained. The rigorous solution of this problem could be carried out by assuming various different bubble shapes of the general form observed and solving the potential flow field at the bubble nose until a shape was

obtained for which Equation (20) was satisfied. This, however, would be a rather tedious procedure.

Very little can be done theoretically towards solving the problem of bubble movement for bubbles of intermediate sizes between the very small and very large bubbles considered above. For these, both inertial and viscous forces are significant and surface tension effects are also present. Other complicating factors which occur in the intermediate regions are unsteady motion and bubble oscillation, and frequently rotation. The bubbles are often deformed and sometimes rise in spiral paths. Probably the most comprehensive compilations of bubble behavior are those of Haberman and Morton (13) and of Harmathy (14).

LARGE BUBBLES IN TUBES I - STAGNANT MEDIA

For large bubbles rising in infinite media, it was shown in the previous section that, on the basis of experimental results in the literature, the rates of rise of bubbles having volumes greater than 4.2 cubic centimeters (i.e. equivalent spherical radii greater than 1 centimeter) are controlled by the inertial flow at the nose of the bubble. In the case of bubbles rising in tubes, the definition of the size of bubble controlled by inertial flow is more difficult. Pending further investigation, however, it would be supposed that the largest bubbles possible would be inertial bubbles and consideration restricted to bubbles with equivalent spherical radii greater than the radius of the tube. This restriction is not entirely in agreement with experimental observation and will be considered further in the light of the theory developed. It is also obvious that in very small diameter tubes the shape of the bubble is controlled by surface tension forces and not by the dynamics of the liquid flow past the bubble. This effect of surface tension on the mechanics of bubble movement will also be considered further in a later section.

Large bubbles in tubes have been observed by a number of investigators (6,7, 20, 15, 30). These bubbles exhibit a blunt or spherical nose followed by a tapered transition section and a cylindrical tail section. For short bubbles, of course, the bubble profile may not be fully developed and the cylindrical section may not be present. These bubbles have the same shape as the cavity formed in a tube filled with liquid when the liquid is allowed to drain from the bottom of the tube and it has been shown that the velocities of bubble and cavity are the same (24). These large bubbles will be referred to as Taylor bubbles following an earlier suggestion in the literature (23). A photograph of such a Taylor bubble is shown in Figure 2.

1. Bubble Characteristics in Inviscid Liquids

Consider the problem of determining the rate of rise of a large bubble of the Taylor type through an inviscid fluid in a tube of radius R. The physical situation has been illustrated in Figure 3 where, again for convenience, the liquid is shown approaching the stationary bubble with a velocity V_b°. Initially, at least, it is not necessary to make any assumption about the specific shape of the bubble.

FIGURE 2

A TAYLOR BUBBLE

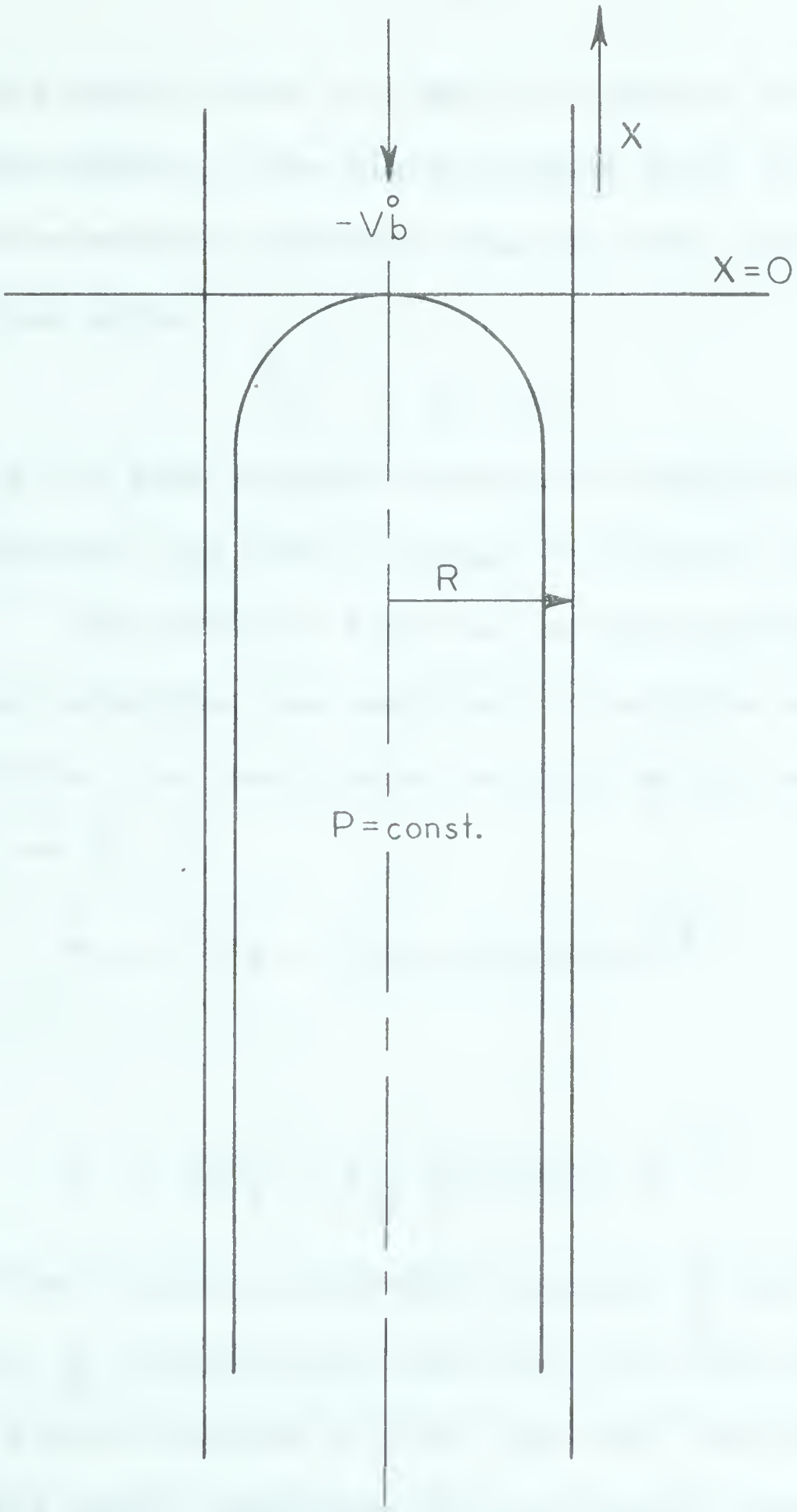

FIGURE 3

A TAYLOR BUBBLE

Since the bubble fluid is a gas, its density is much less than the density of the liquid through which it is rising and the force-momentum equation, Equation (10), for the steady state case gives

$$V_i^2 = 2g\,(-x_i) \qquad (20)$$

which is the same boundary condition as applied in the rise of a spherical-cap bubble through an infinite liquid.

The potential function and corresponding stream function satisfying the conditions of uniform velocity, $-V_b^\circ$, at infinite x and zero radial velocity at the tube wall, r = R, are (6, 7)

$$\Phi = -V_b^\circ x + \sum_j C_j\, J_o(\beta_j \gamma)\, e^{-\beta_j \eta} \qquad (26)$$

and

$$\Psi = V_b^\circ \frac{r^2}{2} + r \sum_j C_j J_1(\beta_j \gamma)\, e^{-\beta_j \eta} \qquad (27)$$

where γ and η denote the radial position, $\frac{r}{R}$, and the axial position, $\frac{x}{R}$, respectively, and the β_j are the null points of the Bessel function of first type and first order. The axial and radial components of the velocity vector are then, respectively,

$$v = \frac{\partial \Phi}{\partial x} = -V_b^\circ - \sum_j \frac{C_j \beta_j}{R} J_o(\beta_j \gamma)\, e^{-\beta_j \eta} \qquad (28)$$

and

$$u = \frac{\partial \Phi}{\partial r} = - \sum_j \frac{C_j \beta_j}{R} J_1(\beta_j \gamma) \, e^{-\beta_j \eta} \qquad (29)$$

At this point one difference between this solution and the solution developed in the previous section for a spherical-cap bubble rising in an infinite medium becomes apparent. Since the bubble shape is not known, the condition that the interface be a surface of constant Ψ (i.e. that the surface be formed by the traces of streamlines) must be satisfied explicitly whereas this condition was implicit in the previous solution where the bubble shape was assumed. The value of Ψ on the surface can be obtained from consideration of Equation (27) at the stagnation point which is one point on the surface. Therefore

$$\Psi_i = \Psi(0,0) = 0 \qquad (30)$$

is the additional condition which must be satisfied to determine the bubble shape as well as the velocity.

In principle, then, Equations (20), (28), (29) and (30) can be solved simultaneously to obtain the bubble velocity and the bubble shape since

$$V_i^2 = v_i^2 + u_i^2 \qquad (31)$$

Thus, for any n arbitrary radial coordinates of the gas-liquid interface, r_i, plus the stagnation point (the stagnation point yields only one equation since Equation (30) is satisfied there implicitly), 2n - 1 equations are available to solve for the unknowns - n constants C_j, the n axial coordinates of the gas-liquid interface, x_i, corresponding to the chosen values of r_i, and the bubble velocity, V_b°. The procedure becomes rapidly more complex, however, with increasing n. Davies and Taylor (6) have carried out the solution for n = 1 using the mid-radius, r/R = 0.5, as the arbitrary radial coordinate of the interface, r_i. The solution that they obtained for the bubble velocity by this method was

$$V_b^\circ = 0.464\sqrt{gR} \qquad (32)$$

Nicklin (24) used the same procedure for several single values of r_i and found that the coefficient in Equation (32) approached asymptotically the value 0.503 as values of r_i nearer the stagnation point were chosen. This result recalls the similar behavior of the solution for a spherical-cap bubble rising in an infinite liquid where the asymptotic solution at the stagnation point predicted the bubble velocity reasonably well.

Before comparing the predictions of Equation (32) with experimental values for the bubble velocity, an alternate method of solution of Equations (20), (28), (29), and (30) will be considered. Substitution of the stagnation conditions

$$v(0,0) = u(0,0) = 0 \tag{33}$$

into Equations (28) and (29) leads to the relation

$$V_b^\circ = -\sum_j \frac{C_j \beta_j}{R} \tag{34}$$

If the bubble shape is now expanded in a general power series in the bubble radius

$$-\eta_i = \sum_k \xi_k \gamma_i \tag{35}$$

and Equations (34) and (35) substituted into Equations (27), (28), and (29) with both the Bessel function and exponential terms being expanded, the stream function and the velocity components are obtained as power series in the bubble radius, the coefficients being functions of the constants C_j and the shape factors ξ_k. These series can now be substituted into the boundary conditions, Equations (20) and (30), to obtain two power series in bubble radius from which the relations between the constants, C_j, and the shape factors, ξ_k, are obtained by equating the coefficients of equal powers of the

bubble radius on either side of the equation for each equation. This procedure, then, results in a general solution of the potential flow around a cavity subject to the condition that the surface of the cavity is a surface of constant pressure and provided that the shape of the cavity can be expressed in a power series in the radial coordinate as expressed in Equation (35).

Dumitrescu (7) carried out this procedure for the case of a spherical nose for which Equation (35) becomes

$$-\frac{\eta_i}{\chi} = \frac{1}{2}\left(\frac{\gamma_i}{\chi}\right)^2 + \frac{1}{8}\left(\frac{\gamma_i}{\chi}\right)^4 + \frac{1}{16}\left(\frac{\gamma_i}{\chi}\right)^6 + \cdots \qquad (36)$$

where χ is the relative frontal radius of curvature of the bubble, r_o/R. This resulted in a solution in terms of the radius of curvature of the nose of the bubble; however, to complete the solution, an additional relation was necessary to define this radius of curvature. To obtain this additional relation, Dumitrescu considered the asymptotic behavior at large distances from the nose of the bubble (i.e. at large -x). The macroscopic material balance for the liquid flowing in the film between the bubble surface and the tube wall can be written as

$$2\pi\int_{r_i}^{R} vr\,dr = -\pi R^2 V_b^\circ \qquad (37)$$

where the negative sign arises from the sign convention used. For large -x, the film becomes thin and the pressure gradient across the film will vanish since it is a result of the radial component of velocity. Therefore, the velocity in the film for large -x is constant for a given value of -x and has the value given by Equation (20). For these conditions, Equation (37) becomes

$$\sqrt{2g(-x)}\ (R^2 - r_i^2) = V_b^\circ\ R^2 \qquad (38)$$

which provides a second relation between the bubble velocity and the bubble geometry.

Dumitrescu showed that the film shape as expressed in Equation (38) joined the spherical nose profile tangentially only for the values

$$V_b^\circ = 0.496\sqrt{gR} \qquad (39)$$

and

$$r_o = 0.75R \qquad (40)$$

and that the two solutions joined at the position $-x_i = 0.50R$, $r_i = 0.71R$. This he assumed to be the correct solution for the overall flow problem.

This analysis of the potential film requires further comment. Equation (38) is quite correct for large distances

from the bubble nose not only because the radial component of velocity can be neglected, but also because the momentum flux at x = 0 will be small compared to the film momentum flux. For this reason as well as the fact that the radial velocity is not negligible for small -x, the applicability of Equation (38) at the point of tangency obtained above is questionable.

Entirely apart from these comments on the solution of the potential film problem, there is the question of how well the solution can be expected to apply to an actual situation where the flow in the film will not approach potential flow. Further discussion of this aspect of the problem, as well as attempts to obtain a better approximation of the actual flow case, will occupy much of the remainder of this section on bubbles in stagnant media.

To test the applicability of these theoretical relations, Equations (32) and (39), which were developed on the basis of potential flow theory, to actual systems, a series of determinations of bubble velocities were made for air bubbles rising through the liquid in a 1.038-inch diameter tube. The properties of the liquids used in these experiments are given in Table I while the details of the experimental

TABLE I

LIQUID PROPERTIES

Liquid	Density lb/ft^3	Kinematic Viscosity $ft^2/sec \times 10^5$	Surface Tension lb/sec^2
Water	62.3	1.055	0.1603
Varsol	49.1	1.29	0.0538
Marcol	54.0	23.65	0.0651
Primol	55.0	173.9	0.0673

equipment and procedures used are included as Appendix I. The results of the velocity determinations for these bubbles are shown in Table II along with the predictions of Dumitrescu (Equation (39)), of Davies and Taylor (Equation (32)) and of the method of Davies and Taylor applied at the stagnation point (this extrapolated value being obtained by Nicklin (24) - see the discussion of Equation (32)). The agreement of Equation 39 with the experimental results for liquids of low viscosity is quite good, as has been demonstrated before (7, 24). The prediction obtained from Equation (32) is considerably below the experimental values for these liquids, however, due probably to the fact that only two points were used to define the bubble. The limiting solution of the Davies and Taylor type at the stagnation point appears to give a slightly better result. Consideration of the experimental results for the more viscous oils, however, indicates that the liquid viscosity has a significant effect on the rate of rise of a Taylor bubble and indicates the inadequacy of the potential model for predicting bubble velocities in actual systems.

TABLE II

EXPERIMENTAL BUBBLE VELOCITIES

Liquid	Bubble Velocity V_b°, ft/sec	$\frac{V_b^\circ}{\sqrt{gR}}$
Water	0.577	0.489
Varsol	0.571	0.484
Marcol	0.558	0.472
Primol	0.494	0.418
Ideal		
- Dumitrescu (Equation (39))		0.496
- Davies and Taylor		
- (Equation (32))		0.464
- Extrapolated to stagnation		0.503

2. Macroscopic Balances - Stagnant Media

Before considering specific aspects of the fluid mechanics of bubble movement, the macroscopic material and force-momentum balances will be applied to the case of a gas bubble rising through stagnant liquid. While these macroscopic balances are derivable by integrating the differential balances over the volume being considered, it is often simpler to proceed directly from the basic definitions of the balances. Thus, the macroscopic material balance is simply the representation of the statement

(Liquid flowing in) - (Liquid flowing out) = (Accumulation)

for the volume being considered. Similarly, the force-momentum balance is the representation of the statement

(Momentum flux in) - (Momentum flux out) = (Net force)

The physical situation being considered is shown schematically in Figure 4 where a Taylor bubble is shown in a tube of radius R. Once again, the coordinate transformation has been made to obtain a stationary bubble with the liquid velocity at infinity being $-V_b^\circ$. It should be noted that the velocity of the tube is also $-V_b^\circ$ in the transformed coordinates. The density and viscosity of the gas in the bubble are considered negligible relative to the density and viscosity of

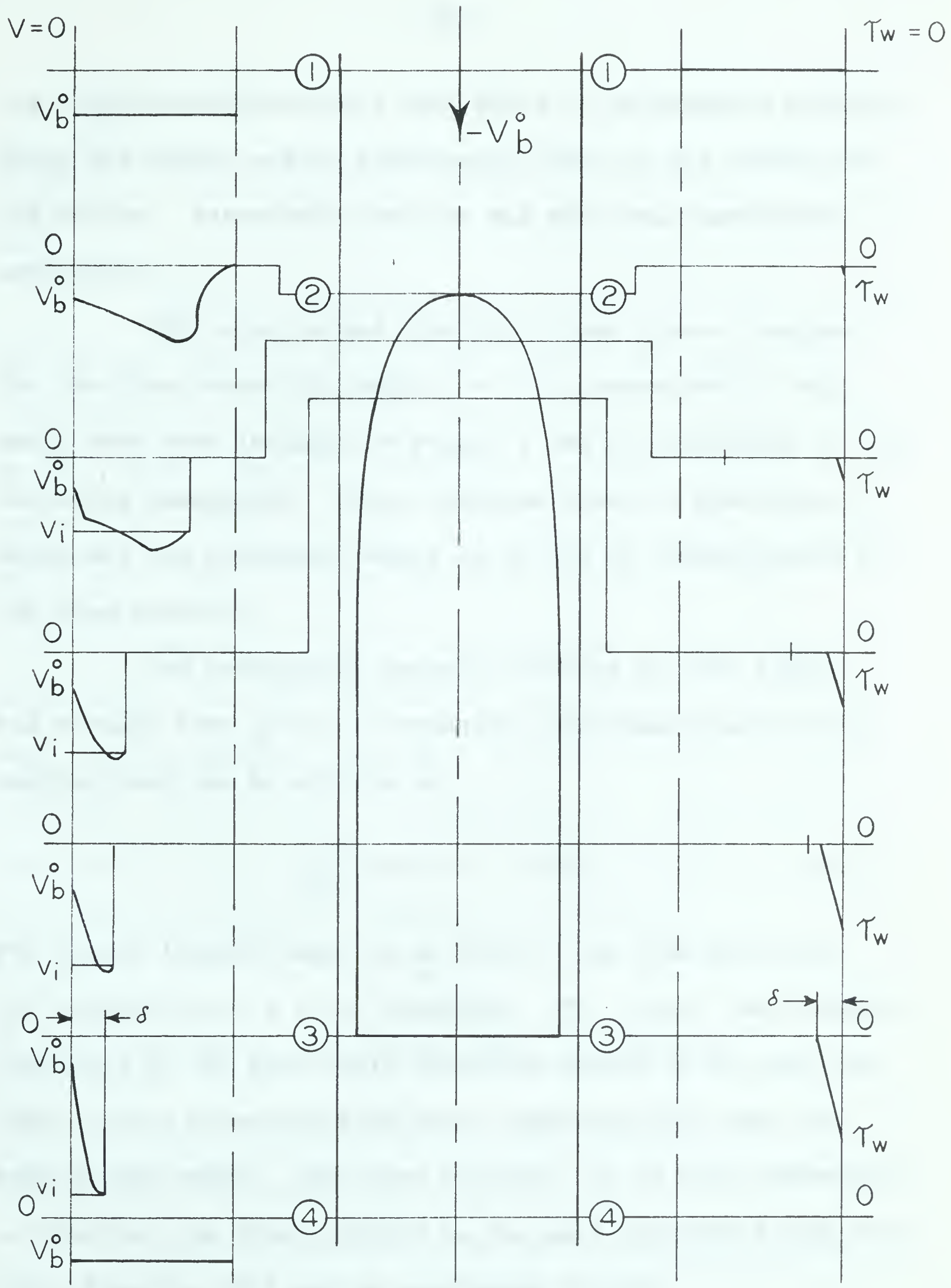

FIGURE 4

PROPOSED MODEL OF TAYLOR BUBBLE

the liquid with the result that there is no pressure gradient along the bubble and no interfacial shear at the surface of the bubble. Interfacial tension has also been considered negligible.

The velocity and idealized shear stress diagrams for the flow around the bubble as it is conceived in this study have been included in Figure 4 and are explained in the following paragraphs. These diagrams have not been drawn to scale and are presented merely as an aid to visualization of the flow behavior.

The macroscopic material balance for the liquid has already been given in connection with Dumitrescu's film analysis and can be written as

$$2\int_{r_i}^{R} vrdr = - R^2 V_b^\circ \qquad (41)$$

For actual liquids there is no slip at the tube wall and the velocity at r = R is, therefore, $-V_b^\circ$. Also, the boundary condition at the gas-liquid interface should be the same as that for the potential flow case, Equation (20), near the nose of the bubble. For some purposes, it is more convenient to consider the flow relative to the wall separately and, for this, Equation (41) can be rearranged to give

$$2\int_{r_i}^{R} (v + V_b^\circ)\, r\,dr = - V_b^\circ r_i^2 = V_F\,(R^2 - r_i^2) \qquad (42)$$

where V_F is the average velocity in the film relative to the wall.

The force-momentum balance cannot be solved exactly due to the complexity of the flow in the nose region. The difficulty arises due to the radial pressure gradient caused by the radial component of flow near the nose. Since, however, the liquid velocity is relatively low near the nose, the radial component should not cause any great radial pressure gradient and it will be neglected. This means, essentially, that the pressure is assumed to be constant or very nearly constant across any transverse section through the tube. To this degree of approximation, the macroscopic force-momentum balance becomes, for a differential length, dx, which is stationary relative to the bubble,

$$\frac{2\rho}{g_c} \frac{\partial \left(\int_{r_i}^{R} v^2 r\,dr\right)}{\partial x} = - (R^2 - r_i^2)\left(\frac{\partial P}{\partial x} + \frac{\rho g}{g_c}\right) + 2R\,\tau_w \qquad (43)$$

The velocity, v, in the integral term of Equation (43) is the local axial velocity.

These relations for the material and force-momentum balances can now be integrated over the length of the bubble

to obtain the overall balances. For this purpose, four sections have been indicated on Figure 4. Sections 1 and 4 are assumed to be sufficiently far from the bubble that the liquid is stagnant with respect to the tube and has a velocity $-V_b^\circ$ in the coordinate system being used. Section 2 is at the stagnation point and section 3 at the tail of the bubble.

The material balance, Equation (41), yields the relations

$$2\left(\int_o^R vr\,dr\right)_2 = -V_b^\circ R^2 \qquad (44)$$

and

$$2\left(\int_{r_i}^R vr\,dr\right)_3 = -V_b^\circ R^2 \qquad (45)$$

To solve the integrals in Equations (44) and (45), the velocity distributions at the sections must be known. Equation (45) for the tail region will be referred to in a later section when the flow in the tail region is being considered.

Considering the force-momentum balance over the length 1-2 of Figure 4, Equation (43) becomes

$$\frac{2\rho}{g_c}\left[\left(\int_o^R v^2 r\, dr\right)_2 - \frac{V_b^{\circ 2} R^2}{2}\right]$$

$$= - R^2 (P_2-P_1) + 2R\int_1^2 \tau_w\, dx - \frac{\rho g}{g_c} R^2 (x_2-x_1) \qquad (46)$$

The velocity distribution at section 2 is not known although, as indicated in Figure 4, it should be fairly well approximated by the velocity distribution for potential flow except in the immediate vicinity of the wall. However, the change in momentum flux over the length 1-2 should not be large since from Equation (44), the average velocity at section 2 is the same as at section 1. The change in momentum flux will, therefore, be neglected. It also seems proper to neglect the increase in pressure at the stagnation point, $\Delta P = \frac{\rho}{g_c} \frac{V_b^{\circ 2}}{2}$ since the velocities encountered are so low. The force-momentum balance over the length 1-2 simplifies to

$$P_2 = P_1 - \frac{\rho g}{g_c} (x_2-x_1) \qquad (47)$$

under these conditions.

Application of Equation (43) to the length 2-3 of Figure 4 leads to the relation

$$\frac{2\rho}{g_c}\left[\left(\int_{r_i}^{R} v^2 r\, dr\right)_3 - \frac{V_b^{\circ 2} R^2}{2}\right]$$

$$= 2R\int_2^3 \tau_w\, dx - \frac{\rho g}{g_c}\int_2^3 (R^2 - r_i^2)\, dx \qquad (48)$$

At this point, it is appropriate to consider the flow behavior in the length 2-3. As shown in Figure 4, the flow at the forward stagnation point is very nearly potential flow with the possible exception of a small region near the tube wall. With increasing distance from the nose, however, the region of viscous influence or the boundary layer on the wall of the tube extends into the film as the liquid accelerates under the influence of gravity. Ultimately, of course, the entire flow in the film is supported by the wall shear and the liquid no longer accelerates but forms a stable 'equilibrium' film. This equilibrium film presumably may be either laminar or turbulent although probably laminar flow would be obtained most frequently.

Since section 4 has been chosen in a region outside the influence of the bubble, Equation (43) gives

$$\frac{2\rho}{g_c}\left[\frac{V_b^{\circ 2} R^2}{2} - \left(\int_{r_i}^{R} v^2 r\, dr\right)_3\right]$$

$$= -R^2(P_4 - P_3) + 2R\int_3^4 \tau_w dx - \frac{\rho g}{g_c} R^2 (x_4 - x_3) \qquad (49)$$

The pressure increase in the wake resulting from the deceleration of the liquid in the film will be referred to as the pressure recovery in the wake, ΔP_R, (after Nicklin (24)) and, with this notation, Equation (49) becomes

$$- \Delta P_R R^2 = - R^2 (P_4 - P_3) + 2R\int_3^4 \tau_w dx - \frac{\rho g}{g_c} R^2 (x_4 - x_3) \qquad (50)$$

In the tube between sections 3 and 4 the shear stress will act upward immediately behind the bubble but will rapidly decrease to zero as the momentum of the annular jet formed at the rear diffuses into the wake. If this force term is neglected, the overall balance over the length 3-4 is

$$- \Delta P_R R^2 = - R^2 (P_4 - P_3) + \frac{\rho g}{g_c} R^2 (x_4 - x_3) \qquad (51)$$

Equations (47) and (51) can be combined to obtain the overall pressure drop between sections 1 and 4 if it is recalled that $P_3 = P_2$. The overall balance so obtained is

$$P_4 - P_1 = \Delta P_R + \frac{\rho g}{g_c} \left[(x_4 - x_3) + (x_2 - x_1) \right] \qquad (52)$$

A second form of the overall force-momentum balance can be obtained by substituting for the pressure recovery in the wake from Equation (48)

$$P_4 - P_1 = \frac{2}{R}\int_2^3 \tau_w \, dx$$

$$- \frac{\rho g}{g_c}\left[(x_4-x_3) + (x_2-x_1) + \int_2^3 \left(\frac{R^2-r_i^2}{R^2}\right) dx\right] \qquad (53)$$

3. Bubble Characteristics in Actual Liquids

a. The Film Region

Through the macroscopic material and force-momentum balances outlined in the previous section, the behavior of Taylor bubbles in actual liquids can be considered. The flow in the liquid film between the bubble and the wall will be treated first.

The assumption of potential flow in the film for large -x, as developed by Dumitrescu, led to Equation (38) which can be rewritten in terms of the film thickness,

$$\delta = R - r_i \qquad (54)$$

to obtain

$$\zeta = \frac{V_b^\circ}{\sqrt{8gR\eta}} \qquad (55)$$

where the relative film thickness, $\frac{\delta}{R}$, has been denoted by ζ and the axial coordinate, as before, by η. Equation (55) can be checked experimentally for actual systems by observation of the variation of film thickness along the

bubble. This has been done both by Davies and Taylor (6) for air bubbles rising through water in a 3.13-inch diameter tube and by Goldsmith and Mason (8) for air bubbles rising through silicone oil (viscosity = 5.6 centipoise) in a 0.197-inch diameter tube. Despite the fact that the observed bubble velocities were quite well represented by Equation (39) in each case, Davies and Taylor's film measurements indicated a thickness about 30 per cent greater than predicted by Equation (55) while Goldsmith and Mason obtained film thicknesses which were about 90 per cent greater. These results are not entirely unexpected; however, they do emphasize the errors involved in applying potential analysis in a region where potential flow behavior would not be expected.

While the principle of analyzing the flow in the transition region between the spherical nose and the cylindrical tail region is quite reasonable, the difficulties involved in solving the equations of motion in this region are considerable. In Equation (43) expressing the force-momentum balance, for example, evaluation of the acceleration term requires detailed knowledge of the velocity distribution in the film as does evaluation of the shear force term.

For this reason, the transition region is not particularly favorable for further analysis.

Consider, however, the annular film of constant thickness which must exist at the rear of long Taylor bubbles. In this region the acceleration of the liquid is zero so that the force-momentum balance, Equation (43), reduces to

$$0 = 2R\tau_w - \frac{\rho g}{g_c}(R^2 - r_i^2) \qquad (56)$$

In addition, the simple geometry permits the application of the differential material and force-momentum balances to determine the velocity distribution. There are two major questions which arise in connection with the application of an analysis carried out in this region, however, the first of which will be considered here and the second when it arises. The first question, then, is whether or not the results of an analysis of long Taylor bubbles rather than a bubble of arbitrary size will be limited in application. Fortunately this is not the case, as experiments (24) have indicated that the velocity of non-expanding Taylor bubbles is independent of bubble length from bubbles one tube diameter in length up to the infinite bubbles obtained by draining the liquid from tubes. It should be noted, however, that bubbles

rising in a tube open to the atmosphere will indicate an effect of bubble length since the velocity of the liquid above the bubble will be a function of the rate of volumetric expansion of the bubble which, in turn, will depend on the bubble size. This effect has been noted experimentally by Laird and Chisholm (20) and by Nicklin (24) and was first explained by Nicklin. For non-expanding bubbles, then, the principles of bubble movement developed from consideration of the cylindrical tail of the bubbles should apply regardless of whether or not the cylindrical tail is present in the actual case being considered.

If the flow in the cylindrical tail region, which will be referred to as the equilibrium film, is assumed to be laminar, Equations (1) and (2) can be solved to obtain the velocity distribution for the steady-state case. This derivation has been carried out in Appendix II and leads to the result

$$V_b^\circ = \frac{\rho g}{\mu} \frac{R^2}{(1-\zeta)^2} \left[\frac{2}{3} \zeta^3 (1-\zeta) + \frac{1}{10} \zeta^5 + \frac{1}{60} \zeta^6 + \text{----} \right] \qquad (57)$$

for the case being considered here with the density and viscosity of the gas being neglected. Equation (57) relates the bubble velocity, V_b°, and the relative thickness, $\zeta = \frac{\delta}{R}$,

of the equilibrium laminar film formed on the wall of the tube around Taylor bubbles. If terms of higher order are neglected, the more familiar result

$$V_b^\circ = \frac{2}{3} \frac{\rho g}{\mu} R^2 \zeta^3 \tag{58}$$

is obtained. For most of the cases considered in this study, it was possible to neglect orders higher than the fourth and the form of Equation (57) which was used is

$$V_b^\circ = \frac{2}{3} \frac{\rho g}{\mu} R^2 \frac{\zeta^3}{(1-\zeta)} \tag{59}$$

The assumption of laminar flow in the equilibrium film has been quite well established experimentally. Nicklin (24), in his experiments with air bubbles rising through water in a 1.02-inch diameter tube measured the film volume by obtaining the change in water level when a bubble reached the free surface, a method also used by Laird and Chisholm in their earlier work (20). Nicklin's results indicated that, as the bubble length increased, the film volume approached asymptotically the value which would result if the film were laminar. An additional check on the film volume was made by trapping the tail region of an infinite bubble and measuring the volume of liquid so obtained.

Agreement in both cases with the predicted laminar film thickness was within 6 per cent.

Additional confirmation that the flow in the film is laminar or, at least, that film thicknesses can be calculated from laminar film theory is provided by White (29) who reports, for a variety of liquids and tube sizes covering a range of Reynolds numbers ($Re = 2V_b^\circ \rho (R-\delta)^2/R\mu$) from 0.01 to 4000, the result

$$\zeta = \alpha \sqrt[3]{\frac{3}{2} \frac{V_b^\circ \mu}{R^2 \rho g}} (1-\zeta) \qquad 0.90 < \alpha < 0.95 \qquad (60)$$

It can be assumed, therefore, without fear of serious error, that the flow in the equilibrium film at the rear of Taylor bubbles is laminar. This conclusion will be recalled once consideration has been given to the flow at the nose of Taylor bubbles.

b. The Nose Region

As has been stated previously, the theoretical analysis of Dumitrescu for the flow at the nose of a Taylor bubble rising in a non-viscous liquid was based on the assumption that the nose was a portion of a spherical surface and determined that the frontal radius was related

to the radius of the tube through the expression

$$\frac{r_o}{R} = 0.75 \qquad (61)$$

In connection with the bubble velocity determinations which were summarized in Table II, the bubble shapes were obtained from analysis of photographs of the bubbles to determine the effect on the shape of the liquid viscosity. As was shown in Table II, the velocities of air bubbles rising through the liquids were a function of the liquid viscosity and this effect would be expected to correspond to a change in the shape of the bubble. The experimental equipment and methods used are given in Appendix I.

The shapes of the nose sections for Taylor bubbles rising through the four liquids listed in Table I are shown individually in Figures I-3 through I-6 in Appendix I and have been combined in Figure 5 to illustrate better the difference in bubble shapes in the different liquids. Also shown in Figure 5 is the theoretical shape for bubbles in ideal liquids as derived from Dumitrescu's analysis.

Comparison of the experimental bubble shapes with the theoretical shape shows that the deviation from the theoretical shape becomes greater as the distance from the

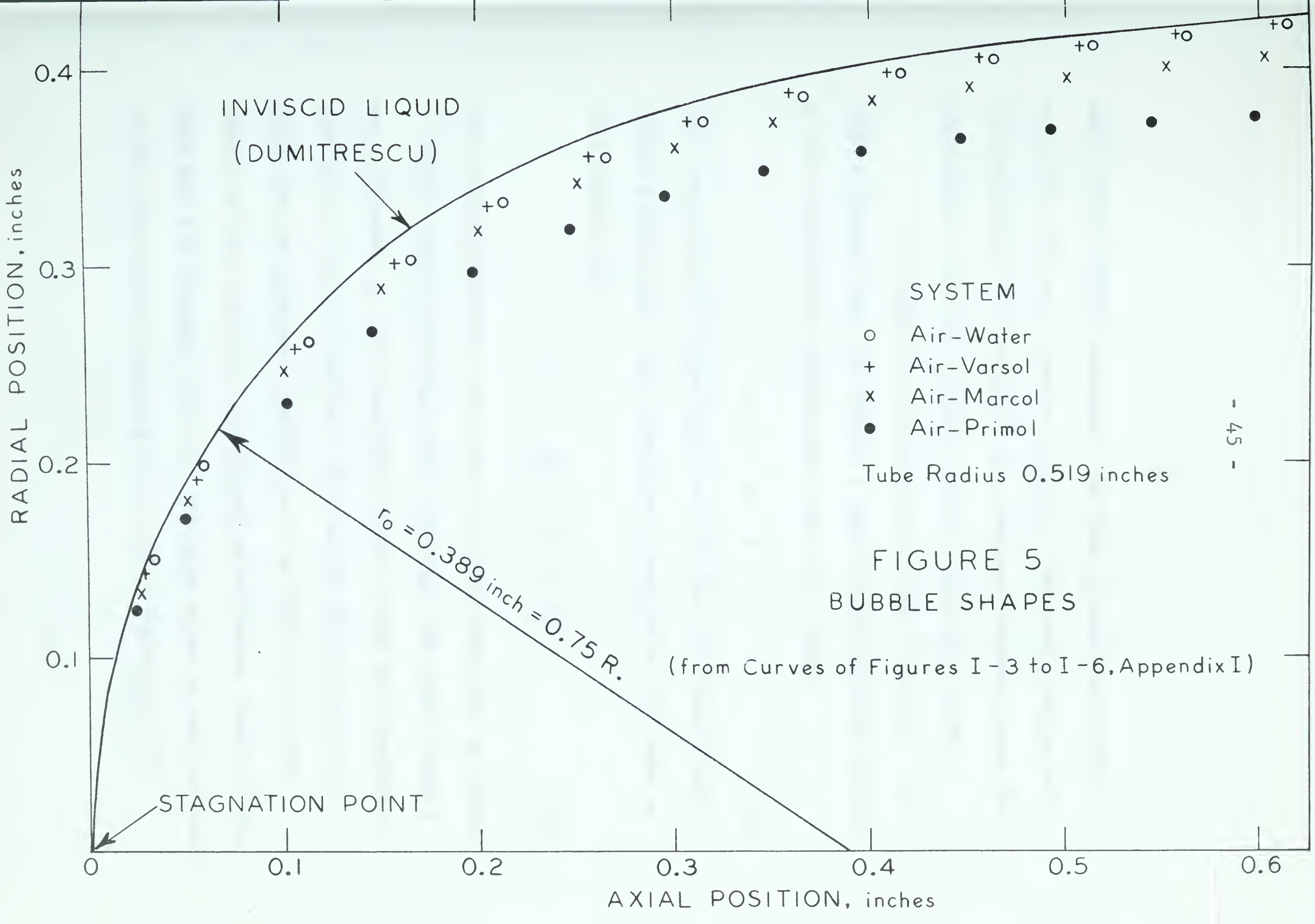

FIGURE 5

BUBBLE SHAPES

(from Curves of Figures I-3 to I-6, Appendix I)

nose of the bubble increases and that greater deviations occur for the more viscous liquids. The shortcomings of the potential film analysis are obvious, however, even for the lowest viscosity liquids tested, water and varsol.

To compare the geometries of the 'cavities', the bubble shapes shown in Figure 5 were normalized with respect to the equilibrium cylindrical radii, R_c, where

$$R_c = R - \delta \tag{62}$$

and δ was obtained from Equation (59) for the appropriate liquid properties. The normalized coordinates obtained in this manner are

$$r' = \frac{r}{R_c}; \quad x' = \frac{x}{R_c} \tag{63}$$

The cavity geometries are shown in normalized form in Figure 6. This figure indicates that, although the cavity shapes are different in the transition region, they are remarkably similar in the nose region. The second interesting fact which can be obtained from Figure 6 is that the frontal radius of the cavity in normalized coordinates, which is the same for all liquids, is 0.75, the same value as was obtained in the theoretical analysis which led to Equation (39).

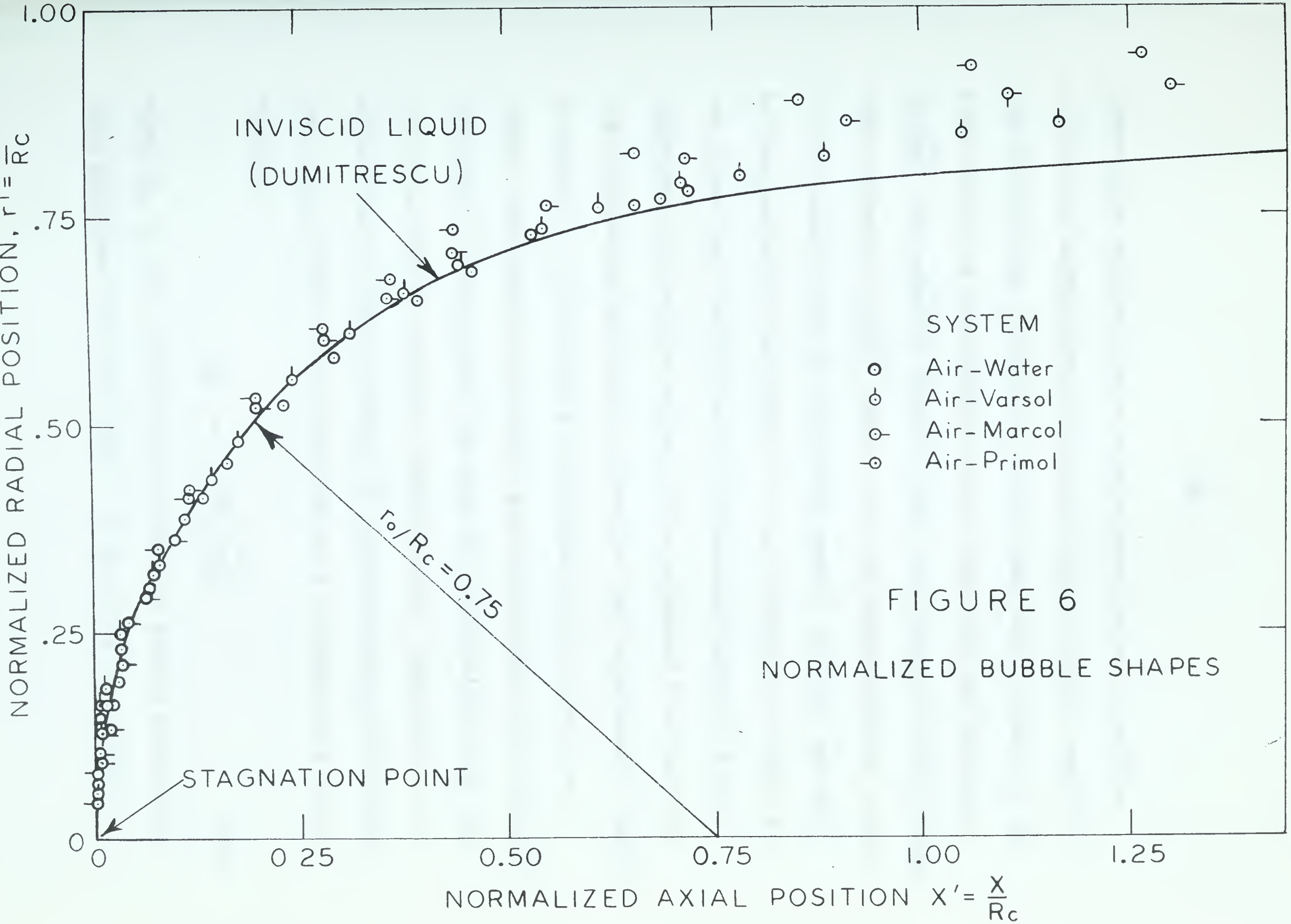

FIGURE 6

NORMALIZED BUBBLE SHAPES

Since this implied that a simple correlation of bubble velocities independent of liquid viscosity might result if the equilibrium cylindrical radius was used instead of the tube radius as the characteristic length in the parameter $V_b^\circ/\sqrt{gR}$, the velocity results were recalculated on this basis. (The parameter $V_b^\circ/\sqrt{gL}$, where L is the characteristic length, is the square root of the Froude number, $V_b^{\circ 2}/gL$, and will be designated by the symbol Γ.) Accordingly, in Table III are given the equilibrium film thickness obtained from Equation (59) and the value of the parameter Γ as well as the information previously given for the experimental results in Table II. The results calculated on this basis do, indeed, indicate a reasonably good correlation with the coefficient Γ being about the same as was obtained from the potential theory analysis, namely 0.496. Therefore, the velocities of Taylor bubbles in liquids having viscosities less than 0.095 lb/(ft)(sec) are well represented by the relation

$$V_b^\circ = 0.496\sqrt{gR_c} \qquad (64)$$

where R_c is the equilibrium cylindrical radius calculable from Equations (62) and (59). It is to be hoped that

TABLE III

EXPERIMENTAL BUBBLE VELOCITIES

Liquid	Bubble Velocity V_b°, ft/sec	$\frac{V_b^\circ}{\sqrt{gR}}$	δ[a] inches	$\frac{V_b^\circ}{\sqrt{g(R - \delta)}}$
Ideal	0.586	0.496	0	0.496
Water	0.577	0.489	0.0272	0.502
Varsol	0.571	0.484	0.0290	0.498
Marcol	0.558	0.472	0.0733	0.510
Primol	0.494	0.418	0.1302	0.484

a Calculated from the bubble velocity with Equation (57)

Equation (64) applies to liquids of greater viscosity also, however, since the correlation as developed here is based on an experimentally observed relation between the frontal radius of the bubble and the equilibrium film thickness, its use for systems beyond the range of observation is open to question.

Before proceeding to apply Equation (64) to further analysis, it may be fruitful to consider the significance of the equation. It indicates that the flow at the nose of a Taylor bubble is well described by potential flow theory regardless of the viscosity of the liquid through which the bubble is rising (subject, of course, to the above comments on the range of viscosity). As a result, the relation between the bubble velocity and the bubble geometry is independent of the liquid, the only effect of the properties of the liquid being to modify the relation between the bubble geometry and the tube geometry. This lack of dependence on the liquid properties which arises from the inertial character of the flow around the bubble is similar to the result obtained by Haberman and Morton (13) for spherical-cap bubbles rising in infinite media where the relation

$$V_b^\circ = 0.645\sqrt{gr_o} \qquad (25)$$

was found to apply over a wide range of liquid viscosities. The velocity of a Taylor bubble can also be expressed in terms of the frontal radius of curvature by substituting into Equation (64) the frontal radius of curvature from Figure 6, $r_o = 0.75\ R_c$. The resulting relation is

$$V_b^\circ = 0.572\sqrt{gr_o} \qquad (65)$$

The difference between Equation (25) and Equation (65) is due almost entirely to the different potential flow situation.

c. General Correlation

Equation (64) relates the bubble velocity to the equilibrium film thickness for a Taylor bubble. It can, therefore, be solved simultaneously with Equation (57) which relates the equilibrium film thickness to the velocity of any inviscid, weightless bubble rising through the liquid in a tube. Eliminating the bubble velocity between these two equations results in the following expression for the equilibrium film thickness.

$$\delta = \frac{-1 + \sqrt{1 + 2CR}}{C} \qquad (66)$$

where

$$C = \sqrt[3]{14.5 \frac{\rho^2 g}{\mu^2}} \tag{67}$$

Substituting back into Equation (64) gives the desired expression for the bubble velocity,

$$V_b^\circ = 0.496\sqrt{gR}\sqrt{1 - \frac{-1 + \sqrt{1 + 2CR}}{CR}} \tag{68}$$

Thus, the second major question about an analysis carried out in the equilibrium film region - whether the solution in this region can be linked to the potential solution at the nose - can now be answered in the affirmative. The experimentally observed similarity in the frontal radii of curvature when normalized with respect to the equilibrium cylindrical radii for the flow at the rear of the bubbles has permitted the solution in the equilibrium film region to be joined to the potential solution at the nose without consideration of the transition region.

d. Limit of Applicability

As Equation (68) is being proposed as a general expression for the velocity of rise of Taylor bubbles in liquids, some consideration must be given to the range of situations to which the equation applies, or, in other words, to the necessary conditions for which a bubble behaves as

a Taylor bubble. As was intimated earlier, with increasing gas-liquid interfacial tension, or surface tension, or with decreasing tube diameter, the surface tension force begins to affect the shape of the bubble and it is no longer controlled entirely by the external flow. In this section, an attempt will be made to determine the limit of this surface tension effect or, at least, to determine the pertinent variables for the empirical correlation of the effect.

It was shown in Part b that a Taylor bubble rises at a velocity given by the equation

$$V_b^\circ = 0.572\sqrt{g r_o} \tag{65}$$

If the shape of the nose of the bubble was determined by the surface tension force, on the other hand, the velocity would be related to the frontal radius by the equation

$$V_b^\circ = 2\sqrt{\frac{\sigma}{\rho r_o}} \tag{69}$$

which is easily derivable from a force balance on an element of the spherical surface assuming that the pressure excess within the bubble due to the surface tension is equal to the stagnation pressure. In Equation (69), σ represents the surface tension. It will be noted that the change of velocity

with frontal radius is opposite in these two cases, therefore at some radius the flow occurring under the Taylor bubble hypothesis will also be consistent with the hypothesis of surface tension control. If only the 'pure' mechanisms occurred, the transition would be predictable by equating Equations (65) and (69). In any actual case, however, there should be a region of transition over which a combined mechanism determines the bubble behavior. Solution of the ideal case should indicate the important parameters governing the bubble behavior. For the ideal case, then, the condition for potential flow is obtained from Equations (65) and (69) as

$$0.327 g r_o > \frac{4\sigma}{\rho r_o} \tag{70}$$

which becomes, upon rearrangement,

$$\frac{\rho g r_o}{\sigma}^2 > 12.23 \tag{71}$$

Substitution into Equation (71) of the relation $r_o = 0.75\ R_c$, along with Equations (62) and (66) yields the condition

$$\frac{\rho g R^2}{\sigma} \left(1 - \frac{-1 + \sqrt{1 + 2CR}}{CR}\right)^2 > 21.8 \tag{72}$$

The parameter on the left-hand side of Equation (72) should be useful for correlating the effect of surface tension on

bubble velocity although the numerical value obtained would not be expected to be valid.

e. Comparison with Literature Results

The velocity prediction of Equation (68) as well as the value of the parameter obtained in Equation (72) for correlating the effect of surface tension on the bubble velocity can now be compared with experimental results from the literature.

The dimensionless parameter 2CR which arose in the development of Equation (68) is equivalent to the property group used by White and Beardmore (30) to correlate their experimental results for velocities of 'cylindrical' bubbles in the region where the effect of surface tension is negligible. Their correlation extends to 2CR = 113 and for 2CR$>$ 160, they recommend the relation

$$\Gamma = \frac{V_b^\circ}{\sqrt{gR}} = 0.488 \qquad (73)$$

The correlation of White and Beardmore and their recommended line for high values of the parameter 2CR are shown in Figure 7 as dashed curves while Equation (68) has been shown as a solid curve. Experimental values of the parameters

FIGURE 7

BUBBLES IN STAGNANT MEDIA COMPARISON WITH EXPERIMENTAL RESULTS

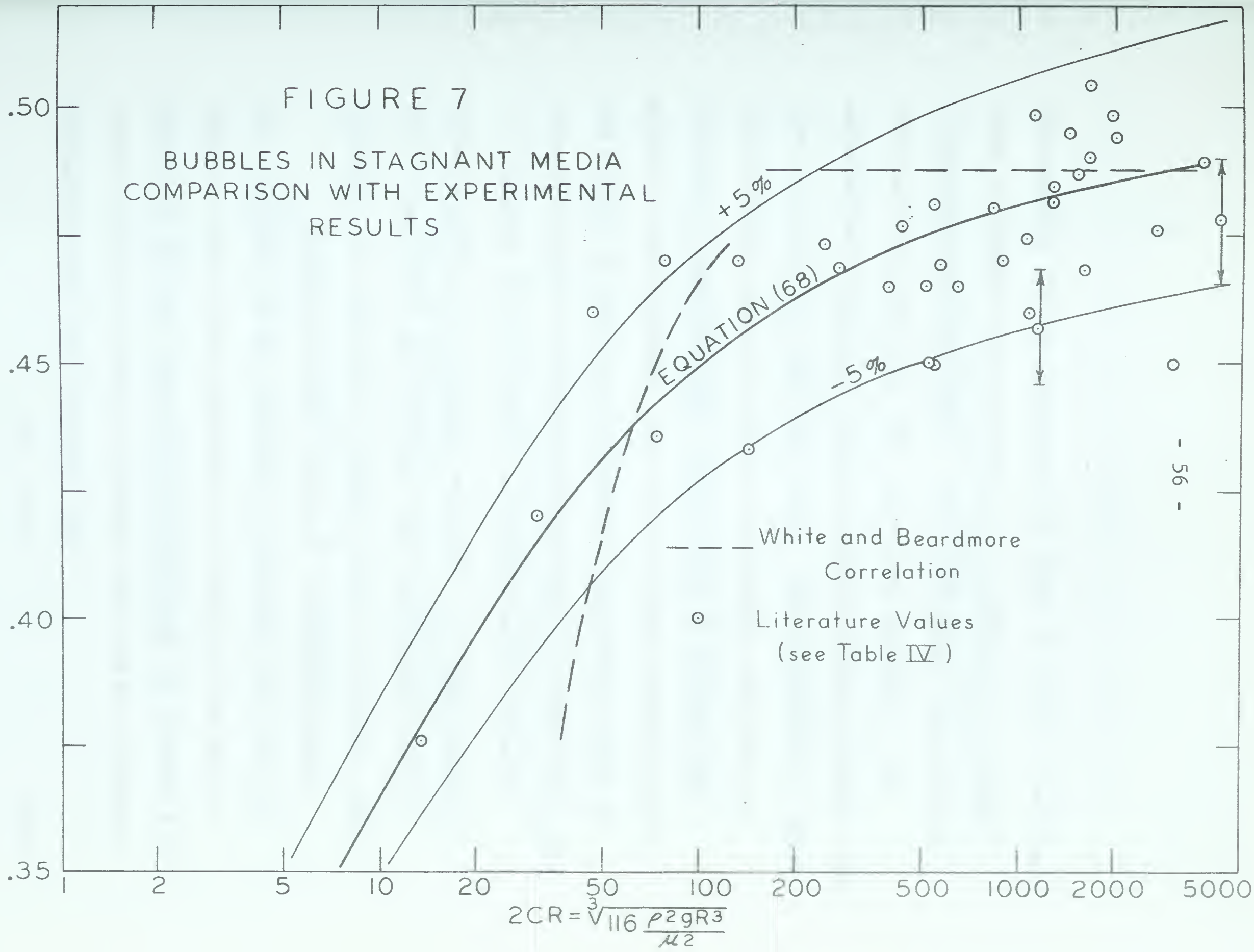

from results in the literature are shown in Figure 7 and are given in tabular form in Table IV. To indicate the degree of agreement on this Figure, lines indicating five per cent deviation from Equation (68), have been included. The experimental results are quite scattered; however, Equation (68) does represent the data quite well. The predictions of White and Beardmore appear to differ considerably from the predictions of Equation (68); however, this is believed due mainly to the different approach of the two investigations. The section of White and Beardmore's correlation which is shown in Figure 7 is the transition region between the region of 'creeping viscous motion' and Taylor bubble behavior. Their proposal of a constant value of Γ at high values of 2CR is reasonably good although the experimental results available are represented somewhat better by Equation (68).

In Table IV, the values of the Eötvös number ($Eo = \rho g R^2/\sigma$) and the parameter of Equation (72) are also shown to enable some comparison to be made of the applicability of the two relations for predicting the threshold of control by surface tension, Equation (72) and the condition proposed by White and Beardmore (30)

$$Eo > 17.5 \qquad (74)$$

TABLE IV

BUBBLES IN STAGNANT MEDIA - COMPARISON WITH EXPERIMENTAL RESULTS

Liquid[a]	Tube Radius inches	Kinematic Viscosity $ft^2/sec \times 10^5$	Surface Tension lb/sec^2	$2CR^b \times 10^{-3}$	Eo[c]	$Eo(1-\xi)^{2d}$	Γ	
							Predicted[e]	Experiment
(1)	(2)	(3)	(4)	(5)	(6)	(7)	(8)	(9)
A1	1.0	1.055	0.1603	2.688	86.9	80.5	0.487	0.476
A2	0.51	1.167	0.1617	1.282	22.4	20.1	0.483	0.484
		0.902	0.1578	1.522	22.9	20.7	0.484	0.487
		0.798	0.1557	1.651	23.17	21.0	0.4845	0.490
A3	0.195	1.055	0.1603	0.515	3.42	2.87	0.475	0.2865
	0.394			1.06	14.0	12.4	0.482	0.474
	0.74			1.99	49.4	45.1	0.485	0.494
	1.38			3.71	171.3	160.5	0.489	0.489
A4	0.242	1.055	0.1603	0.651	5.09	4.35	0.479	0.407
	0.425			1.143	15.7	13.96	0.482	0.457
	1.563			4.20	212.5	200.	0.490	0.478
A5	0.25	1.407	0.164	0.555	5.32	4.49	0.475	0.427
	0.375	1.407	0.164	0.833	11.99	10.44	0.480	0.480
		0.623	0.1510	1.432	12.83	11.56	0.483	0.495
	0.50	1.407	0.164	1.11	21.27	18.9	0.482	0.498
		0.601	0.1503	1.96	22.97	21.0	0.485	0.498
B	0.197	2.92	0.0413	0.1333	12.1	8.55	0.455	0.47
		6.55	0.0430	0.0779	11.6	7.39	0.443	0.47
		14.03	0.0444	0.0469	11.26	6.29	0.430	0.46
		25.7	0.0483	0.0313	10.33	5.08	0.415	0.42

(1)	(2)	(3)	(4)	(5)	(6)	(7)	(8)	(9)
A6	0.59	1.05	0.1606	1.59	30.2	27.3	0.484	0.468
	1.12			3.02	108.9	101.2	0.488	0.45
C	0.59	14.5	0.0715	0.276	58.6	46.1	0.468	0.468
	1.12			0.525	211.5	177.8	0.475	0.45
D	0.59	103.7	0.0750	0.07445	57.0	35.9	0.443	0.436
	1.12			0.1415	205.5	146.7	0.456	0.433
E	0.434	0.611	0.058	1.678	71.9	65.2	0.485	0.504
F	0.716	7.09	0.144	0.5415	57.0	48.0	0.475	0.481
G		23.38	0.1033	0.2444	76.8	59.5	0.465	0.473
H	0.437	855.	0.142	0.01353	23.6	4.63	0.380	0.376
	0.280			0.00866	9.67	2.27	0.356	0.267
I	0.437	1.62	0.0486	0.884	43.6	38.2	0.480	0.470
	0.280			0.566	17.9	15.12	0.475	0.469
	0.252			0.510	14.5	12.11	0.475	0.465
	0.234	1.91	0.0486	0.425	12.54	10.35	0.473	0.477
	0.216			0.393	10.70	8.75	0.471	0.465
	0.1595			0.290	5.83	4.61	0.468	0.406
J	0.216	0.324	0.0382	1.282	12.56	11.25	0.483	0.482
	0.183			1.088	9.03	7.99	0.482	0.460
	0.150			0.890	6.05	5.29	0.480	0.402
K	0.216	0.909	0.0640	0.644	9.13	7.80	0.478	0.465
	0.183			0.545	6.55	5.51	0.480	0.450
	0.1595			0.475	4.98	4.15	0.475	0.419
A7	0.519	1.055	0.1603	1.394	23.4	21.0	0.484	0.489
L		1.29	0.0538	1.220	55.0	49.1	0.482	0.484
M		23.65	0.0651	0.1752	49.9	36.9	0.460	0.472
N		173.9	0.0673	0.0464	49.2	27.45	0.429	0.418

a See Code for Table IV listing Liquids and Sources on following page.

b $2CR = \sqrt[3]{116 \frac{\rho^2 g R^3}{\mu^2}}$

c $Eo = \frac{\rho g R^2}{\sigma}$ (See Equation (74))

d See Equation (75).

e $\Gamma = 0.496\ (1-\varepsilon)^{1/2}$ (See Equation (68))

CODE FOR TABLE IV

Designation in Table IV	Liquid	Source
A1	Water	Laird and Chisholm
A2	Water	Nicklin
A3	Water	Dumitrescu
A4	Water	Davies and Taylor
A5	Water	Griffith and Wallis
A6	Water	O'Brien and Gosline
A7	Water	This Investigation
B	Silicone Oils	Goldsmith and Mason
C	Mineral Seal Oil	O'Brien and Gosline
D	Livestock Oil	O'Brien and Gosline
E	Carbon Tetrachloride	Harmathy
F	Glycerine Solution	Uno and Kintner
G	Diethylene Glycol	Uno and Kintner
H	Glycerine	Hattori
I	Ethyl Alcohol	Hattori
J	Ether	Hattori
K	Benzene	Hattori
L	Varsol	This Investigation
M	Marcol	This Investigation
N	Primol	This Investigation

The experimental and predicted velocities for tests in which the surface tension effect is significant have been indented to permit easier comparison of the agreement. Neither Equation (72) nor Equation (74) predict the surface tension effect very well; however, the form of Equation (74) seems to reflect the experimental behavior more adequately. This would indicate that the surface tension alone is not sufficient to determine whether Taylor bubble behavior is obtained and the viscosity must also be considered. From Table IV, the criterion of Taylor bubble behavior can be obtained by inspection as

$$Eo \left(1 - \frac{-1 + \sqrt{1 + 2CR}}{CR}\right)^2 > 5.0 \qquad (75)$$

Actually, the constant may be somewhat lower since in all but one case Equation (68) applies for values greater than 4.62.

f. Minimum Size of Taylor Bubbles

In the initial discussion of the movement of Taylor bubbles in tubes, a very rough definition of a bubble which would be expected to behave as a Taylor bubble was given as a bubble with an equivalent spherical radius greater than the radius of the tube. While no experimental

results were obtained in this study to check the approximation, consideration of the bubble mechanics developed would indicate that a better criterion might be that a bubble would behave as a Taylor bubble if it has an equivalent spherical radius equal to or greater than the frontal radius of a Taylor bubble rising through the liquid in the tube. In terms of the relations developed above, this condition can be expressed as

$$r_e > 0.75R \left(1 - \frac{-1 + \sqrt{1 + 2CR}}{CR}\right) \qquad (76)$$

To check the applicability of this condition, the results of O'Brien and Gosline (25) and of Uno and Kintner (28) can be considered. In both of these investigations, the effect of bubble size on bubble velocity in various sizes of tubes was obtained experimentally for a number of liquids. Using only the tests for which transition to bubbles rising at constant velocity was observed, this comparison is given in Table V. These results show that Equation (76) does give a better approximation for the size of bubbles which will behave as Taylor bubbles; however, the approximation is still not good. In the case of larger tubes, it appears that relatively small bubbles will behave as Taylor bubbles - probably indicating that the bubbles attain the shape of spherical-cap

TABLE V

MINIMUM SIZES FOR TAYLOR BUBBLES

Liquid	Tube Radius inches	Equivalent Radius, r_e inches	
		Calculated[a]	Experimental
Water	0.59	0.42	0.37
	1.12	0.81	0.48
Mineral Seal Oil	0.59	0.39	0.24
	1.12	0.77	0.37
Livestock Oil	0.59	0.35	0.32
	1.12	0.71	0.38
Glycerine Solution	0.716	0.49	0.35
Diethylene Glycol	0.716	0.47	0.24

a Calculated from Equation (76)

bubbles as shown in Figure 1 with a frontal radius equal to the frontal radius of a Taylor bubble.

g. Summary

A model is proposed for the movement of a large gas bubble in a tube filled with liquid which takes into account the viscous flow along the wall of the tube as well as the inertial flow at the nose of the bubble. On the basis of an observed similarity in the geometries of bubbles rising through liquids of different viscosities, an equation is developed which describes the behavior of these bubbles over a considerable range of liquid and tube properties, this equation being

$$V_b^\circ = 0.496\sqrt{gR}\sqrt{1 - \frac{-1 + \sqrt{1 + 2CR}}{CR}} \qquad (68)$$

where

$$C = \sqrt[3]{14.5\,\frac{\rho^2 g}{\mu^2}} \qquad (67)$$

The condition for which Equation (68) describes the bubble velocity is found by semi-empirical means to be

$$Eo\left(1 - \frac{-1 + \sqrt{1 + 2CR}}{CR}\right)^2 > 5.0 \qquad (75)$$

The minimum size of Taylor bubbles is considered and it is

found that bubbles which satisfy the condition

$$r_e > 0.75R \left(1 - \frac{-1 + \sqrt{1 + 2CR}}{CR}\right) \qquad (76)$$

all appear to be described by Equation (68). However, Equation (68) also describes quite well the behavior of smaller bubbles, especially in large size tubes, so Equation (76) is not an accurate description of the minimum size of Taylor bubbles.

LARGE BUBBLES IN TUBES II -- MOVING MEDIA

In the foregoing sections dealing with the movement of large bubbles in tubes, it has been shown that the behavior of the bubbles can be quite well described for a wide range of systems if the viscous flow in the film is taken into account.

In the following sections, the same type of model will be tested for the velocity of bubbles in moving liquid streams. Initially considered will be the rise of a single bubble in a moving stream of liquid in a tube following which the case of gas-liquid slug flow will be treated. Before becoming involved with the behavior of actual bubbles, however, it will be profitable to consider the changes that occur in the macroscopic balances as a result of the movement of the medium through which the bubble is rising.

1. Macroscopic Balances - Moving Media

a. Single Bubble

Figure 8 illustrates schematically the problem being considered. As before, sections 1 and 4 are considered to be in regions of fully developed flow in the tube. If the axial velocity is denoted by v, as before, the average

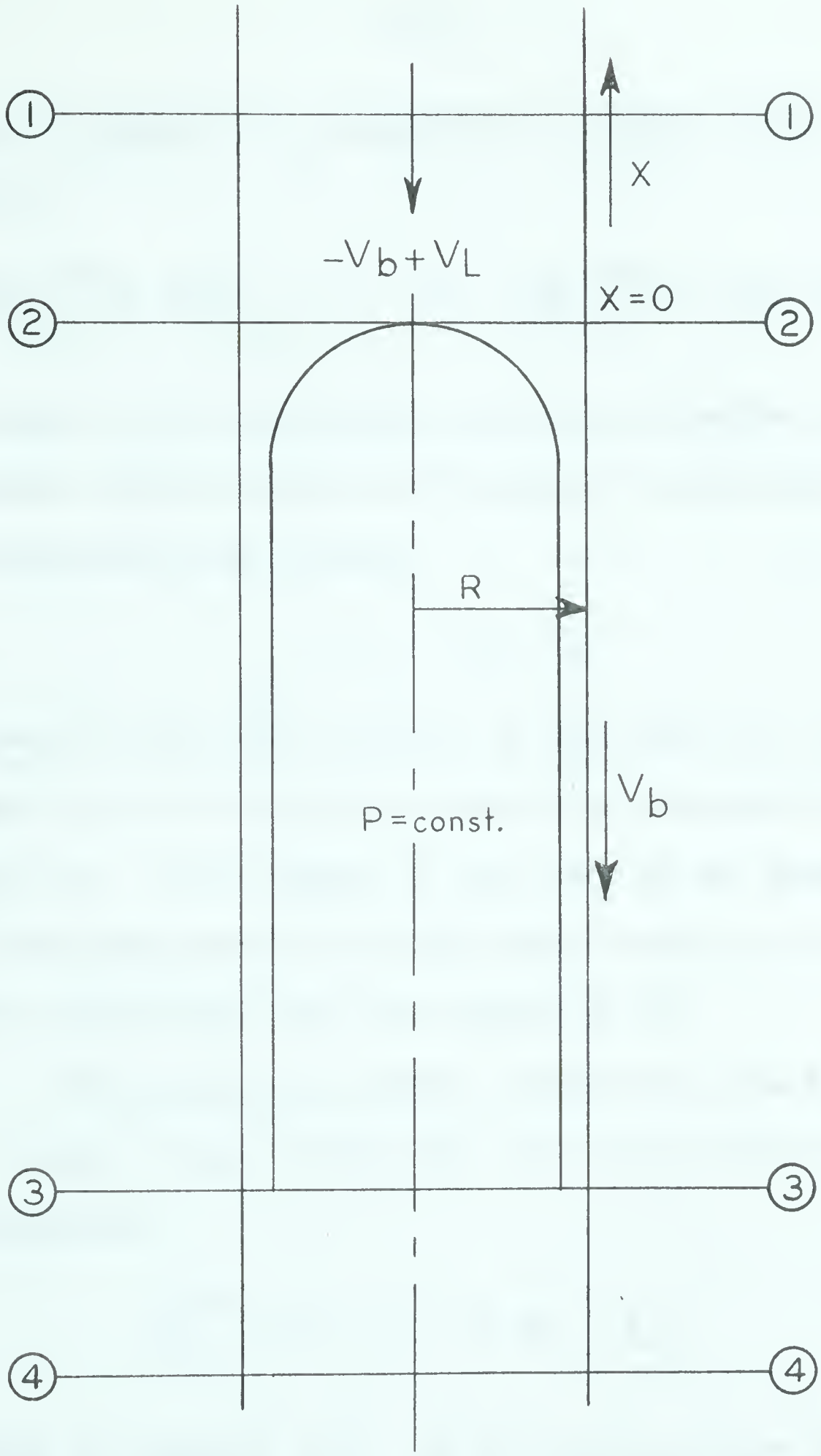

FIGURE 8

A TAYLOR BUBBLE IN MOVING LIQUID

velocity is obtained by integration at either section 1 or section 4,

$$\underline{V} = \frac{2}{R^2}\left(\int_o^R vr\ dr\right)_{1 \text{ or } 4} = -V_b + \frac{2}{R^2}\int_o^R (v + V_b)\ rdr \qquad (77)$$

The integral in the right-hand equality of Equation (77) is the average liquid velocity with respect to the tube which will be denoted by V_L, giving

$$\underline{V} = -V_b + V_L \qquad (78)$$

The velocity of the tube relative to the bubble is $-V_b$. The symbol V_b has been used to denote the absolute bubble velocity (i.e. with respect to the tube) in the general case to differentiate it from the bubble velocity in a stagnant liquid which has been denoted by V_b°.

The macroscopic material balance for the flow of liquid around a Taylor bubble for the moving liquid case can be expressed as

$$2\int_o^R vr\ dr = -R^2\ (V_b - V_L) \qquad (79)$$

in analogy to Equation (41). If the flow relative to the wall is considered separately, Equation (79) can be re-arranged to obtain

$$2\int_{r_i}^{R} (v + V_b)\, r\,dr = V_L R^2 - V_b r_i^2 = V_F (R^2 - r_i^2) \quad (80)$$

where, as before, V_F denotes the average velocity in the film with respect to the wall of the tube.

The force-momentum balance, Equation (43), can be integrated along the flow relative to the bubble to obtain the pressure drop across the bubble. This is the same procedure carried out earlier for the bubble moving in stagnant liquid and the results are quite similar. For the flow between sections 1 and 2, the force-momentum balance gives

$$\frac{2\rho}{g_c}\left[\left(\int_o^R v^2 r\, dr\right)_2 - \left(\int_o^R v^2 r\, dr\right)_1\right]$$

$$= - R^2 (P_2 - P_1) + 2R\int_1^2 \tau_w\, dx - \frac{\rho g}{g_c} R^2 (x_2 - x_1) \quad (81)$$

In the stagnant liquid case, the wall shear term and the acceleration of the liquid between the two sections were neglected to give Equation (47). As the velocity of the liquid is increased from zero, however, this approximation becomes poorer due to the increased shear at the wall of the tube. If the change in momentum flux between sections 1 and

2 is still considered negligible, the balance for the moving liquid case can be approximated by

$$P_2 - P_1 = \left(\frac{2}{R}\tau_{w1} - \frac{\rho g}{g_c}\right)(x_2 - x_1) \qquad (82)$$

where the wall shear stress is evaluated for the fully developed flow at section 1. Here, as in the stagnant liquid case, the effect of the bubble nose on the velocity distribution in the liquid ahead of the bubble has been neglected.

For the flow in the film along the bubble, Equation (43) has the form

$$\frac{2\rho}{g_c}\left[\left(\int_{r_i}^{R} v^2 r\, dr\right)_3 - \left(\int_{o}^{R} v^2 r\, dr\right)_1\right]$$

$$= 2R\int_2^3 \tau_w dx - \frac{\rho g}{g_c}\int_2^3 (R^2 - r_i^2)\, dx \qquad (83)$$

since there is no pressure drop along the bubble, the gas in the bubble being considered weightless and inviscid. The assumption of zero pressure drop across the film at the nose of the bubble will be poorer for this case; however, the effect should still be small. The flow in the film, then, is quite similar for both the stagnant liquid and moving liquid cases - there is initially a region of 'free' acceleration or free

fall under the influence of gravity along with which there is a concurrent increase in the wall shear stress until a stable, non-accelerating film supported entirely by the shear stress is attained. It should be noted that the criterion of the stable film is based on the liquid movement relative to the wall, not the movement relative to the bubble.

The force-momentum balance in the wake region between sections 3 and 4 is, from Equation (43),

$$\frac{2\rho}{g_c}\left[\left(\int_o^R v^2 r\, dr\right)_4 - \left(\int_{r_i}^R v^2 r\, dr\right)_3\right]$$

$$= -R^2(P_4 - P_3) + 2R\int_3^4 \tau_w dx - \frac{\rho g}{g_c} R^2 (x_4 - x_3) \qquad (84)$$

which can also be expressed as

$$P_4 - P_3 = \Delta P_R + \frac{2}{R}\int_3^4 \tau_w dx - \frac{\rho g}{g_c}(x_4 - x_3) \qquad (85)$$

by introducing the symbol ΔP_R for the pressure increase in the wake as a result of deceleration of the liquid in the annular film.

$$\Delta P_R = \frac{2\rho}{g_c R^2}\left[\left(\int_{r_i}^R v^2 r\, dr\right)_3 - \left(\int_o^R v^2 r\, dr\right)_4\right] \qquad (86)$$

As before, the exact evaluation of the wall shear stress is

made difficult by the presence of the 'decaying' annular jet behind the bubble. For practical purposes, however, the shear stress can be approximated in the wake region in the same way as it was approximated in the nose region - namely by using the shear stress for the fully developed liquid flow. Introducing this approximation, Equation (85) becomes

$$P_4 - P_3 = \Delta P_R + \left(\frac{2}{R}\tau_{w_4} - \frac{\rho g}{g_c}\right)(x_4 - x_3) \qquad (87)$$

The overall pressure drop can be obtained by combining Equations (82) and (87) since the pressure drop along the bubble is negligible (i.e. $P_2 = P_3$). The overall pressure drop is, then,

$$P_4 - P_1 = \Delta P_R + \left(\frac{2}{R}\underline{\tau}_w - \frac{\rho g}{g_c}\right)\left[(x_4 - x_3) + (x_2 - x_1)\right] \qquad (88)$$

where the shear stresses at sections 1 and 4 have both been denoted by the symbol $\underline{\tau}_w$ in accordance with the assumptions outlined above. Upon elimination of the pressure recovery term through Equation (83), Equation (88) can be written as

$$P_4 - P_1 = \frac{2}{R}\int_2^3 \tau_w\, dx - \frac{\rho g}{g_c}\int_2^3 (R^2 - r_i^2)\, dx + \left(\frac{2}{R}\underline{\tau}_w - \frac{\rho g}{g_c}\right)\left[(x_4 - x_3) + (x_2 - x_1)\right] \qquad (89)$$

2. The Effect of Liquid Velocity on Bubble Velocity

The second and third terms of the material balance relation given in Equation (80) can be solved to give the following form which is explicit in the bubble velocity,

$$V_b = \frac{R^2}{r_i^2} V_L - \frac{R - r_i^2}{r_i^2} V_F \qquad (90)$$

Equation (90) is a general relationship between the bubble velocity, V_b, the geometry of the bubble at any section and the average velocity of the liquid at the same section. To obtain the bubble velocity from Equation (90), it must be possible to specify both the bubble geometry and the velocity of the liquid at some section through the bubble.

In the first part of this investigation, it was demonstrated that the velocities of air bubbles of the Taylor type rising through liquids in confining tubes could be predicted quite well by a theory which depended in part upon the hypothesis that the flow in the annular film at the rear of the bubbles was laminar. In the force-momentum balance considerations of the preceding section, it has also been shown that there is no a priori reason to discard this hypothesis for the case of Taylor bubbles rising in a moving stream of liquid. If it can be assumed, therefore, that

there is an equilibrium annular film in laminar flow at the rear of the bubble, laminar flow theory gives an additional relation between the geometry of the bubble and the liquid flow in this region, and the bubble velocity can be specified as a unique function of either the liquid flow or the equilibrium film thickness. Using the relation developed in Appendix II and previously used in Equation (57), the bubble velocity in a moving stream of liquid can be expressed as

$$V_b = \frac{1}{(1-\zeta^\circ)^2} V_L + \frac{\rho g}{\mu} \frac{R^2}{(1-\zeta^\circ)^2} \left[\frac{2}{3} \zeta^{\circ 3} (1-\zeta^\circ) + \frac{1}{10} \zeta^{\circ 5} + \cdots \right] \quad (91)$$

where the symbol ζ° denotes, as before, the relative film thickness, δ/R. Equation (91) permits prediction of the bubble velocity in a moving stream of liquid if only the thickness of the equilibrium film at the rear of the bubble is known.

As was shown in Equation (66), it is possible to predict the thickness of the equilibrium laminar film as a function of the properties of the system for Taylor bubbles rising through stagnant liquids. For the case of bubbles rising in moving liquid streams, however, there are two general possibilities. First, the equilibrium film thickness could be independent of the liquid velocity, in which case

it would remain the same as the film thickness for the stagnant case and Equation (91) would become

$$V_b = C_o V_L + V_b^\circ \qquad (92)$$

where the constant $1/(1-\zeta)^2$ for a bubble rising through stagnant liquid has been denoted by C_o. The second possibility is that the film thickness could be a function of the liquid velocity, in which case Equation (91) would remain in its general form which can be abbreviated to

$$V_b = C_1(\zeta) V_L + C_2(\zeta) \qquad (93)$$

Before considering experimental results from the literature to determine which of these forms of Equation (91) provides a better description of bubble movement in actual systems, some rather interesting observations can be made on the basis of the equations themselves.

From Equation (92), which applies to the simplest possible case, namely that in which there is no change in the flow in the equilibrium film with increasing liquid velocity, it can be seen that the bubble velocity increases with increasing liquid rate. The reason, of course, is that the equilibrium film moves with a constant average velocity

relative to the wall for a constant film thickness while the velocity of the bubble relative to the wall changes. Hence the average velocity of the film relative to the bubble must change and with it the velocity of the bubble relative to the preceding liquid.

The condition for which the bubble velocity relative to the preceding liquid is independent of the liquid velocity can be obtained from Equation (93) by subtracting V_L from both sides of the equation and differentiating with respect to V_L. Denoting the differentiation with a prime ('), this yields

$$(V_b - V_L)' = 0 = C_1(\zeta) - 1 + V_L C_1'(\zeta) + C_2'(\zeta) \qquad (94)$$

Consideration of the nature of the terms $C_1(\zeta)$ and $C_2(\zeta)$ from Equation (91) indicates that the film thickness must decrease with increasing liquid velocity to maintain a constant bubble velocity relative to the preceding liquid. While this is not impossible, it would seem rather improbable since, for higher liquid velocities, the higher wall shear stress would be imagined to drag more liquid past the bubble.

From this general consideration of the material balance relation, it can be concluded that the bubble velocity

relative to the preceding liquid most likely increases with increasing liquid velocity. Whether or not the thickness of the equilibrium film increases, however, must be decided on the basis of experimental results.

There are available two experimental investigations of the effect of liquid velocity on the velocity of a single bubble rising in the liquid (12, 24). In both of these investigations, a single bubble was injected into a moving stream of water and the bubble velocity measured. The empirical equations for the change of bubble velocity with water velocity which were obtained in these investigations are:

Griffith and Wallis (12)

$$V_b = V_L + C_3 V_b^\circ \tag{95}$$

Nicklin (24)

$$V_b = C_4 V_L + V_b^\circ \tag{96}$$

In Griffith and Wallis' correlation, the parameter C_3 was obtained as a function of the bubble velocity and the kinematic viscosity and velocity of the liquid while for Nicklin's correlation, the parameter C_4 was a function of

bubble length and liquid velocity at low liquid velocities and approached a constant value of 1.2, independent of bubble size, for higher liquid velocities. Nicklin's results for the variation of C_4 at low liquid velocities are shown in Figure 9. Also shown in Figure 9 are the results of Griffith and Wallis for comparable water temperature, calculated from experimental data with Equation (96).

The results of Griffith and Wallis for both tube sizes, 1-inch and 3/4-inch diameter, are in quite good agreement with the results of Nicklin. These investigators, however, noted no effect of bubble length, even at the low velocities where Nicklin obtained a significant variation in bubble velocity with bubble length. It is quite possible, however, that their velocity measurements were not sufficiently accurate to obtain the slight difference in velocity. The velocity measurements of Griffith and Wallis were made by timing the rate of rise by hand while Nicklin's results were obtained by tracking the bubbles with a movie camera, the time being obtained from a watch mounted on the camera platform and in the field of view of the camera.

Comparing Equations (91) and (95), the parameter C_3 is given by the relation

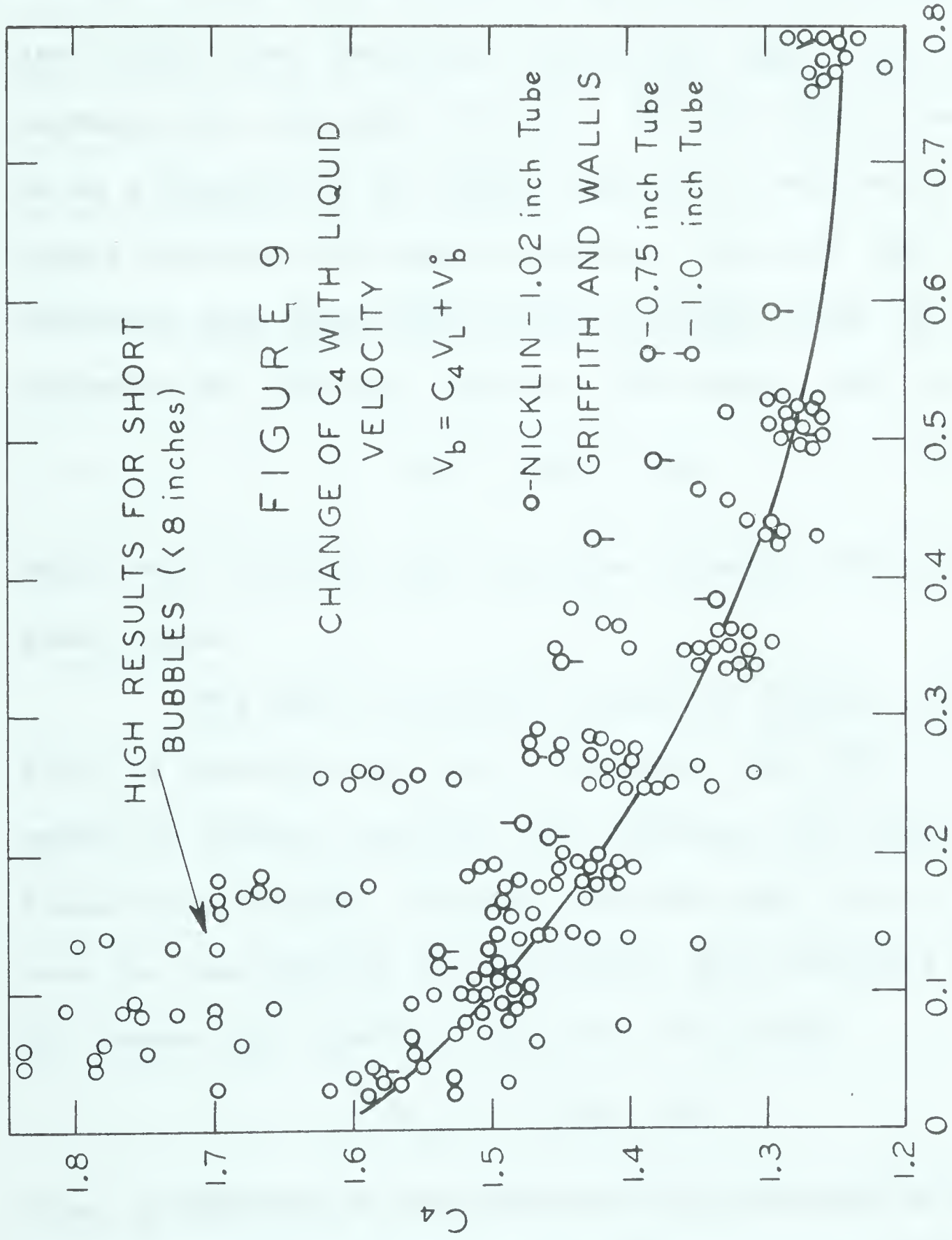
FIGURE 9
CHANGE OF C_4 WITH LIQUID VELOCITY
$V_b = C_4 V_L + V_b^\circ$
o-NICKLIN - 1.02 inch Tube
GRIFFITH AND WALLIS
φ-0.75 inch Tube
δ-1.0 inch Tube
HIGH RESULTS FOR SHORT BUBBLES (< 8 inches)
C_4
LIQUID VELOCITY, V_L, ft./sec.
1.8
1.7
1.6
1.5
1.4
1.3
1.2
0
0.1
0.2
0.3
0.4
0.5
0.6
0.7
0.8

$$C_3 = \frac{1}{V_b^\circ} \left[\frac{\xi(2 - \xi)}{(1 - \xi)^2} V_L + \frac{2}{3} \frac{\rho g R^2}{\mu} \frac{\xi^3}{(1 - \xi)} \right] \qquad (97)$$

where the higher order terms in ξ have been neglected. For zero liquid flow, the first term on the right is zero and the parameter has the value of unity. The fact that C_3 was found to be a function of the bubble velocity as well as of the liquid velocity and liquid properties indicates that the film thickness does change with liquid velocity since, if the film thickness was constant, Equation (97) would reduce to

$$C_3 = C_5 V_L + C_6 \qquad (98)$$

which would indicate that C_3 varied linearly with V_L for a given system.

The form of Nicklin's empirical equation, Equation (96), is identical with that of Equation (92) which would appear to indicate that the film thickness was constant. Closer consideration, however, indicates that this is not the case for substituting the equilibrium film thickness for his system into Equation (91) gives the result

$$V_b = 1.11 V_L + V_b^\circ \qquad (99)$$

This, in addition to the variation of C_4 obtained at low liquid velocities which is clearly not consistent with the

hypothesis of a constant film thickness, confirms the result obtained above - that the film thickness is a function of the liquid velocity. That the variation in film thickness with liquid velocity could lead to the results obtained by Nicklin can be seen by comparing Equations (91) and (96) to obtain for the parameter C_4 the expression

$$C_4 = \frac{1}{(1-\zeta)^2} + \frac{\frac{\rho g R^2}{\mu} \frac{1}{(1-\zeta)^2} \left[\frac{2}{3}\zeta^3(1-\zeta)\right] - V_b^\circ}{V_L} \qquad (100)$$

In Equation (100), the first term on the right-hand side will be rather insensitive to fairly large changes in ζ since $\zeta \ll 1$. The second term on the right will be quite sensitive to changes in ζ since ζ^3 appears in the numerator. At low liquid velocities this second term is significant because of the factor, V_L, in the denominator while at higher liquid velocities it becomes much smaller than the first term and C_4 approaches a nearly constant value. The constant value of C_4 which was obtained by Nicklin must indicate that the film thickness changes approximately as the cube root of the liquid velocity at some intermediate velocities.

The results obtained in Nicklin's investigation and presented in Figure 9 can be used to obtain the change

in film thickness with liquid velocity through Equation (100) and this has been done using the average curve drawn through the results in Figure 9. (This average curve was drawn for this investigation and not by Nicklin.) The variation in film thickness obtained is shown in Figure 10 and indicates that the observed change in C_4 would result from a change in film thickness of about six per cent or about two mils.

To obtain a better idea of the factors causing the change in the relative bubble velocity (relative to the preceding liquid) with increasing liquid velocity, the terms in the force-momentum balance can be evaluated for the approach flow (i.e. section 1, Figure 8) and for the flow in the equilibrium laminar film. For this purpose, the momentum flux of the preceding stream relative to the bubble and the momentum flux in the equilibrium film have been evaluated in Appendix III for plug flow and for laminar flow in the approach flow and for laminar flow in the equilibrium film. The plug flow case can be used as an approximation to the momentum flux in a turbulent approach flow as well. Before considering the force-momentum balance, however, the flow in the film can be analyzed in general terms to make clearer the significance of the calculations.

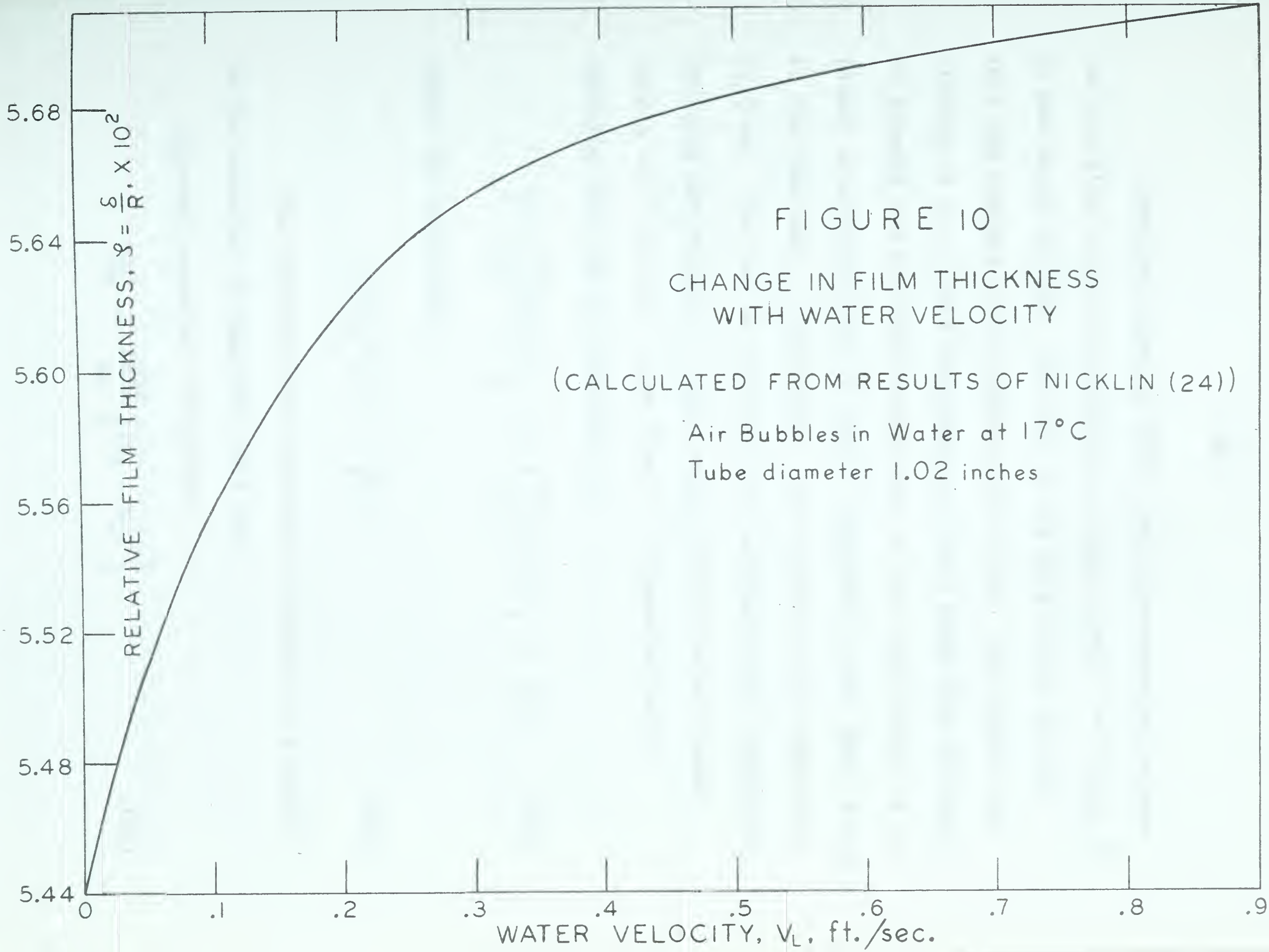

FIGURE 10

CHANGE IN FILM THICKNESS
WITH WATER VELOCITY

(CALCULATED FROM RESULTS OF NICKLIN (24))

Air Bubbles in Water at 17°C

Tube diameter 1.02 inches

Consider Equation (83), the force-momentum balance for the flow in the film between sections 2 and 3 of Figure 8. As was noted earlier, the flow in the film can be divided into two regions on the basis of flow type - one region consisting of the liquid accelerating freely under the influence of gravity and the other consisting of the liquid which is no longer accelerating and is wholly supported by the shear stress at the tube wall. While these two regions are not physically distinct, they can be considered so mathematically; therefore, defining the volume of liquid supported by the wall shear stress as $\mathcal{V}'$ and the volume freely accelerating as $\mathcal{V}''$, Equation (83) can be simplified to

$$2\pi \left(\int_{r_i}^{R} v^2 r \, dr\right)_3 - 2\pi \left(\int_{r_i}^{R} v^2 r \, dr\right)_1 = g\mathcal{V}'' \qquad (101)$$

since, by definition,

$$-2\pi R \int_2^3 \tau_w \, dx = \frac{\rho g}{g_c} \mathcal{V}' \qquad (102)$$

The equations from Appendix III which are required in the solution of Equation (101) are:

Approach momentum - Plug flow

$$\mathring{M}_A = \frac{\pi \rho R^2}{g_c} \left[(V_b - V_L)^2\right] \qquad (103)$$

- Laminar flow

$$\mathring{M}_A = \frac{\pi\rho R^2}{g_c}\left[(V_b - V_L)^2 + \frac{V_L^2}{3}\right] \tag{104}$$

Film momentum (laminar flow)

$$\mathring{M}_F = \frac{\pi\rho R^2}{g_c} V_b^2 \,(2\zeta - \zeta^2)$$

$$+ \frac{\pi\rho^2 g R^4}{\mu g_c} V_b \left(\frac{4}{3}\zeta^3 - \frac{4}{3}\zeta^4 + \frac{1}{5}\zeta^5 + \text{---}\right)$$

$$+ \frac{\pi\rho^3 g^2 R^6}{g_c \mu^2}\left(\frac{4}{15}\zeta^5 - \frac{17}{45}\zeta^6 + \frac{13}{105}\zeta^7 + \text{---}\right) \tag{105}$$

These have been evaluated for the results shown in Figures 9 and 10 and the results are shown in terms of the momentum flux in Table VI. Also given in Table VI is the transition length for development of the equilibrium laminar film which was obtained from Equation (20) for the interface velocity corresponding to an equilibrium laminar film of the thickness being considered. The film momentum and the mass of accelerating liquid (obtained by difference through Equation (101) using the approach momentum) are also shown in Figure 11. In addition, the mass of liquid contained in

TABLE VI

FORCE-MOMENTUM BALANCE RESULTS

Liquid Velocity ft/sec	Bubble Velocity ft/sec	Equilibrium Film Thickness in.	Approach Momentum Flux lb_f	Film Momentum Flux lb_f	Transition Length ft.
.0	0.579	0.0277	0.00368	0.0386	0.810
0.05	0.607	0.0281	0.00405	0.0423	0.855
0.10	0.629	0.0284	0.00439	0.0453	0.894
0.15	0.647	0.0285	0.00470	0.0470	0.907
0.20	0.664	0.02865	0.00498	0.0492	0.927
0.30	0.688	0.0288	0.00524	0.0521	0.946
0.40	0.705	0.02895	0.00550	0.0551	0.965
0.50	0.721	0.0290	0.00574	0.0573	0.970
0.60	0.736	0.0290	0.00600	0.0592	0.970
0.70	0.754	0.02905	0.00628	0.0611	0.978
0.80	0.774	0.0291	0.00662	0.0637	0.985

FIGURE 11

FORCE-MOMENTUM BALANCE

(Nicklins Results see Figures 9 and 10)

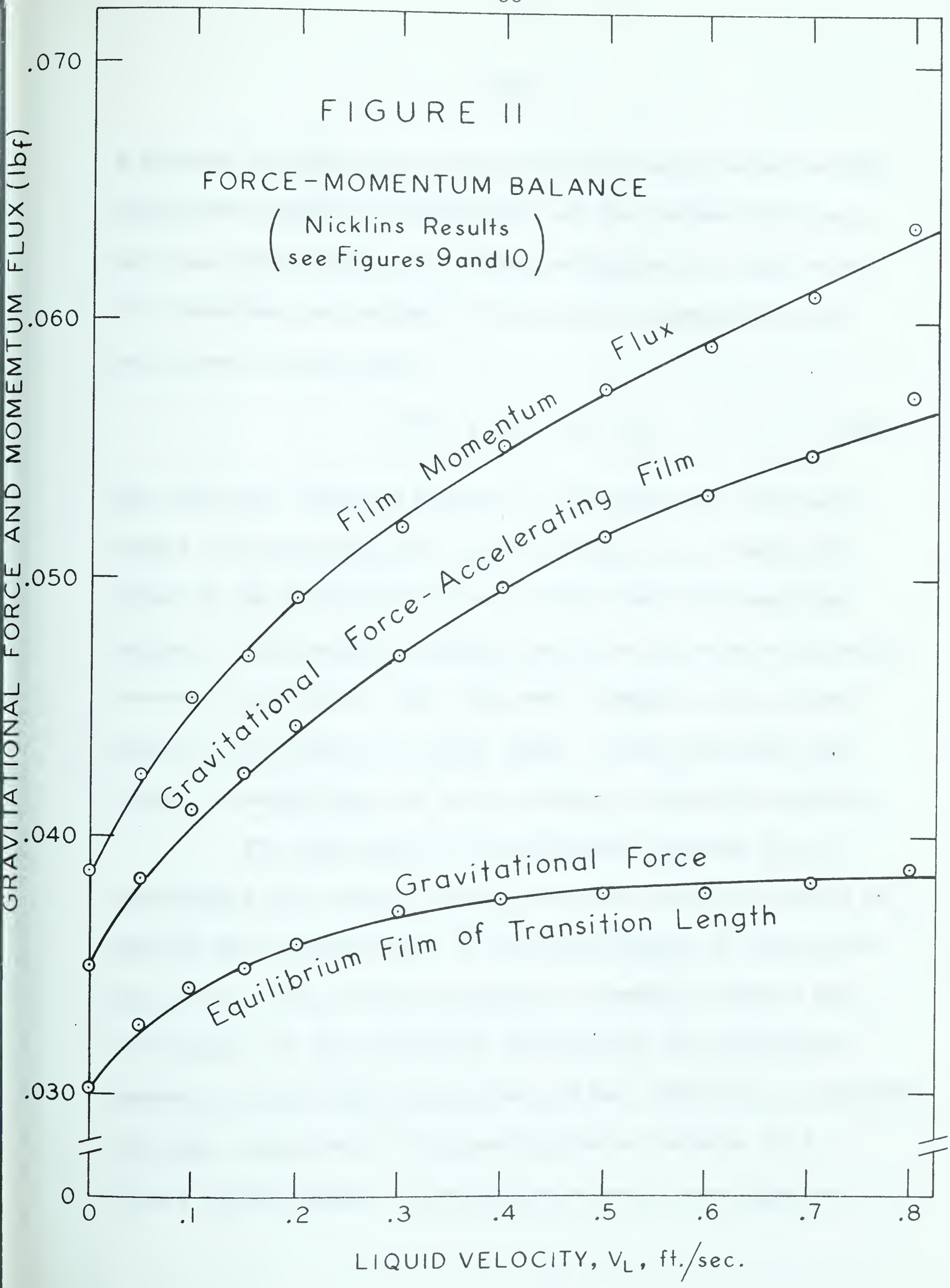

a film of equilibrium thickness and the length equal to the transition length for development of the laminar film, x_e, has been calculated and is shown in Figure 11. This curve is, therefore, an estimate of the liquid supported by the wall shear stress since

$$\mathcal{V}' < \pi (R^2 - r_i^2) x_e \qquad (106)$$

The relations shown in Figure 11 illustrate that the major effect of increasing the liquid velocity is to change the shape of the bubble in the nose region and the transition region. The change in approach momentum is relatively small; however, it is likely that this small change is the primary cause of the change in bubble shape. This would have the effect of magnifying the small change in approach momentum.

The importance of the approach momentum flux in determining the bubble velocity has been noted previously by Moissis and Griffith (23) in an investigation of developing slug flow. This study was directed primarily towards the development of the principles determining the macroscopic geometry of gas-liquid slug flow and was, therefore, concerned with the coalescence of succeeding Taylor bubbles in a moving liquid stream. The results of this investigation

indicated that there was a marked correspondence between the decay of momentum in the wake of a bubble and the velocity of a trailing bubble, the bubble velocity being higher in regions closer to the preceding bubble where the flux of momentum was higher. While Moissis and Griffith were not able to predict the quantitative effect of the approach momentum flux on the bubble velocity, their measurements indicated that the flux of momentum decayed to the value corresponding to the fully-developed stream within six tube diameters of the rear of the bubble which is in agreement with the results of other investigations of the minimum stable slug length (24).

Because of the complexity of the flow around a Taylor bubble and the present lack of knowledge about the factors determining the shape of the bubble in the nose region, it does not appear likely that a general solution for the problem of Taylor bubble movement can be obtained. Accordingly, an empirical correlation for the bubble behavior will be sought on the basis of the physical model of a bubble having a cylindrical portion at the rear with the flow in the annular film between the bubble wall and the tube wall being laminar.

On this basis, then, the only relation available which describes the bubble motion is Equation (91) which relates the bubble velocity to the liquid velocity and the thickness of the equilibrium film. If Equation (91) is divided by Equation (57), the following relation is obtained.

$$\frac{V_b}{V_b^\circ} = \frac{1}{(1-\zeta)^2}\frac{V_L}{V_b^\circ} + f(\zeta,\zeta_o) \qquad (107)$$

Equation (107) indicates that the relation between the parameters V_b/V_b° and $\frac{V_L/V_b^\circ}{(1-\zeta)^2}$ should be independent of the system properties if the model chosen to describe the bubble is correct.

Figure 12 shows the relation between these parameters for the results of Nicklin and of Griffith and Wallis. In addition, some bubble velocities obtained at the University of Alberta for air bubbles in an oil of 19.0 centipoise viscosity and a tube of 1.038-inch diameter are shown. These latter results were obtained for two-phase flow while the other results were from single bubble measurements. The results for the oil fall about ten per cent high on the average; however, the agreement was considered sufficiently good to warrant further consideration of Equation (107).

FIGURE 12

BUBBLE VELOCITIES IN MOVING LIQUID STREAMS

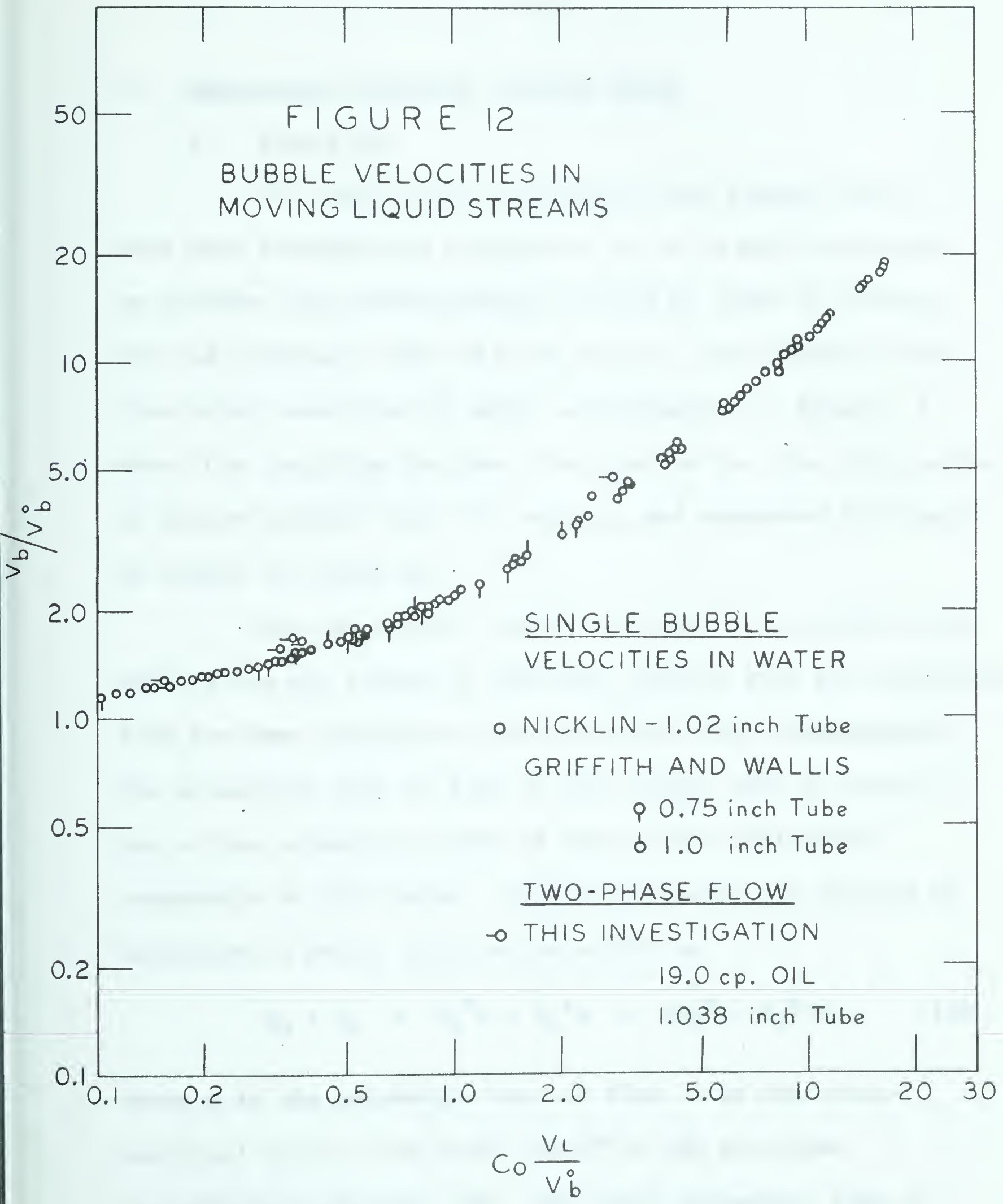

3. Macroscopic Balances - Moving Media

b. Slug Flow

The macroscopic balances for the single bubble case have already been considered, so it is only necessary to consider the modifications required in these to account for the continuous flow of both phases. The physical situation being considered is shown schematically in Figure 13 where the slug flow has been idealized to the rise of a series of Taylor bubbles, each of length ℓ_b and separated by 'slugs' of liquid of length ℓ_s.

For the moment, the steady state case in which the bubbles are all rising at the same velocity will be considered. With the same assumption that the fluids are incompressible, the volumetric rate of flow at any section must be equal to sum of the volumetric rates of flow of the individual components to the system. If the components are denoted by subscripts G and L, this can be stated as

$$Q_G + Q_L = V_G^* A + V_L^* A = (V_G^* + V_L^*) A \qquad (108)$$

where Q is the volumetric rate of flow, A is the cross-sectional area of the tube, and V^* is the so-called 'superficial velocity' (9). The total volumetric rate of

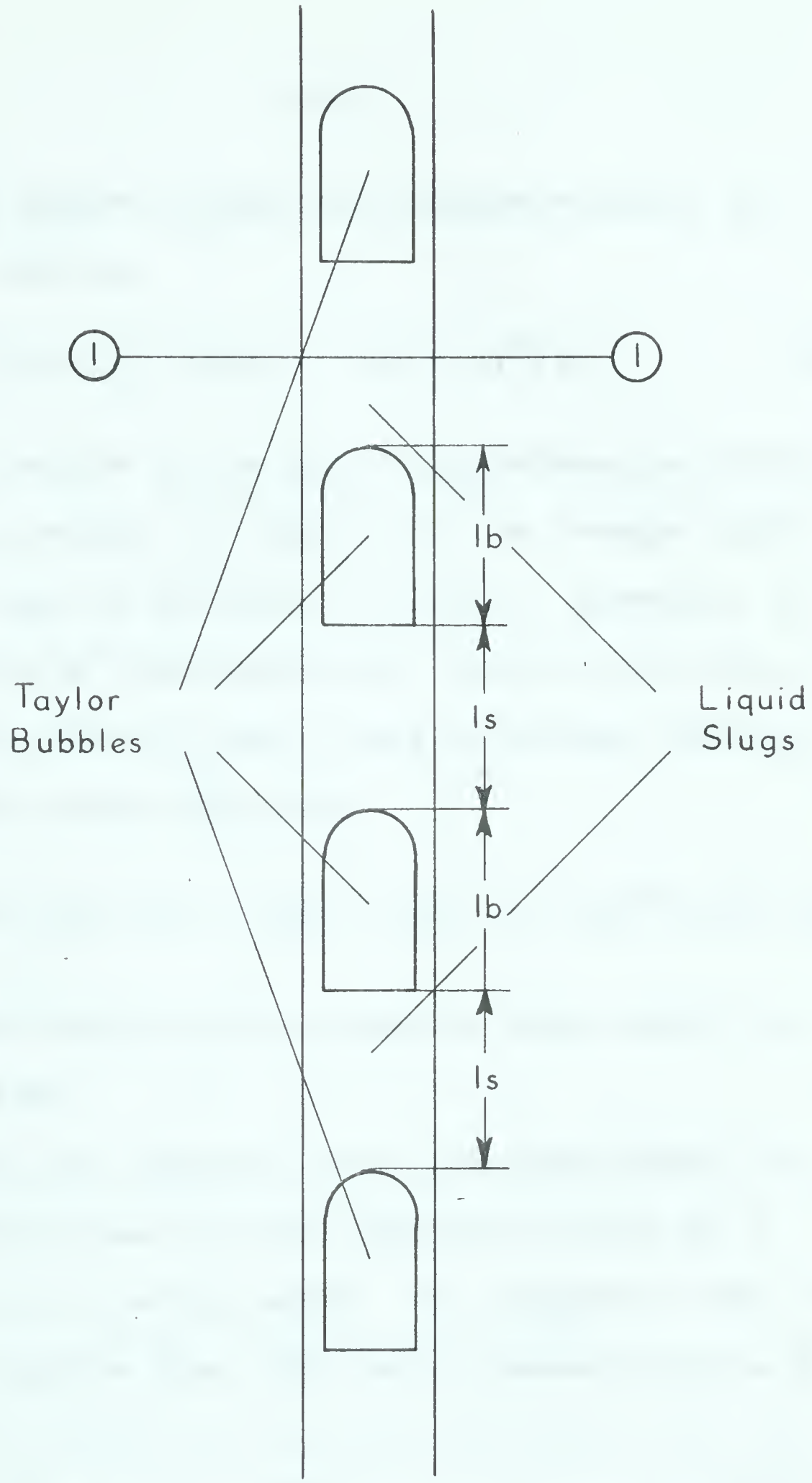

FIGURE 13

SCHEMATIC REPRESENTATION OF SLUG FLOW

flow is often stated in terms of a mixture velocity, V_M, through the relations

$$Q_G + Q_L = V_M A = (V_G^* + V_L^*) A \qquad (109)$$

Considering the flow in the liquid slug between two bubbles (for example, section 1 in Figure 13), the average liquid velocity is equal to the mixture velocity. Therefore, for the application of the single bubble results to the slug flow case, 'liquid velocity' must be read as 'mixture velocity'. Equation (66) becomes, therefore

$$2\int_{r_i}^{R} (V + V_b)\, r\, dr = V_M R^2 - V_b r_i^2 = V_F(R^2 - r_i^2) \qquad (110)$$

and gives the material balance around a single bubble in steady slug flow.

The force balances for an individual bubble in slug flow are the same as those previously listed for a single bubble in a moving medium. For a length of tube, H, containing n bubbles then, the overall pressure drop is given by

$$\Delta P = n\left[\Delta P_R + \left(\frac{2}{R}\tau_w - \frac{\rho g}{g_c}\right)\left[(x_4 - x_3) + (x_2 - x_1)\right]\right] \qquad (111)$$

from Equation (88) or

$$\Delta P = n\left[\frac{2}{R}\int_2^3 \tau_w dx - \frac{\rho g}{g_c R^2}\int_2^3 (R^2 - r_i^2)\, dx \right.$$

$$\left. + \left(\frac{2}{R}\tau_w - \frac{\rho g}{g_c}\right)\left[(x_4 - x_3) + (x_2 - x_1) \right] \right] \qquad (112)$$

from Equation (89). If the bubbles have an average volume of v_b, Equation (112) can be written as

$$\Delta P = n\left[\frac{2}{R}\int_2^3 \tau_w dx + \frac{2}{R}\tau_w \left[(x_4 - x_3) + (x_2 - x_1) \right] \right]$$

$$+ \frac{\rho g}{R^2 g_c}\left(R^2 H - \frac{n}{\pi} v_b \right) \qquad (113)$$

where the volume of liquid in the tube length being considered has been written as

$$v_L = \pi R^2 H - n v_b \qquad (114)$$

Then the amount of bubble fluid or gas contained in the tube must be

$$n v_b = \frac{H}{V_b} Q_G = \frac{H A V_G^*}{V_b} \qquad (115)$$

since a single bubble will traverse the length in time $\frac{H}{V_b}$. The volume fraction of gas in the tube is, then

$$x_G = \frac{n v_b}{HA} = \frac{V_G^*}{V_b} \qquad (116)$$

and the average density of the mixture in the tube is

$$\rho_a = (1 - \frac{V_G^*}{V_b})\rho + \frac{V_G^*}{V_b}\rho' \qquad (117)$$

where ρ' denotes the density of the gas.

Since the gas density is considered negligible,

$$\rho_a = (1 - \frac{V_G^*}{V_b})\rho \qquad (118)$$

Substituting into Equation (113)

$$\Delta P = n\left[\frac{2}{R}\int_2^3 \tau_w dx - \frac{2\ell s}{R}\tau_w\right] + \rho_a \frac{g}{g_c} H \qquad (119)$$

The evaluation of the friction or wall shear terms must be approximated from consideration of the bubble geometry since it is not possible to predict them more rigorously. The effect of the presence of the bubble on the wall shear in the approach and wake regions has already been neglected and the wall shear approximated by the corresponding single-phase wall shear. If the relative thickness of the equilibrium film for the flow being considered is $\zeta = \frac{\delta}{R}$, the liquid being supported by wall shear can be approximated as

$$n\mathcal{V}' = \frac{V_G^*}{V_b} \frac{\pi H R^2}{(1-\zeta)^2} (2\zeta - \zeta^2) \qquad (120)$$

and the length fraction in 'single-phase shear' can be approximated as

$$\frac{n\ell_s}{H} = 1 - \frac{V_G^*}{V_b} \frac{1}{(1 - \zeta)^2} \tag{121}$$

The model of the flow corresponding to these equations is shown in Figure 14, and it is seen that the average pressure gradient is approximated by

$$\frac{\Delta P}{H} = \left(-\frac{2}{R} \tau_w + \frac{g}{g_c} \rho \right) \left(1 - \frac{V_G^*}{V_b} \frac{1}{(1 - \zeta)^2} \right) \tag{122}$$

Therefore the pressure drop in two-phase, gas-liquid slug flow can be estimated if the bubble velocity and equilibrium film thickness for the flow are predictable.

4. Bubble Motion in Slug Flow

In the preceding sections, a model was developed for the flow around a large gas bubble rising through stagnant liquid in a tube which accounts for the viscous flow in the film around the tail of the bubble as well as the inertial flow at the nose. It was also shown that the model applies in part to the movement of a large bubble in a moving stream of liquid in a tube. For this case it is not possible to

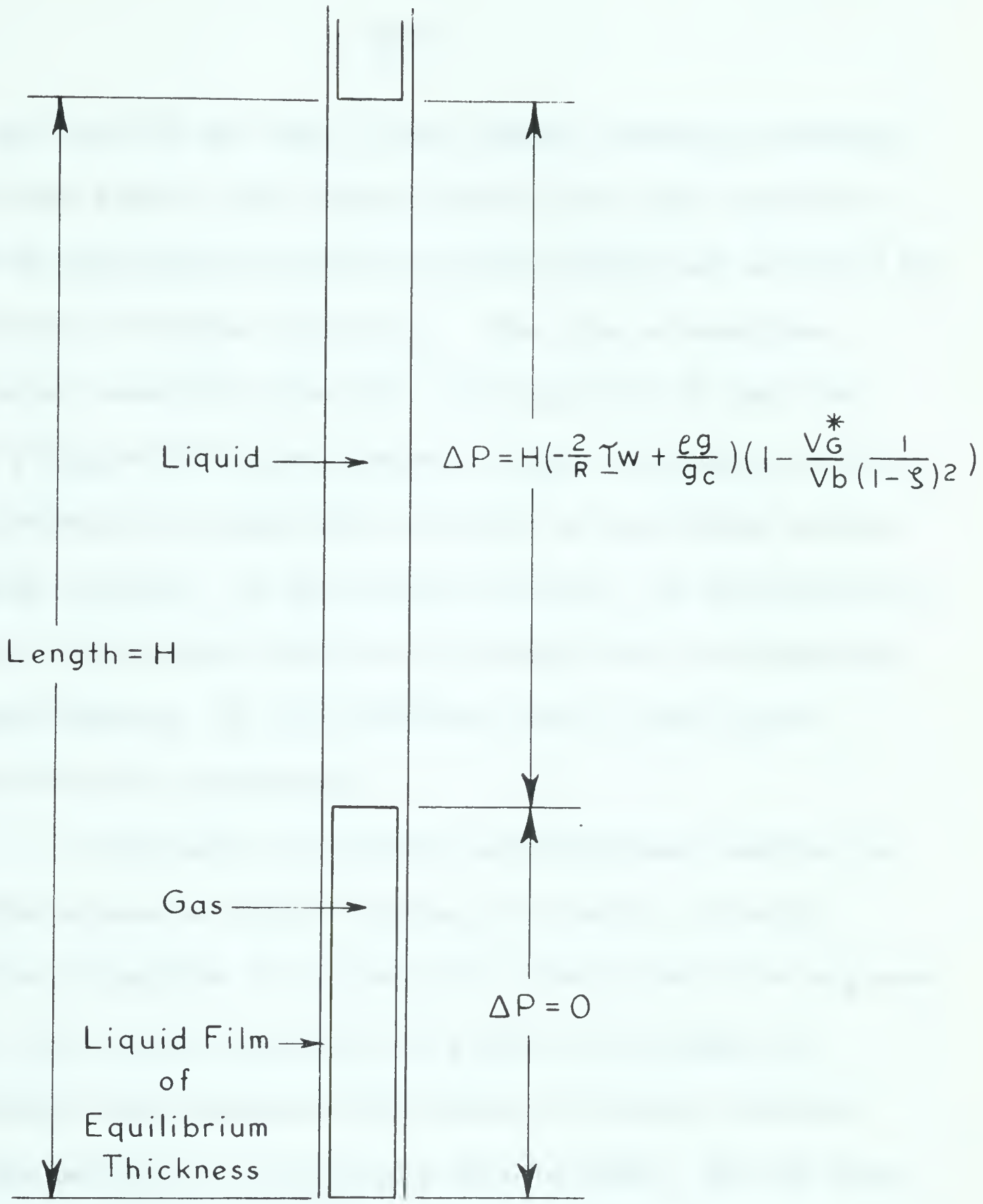

FIGURE 14

MODEL FOR PRESSURE DROP CALCULATIONS

solve the flow at the nose of the bubble; however, consideration of the flow in the viscous film at the rear resulted in a form of the material balance equation which was suitable for correlation of bubble velocities. The form of empirical correlation developed from this consideration of the flow around a single bubble was shown to apply reasonably well for the correlation of measured velocities of individual bubbles in moving liquids. In the present section, the applicability of these conclusions, which were obtained from consideration of single bubbles, to the cocurrent flow of gas-liquid mixtures will be considered.

If the model is correct and individual bubbles in slug flow behave as Taylor bubbles, the bubble velocity should be a function of the mixture velocity only for a given system. Due to the inability to predict the change of equilibrium film thickness with mixture velocity, however, empirical methods of correlation must be used. On the basis of the previous consideration of single bubbles in moving streams of liquid, the velocities of bubbles in different systems should be correlated by the parameters V_b/V_b° and $\frac{V_M/V_b^\circ}{(1-\zeta)^2}$ of Equation (107) (the mixture velocity being

substituted for the liquid velocity for slug flow). If the model for slug flow is correct, the velocities should be predictable from the correlation of velocities of single bubbles shown in Figure 12.

As was shown earlier in the consideration of the macroscopic balances in slug flow, the main interest in the bubble velocity in slug flow stems from its usefulness in predicting the voidage or gas content in the tube which is closely related to the static and frictional pressure drops (i.e. Equations (118) and (119)). For this reason as well as the lack of experimental bubble velocities in slug flow (the limited results of Nicklin (24) being the only ones available), a more realistic comparison should be obtained if bubble velocities calculated from experimental voidage measurements are used. Reference will be made, therefore, to the results of Govier and coworkers (9, 10, 4) at the University of Alberta for the cocurrent flow of air-water mixtures in smooth, vertical tubes of diameters 0.630, 1.025, 1.50 and 2.50 inches and to the results of Hughmark (17) at Louisiana State University for the cocurrent flow of air and a variety of liquids in commercial steel pipe (diameter = 1.049 inches).

In both of these sets of investigations, the liquid content in the tube was obtained by trapping the flowing mixture with full-flow valves installed at the ends of the conduits. The test section for liquid content in each case, then, consisted of the entire conduit from just above the mixing section to the discharge. In Hughmark's tests, this was also the test section for pressure drop, the pressure being measured at both ends of the pipe. In the case of the University of Alberta tests, a calming section was provided before the test section for pressure drop and the mid-point pressure of this test section (i.e. the test section for pressure measurement) was controlled at predetermined values. It would not be expected that the lack of a calming section for the measurement of the liquid content would cause any great errors as, in each case, the test section was quite long. That the effect of the entrance section could be significant for shorter conduits, however, has been shown by Moissis and Griffith (23) whose results indicated that the liquid content in the region of developing slug flow can be considerably higher than in a developed flow for the same flow rates.

The bubble velocity in slug flow can be obtained from Equation (116) as

$$V_b = \frac{V_G^*}{x_G} \tag{123}$$

This equation applies rigorously to the movement of any heterogeneous mixture provided that the average velocity of one of the phases in the conduit (i.e. phase G) is constant, as can be seen from the derivation of Equation (116). Its application in the case of gas-liquid flow assumes that the effect of expansion is negligible if it is to be applied over a considerable length of conduit. In the results of Govier and of Hughmark being considered here, the average gas content for the entire conduit was obtained and the superficial gas velocities corresponding to the mid-point pressure for Govier's results and the average pressure for Hughmark's results will be used.

To obtain the two parameters required for the correlation, it is also necessary to have the bubble velocity in stagnant liquid and the equilibrium film thickness for the mixture velocity being considered. For the bubble velocity, Equation (68), which was developed earlier, can be used. The equilibrium film thickness, however, can be obtained only from a trial and error solution of Equation (91) for the test conditions. Fortunately, however, the film

thickness is so small that the change in the factor $(1 - \xi)^2$ with liquid velocity is slight, enabling the use of the equilibrium film thickness for a bubble rising in stagnant liquid. With this modification, the correlating factors are:

$$\frac{V_b}{V_b^\circ} \quad ; \quad C_o \frac{V_M}{V_b^\circ} \tag{124}$$

The symbol C_o in Equation (124) represents the factor $\frac{1}{(1 - \xi)^2}$ for the stagnant liquid case as in Equation (92). Table VII contains the values of C_o as well as the values of bubble velocity and equilibrium film thickness for stagnant liquid in the systems investigated by Govier and by Hughmark.

In calculating the second parameter of Equation (124), the mixture velocities corresponding to the mid-point pressure and average pressure were used for the results of Govier and of Hughmark, respectively. This, while consistent with the use of an 'average' superficial velocity for the gas, is an approximation to the actual case.

The parameters of Equation (124) for the results of Govier are shown in Figures 15 through 18 while those for the results of Hughmark are shown in Figures 19 through 24.

TABLE VII

SYSTEM CHARACTERISTICS - AIR-LIQUID FLOW TESTS

Liquid	Tube Diameter inches	Kinematic Viscosity $ft^2/sec \times 10^5$	Bubble Velocity V_b° ft/sec	Equilibrium Film Thickness inches	C_o
Water[a]	0.630	1.055	0.441	0.0210	1.15
	1.025		0.566	0.0269	1.12
	1.50		0.689	0.0327	1.09
	2.50		0.892	0.0424	1.07
Water[b]	1.049	1.05	0.575	0.0272	1.11
Varsol[b]		1.484	0.571	0.0304	1.13
Trichlor-ethylene[b]		0.416	0.577	0.0201	1.08
Oil Blend No. 1[b]		7.61	0.560	0.0513	1.23
Oil Blend No. 2[b]		35.43	0.541	0.0828	1.41
Sodium Carbonate Solution[b]		2.865	0.567	0.0375	1.16

a University of Alberta results (9, 10, 3).

b Results of Hughmark (17).

FIGURE 15

CORRELATION OF IN SITU GAS CONTENT
(SEE EQUATION (116))

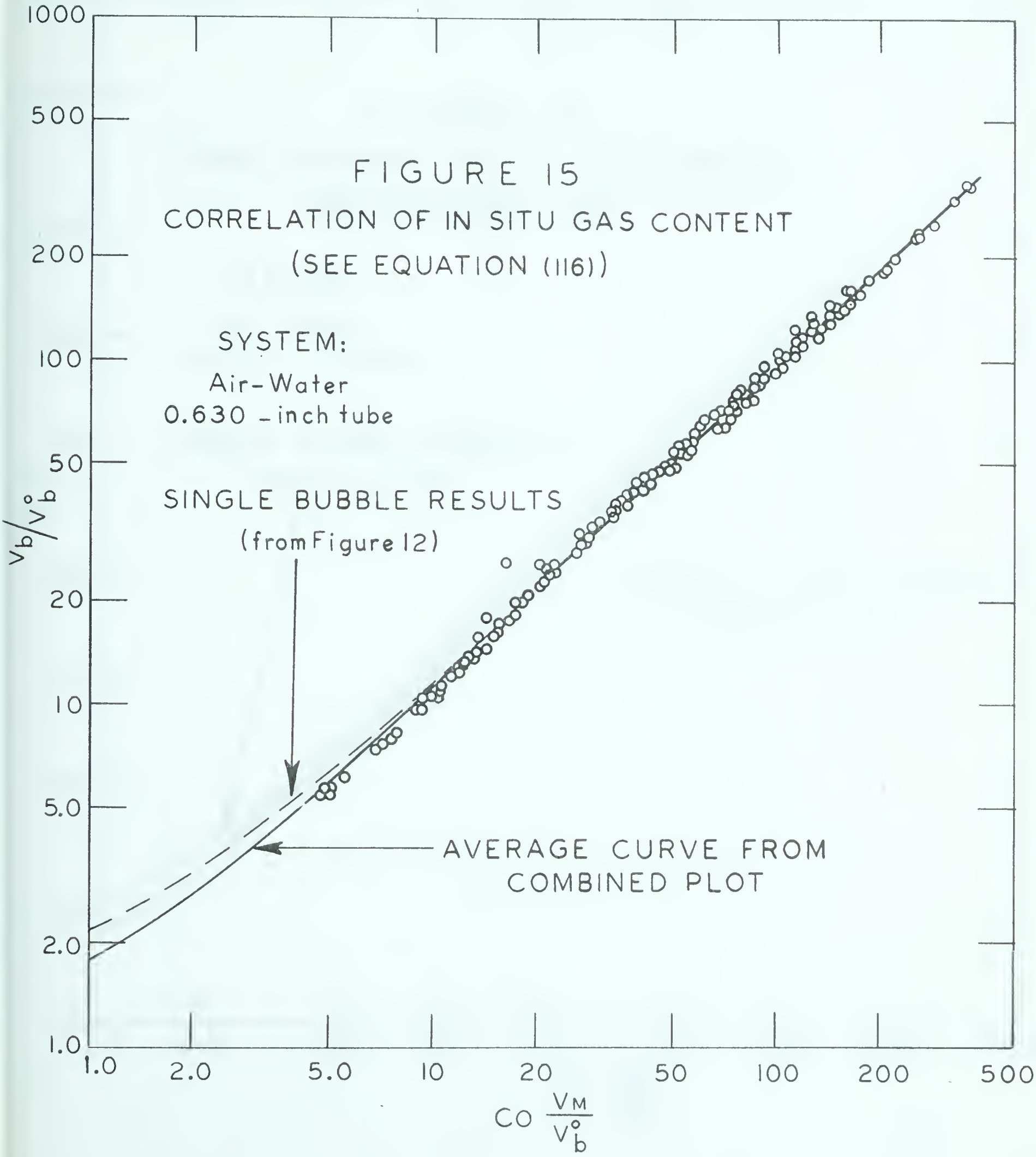

FIGURE 16

CORRELATION OF IN SITU GAS CONTENT

(SEE EQUATION (116))

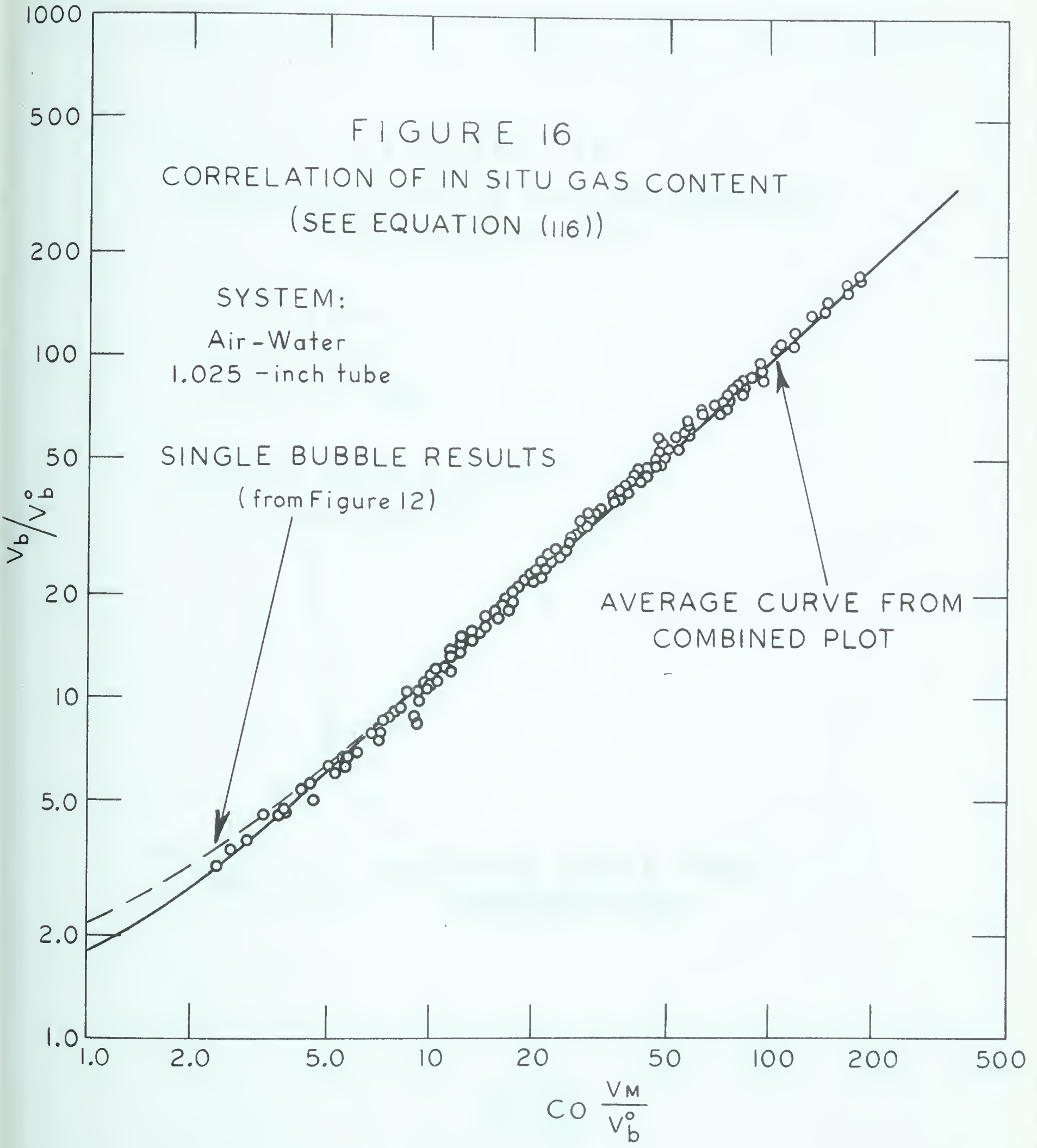

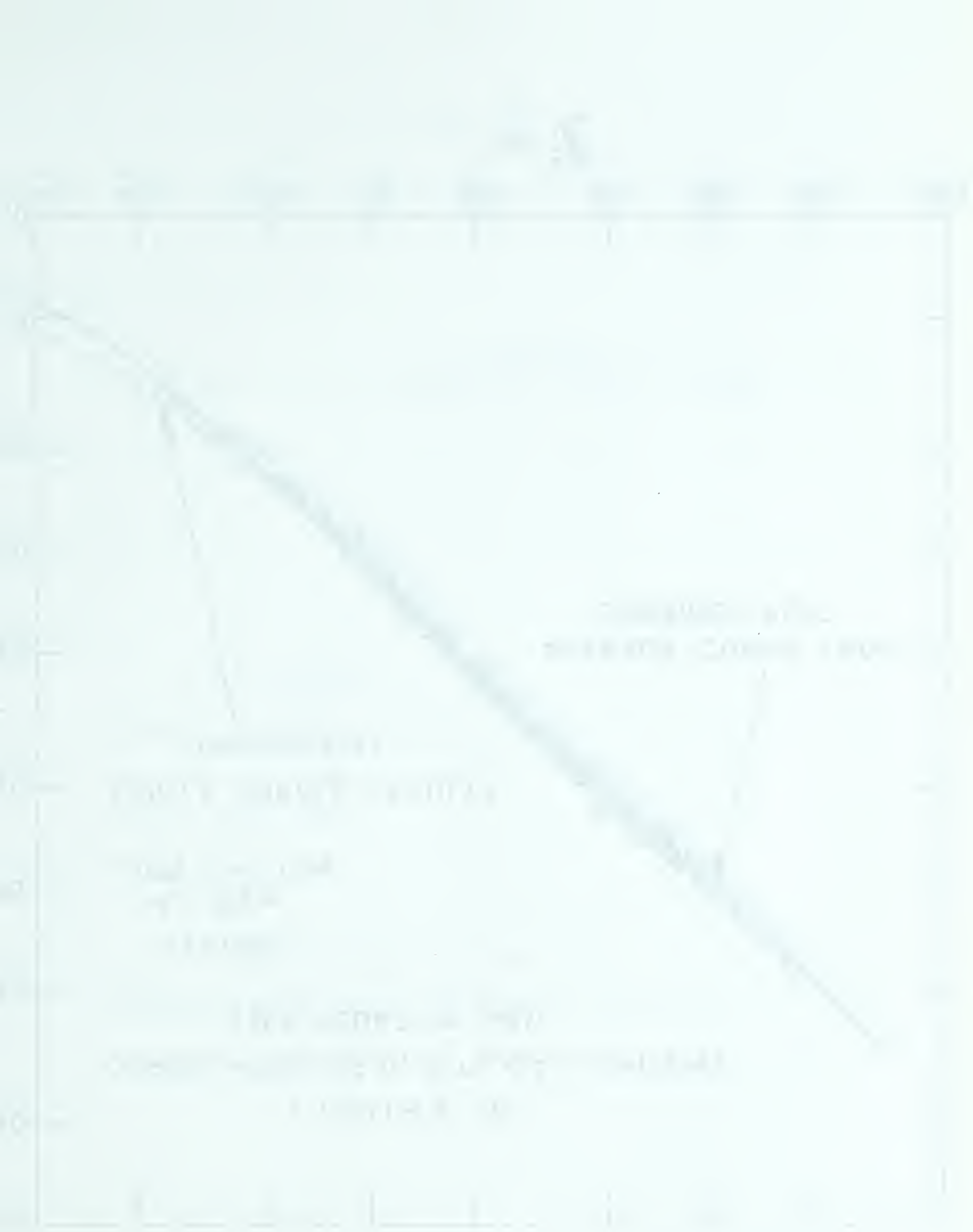

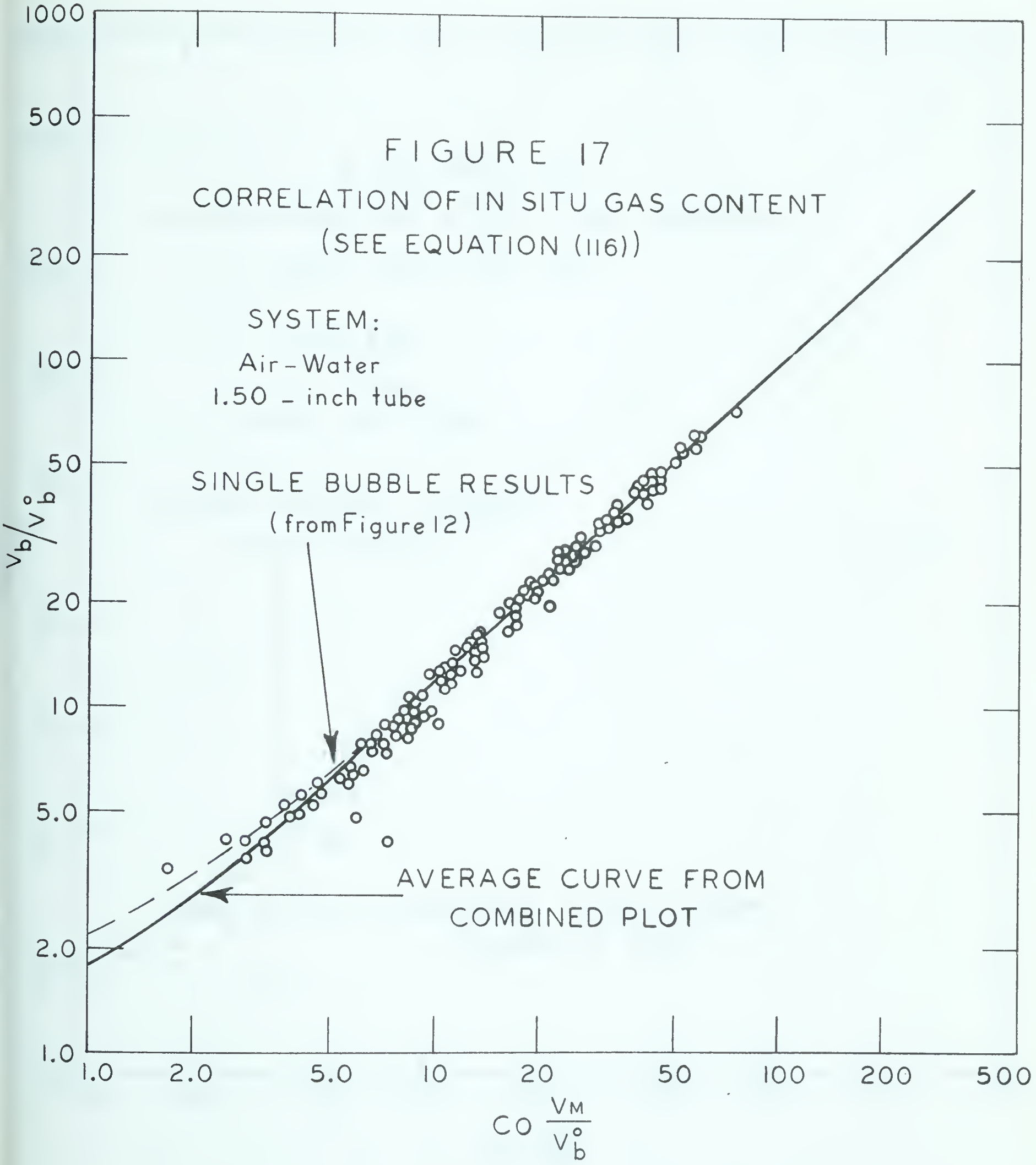
FIGURE 17
CORRELATION OF IN SITU GAS CONTENT
(SEE EQUATION (116))
SYSTEM:
Air-Water
1.50 - inch tube
SINGLE BUBBLE RESULTS
(from Figure 12)
AVERAGE CURVE FROM
COMBINED PLOT
V_b/V_b°
$C_O \frac{V_M}{V_b^\circ}$
1000
500
200
100
50
20
10
5.0
2.0
1.0
1.0
2.0
5.0
10
20
50
100
200
500

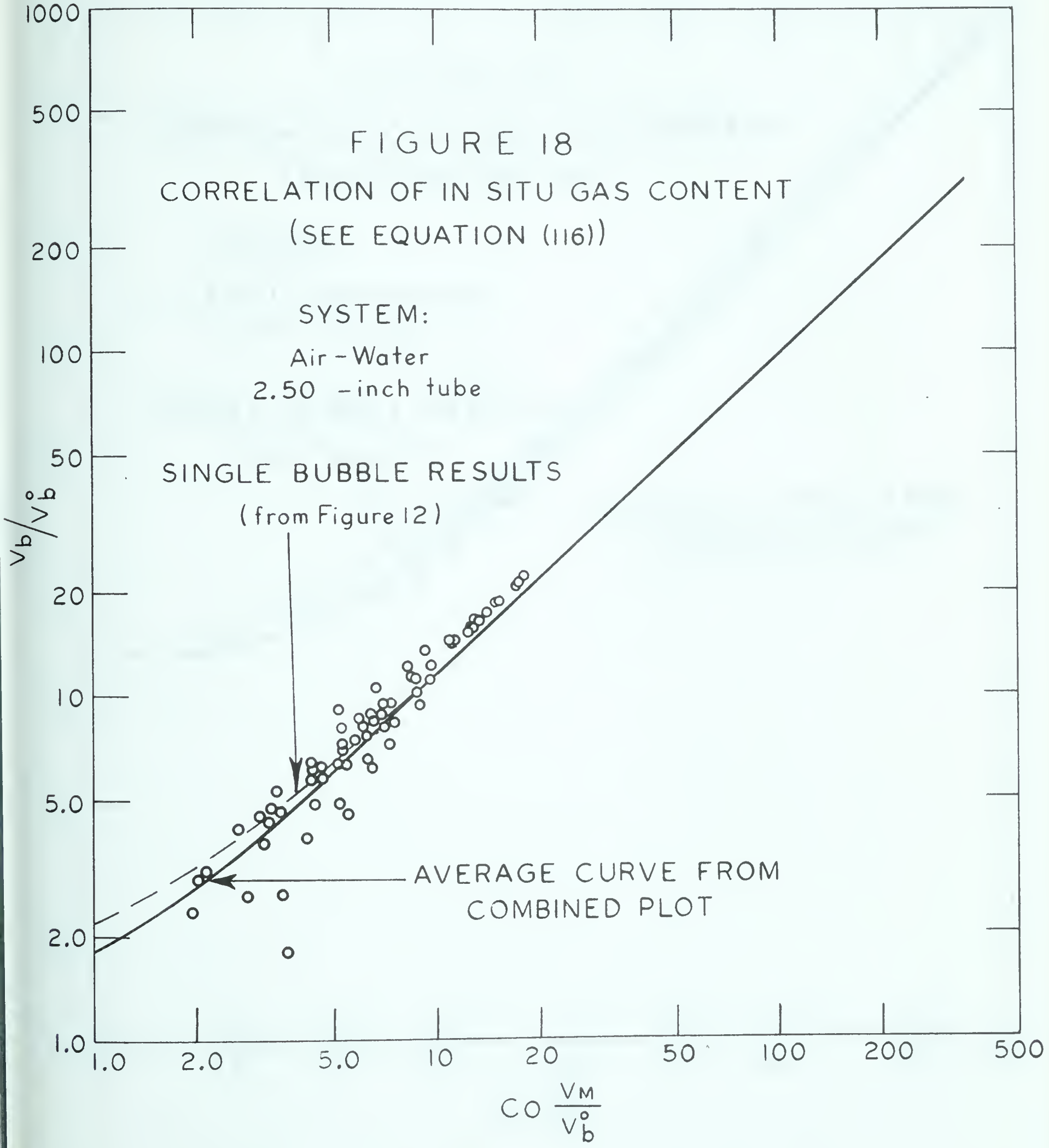
FIGURE 18
CORRELATION OF IN SITU GAS CONTENT
(SEE EQUATION (116))
SYSTEM:
Air - Water
2.50 - inch tube
SINGLE BUBBLE RESULTS
(from Figure 12)
AVERAGE CURVE FROM
COMBINED PLOT
V_b/V_b^o
$C_o \frac{V_M}{V_b^o}$
1000
500
200
100
50
20
10
5.0
2.0
1.0
1.0
2.0
5.0
10
20
50
100
200
500

FIGURE 19

CORRELATION OF IN SITU GAS CONTENT
(SEE EQUATION (116))

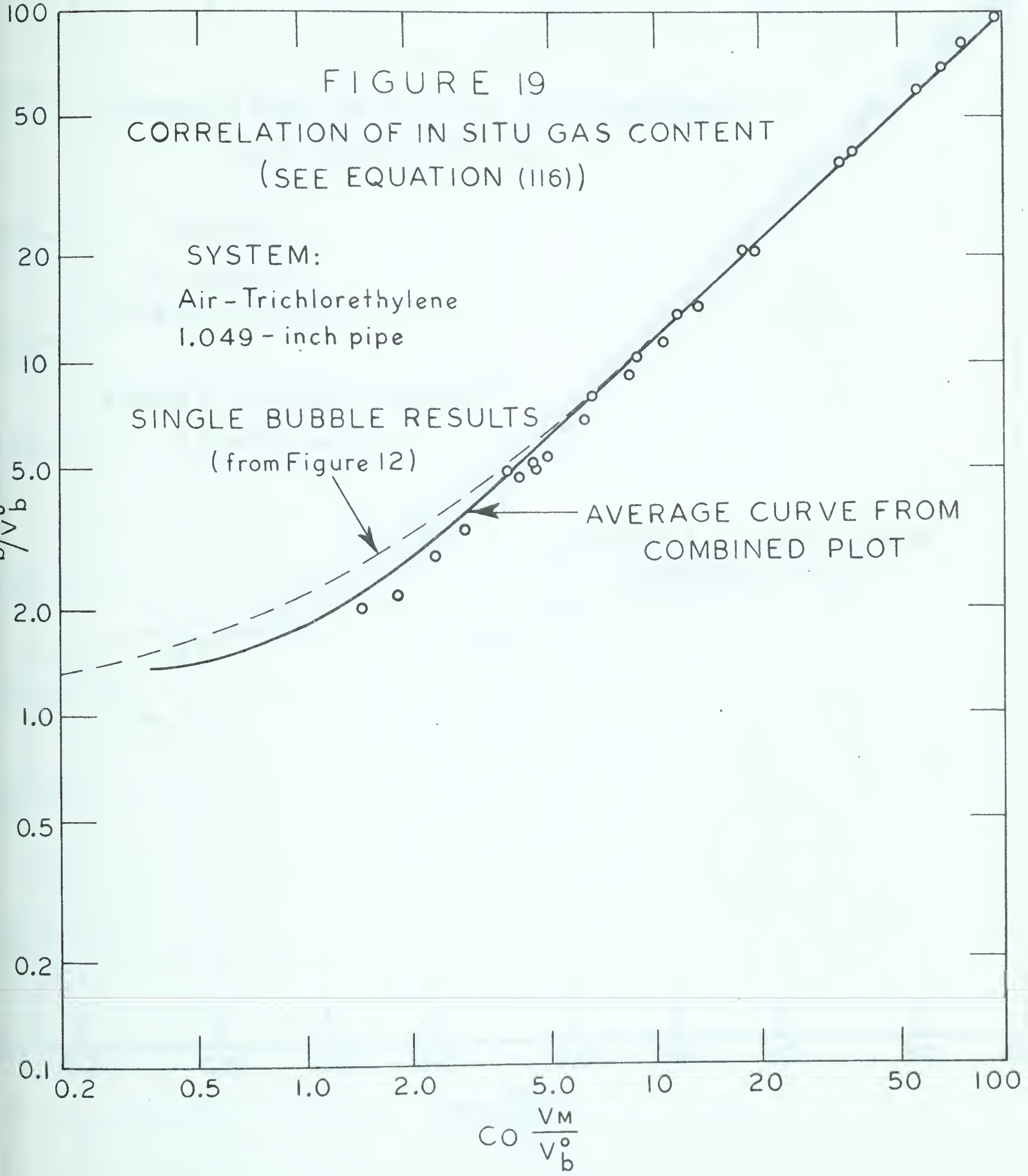

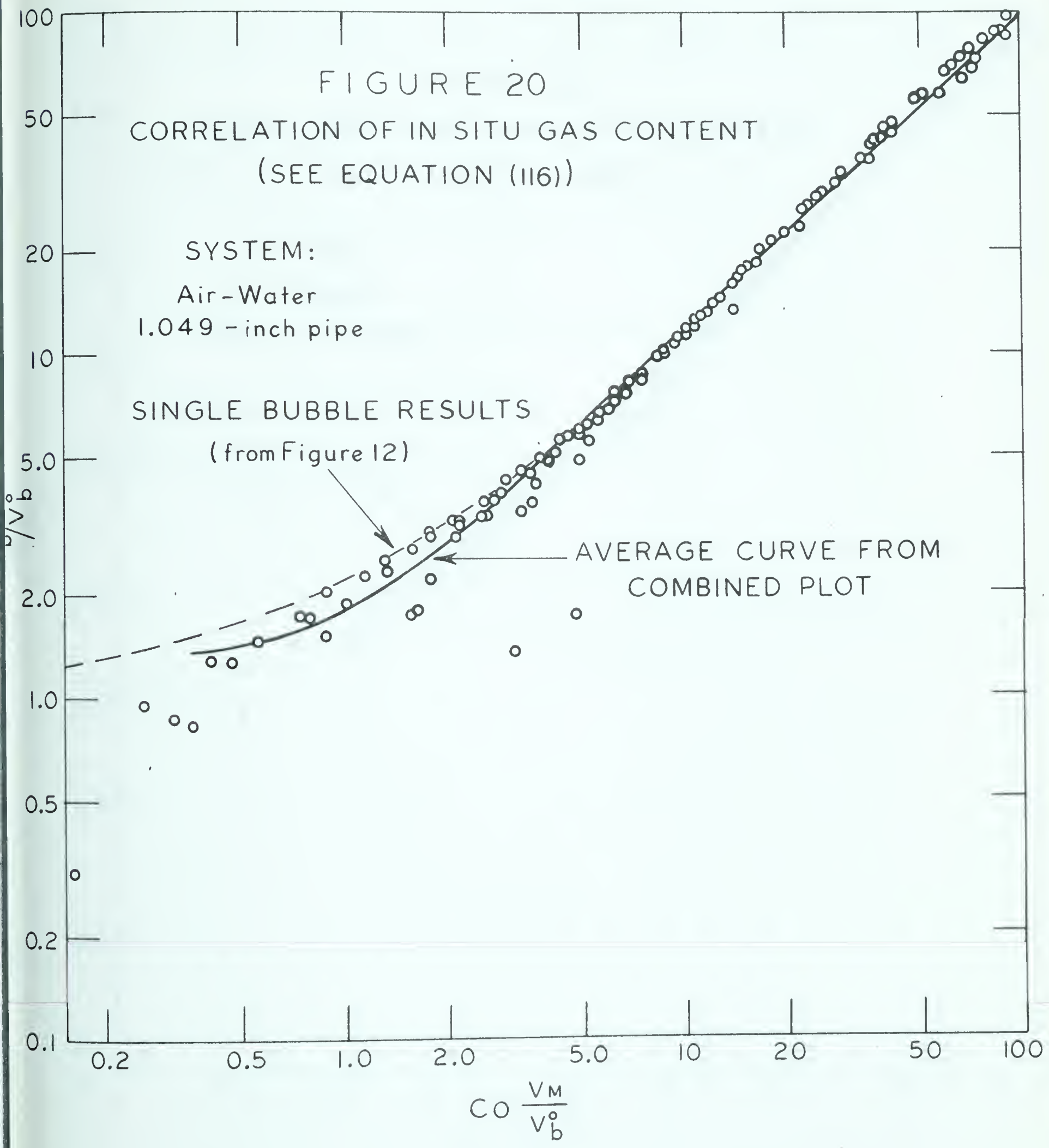
FIGURE 20
CORRELATION OF IN SITU GAS CONTENT
(SEE EQUATION (116))
SYSTEM:
Air-Water
1.049 - inch pipe
SINGLE BUBBLE RESULTS
(from Figure 12)
AVERAGE CURVE FROM
COMBINED PLOT
100
50
20
10
5.0
2.0
1.0
0.5
0.2
0.1
0.2
0.5
1.0
2.0
5.0
10
20
50
100
$C_o \frac{V_M}{V_b^o}$
$\frac{V_M}{V_b^o}$

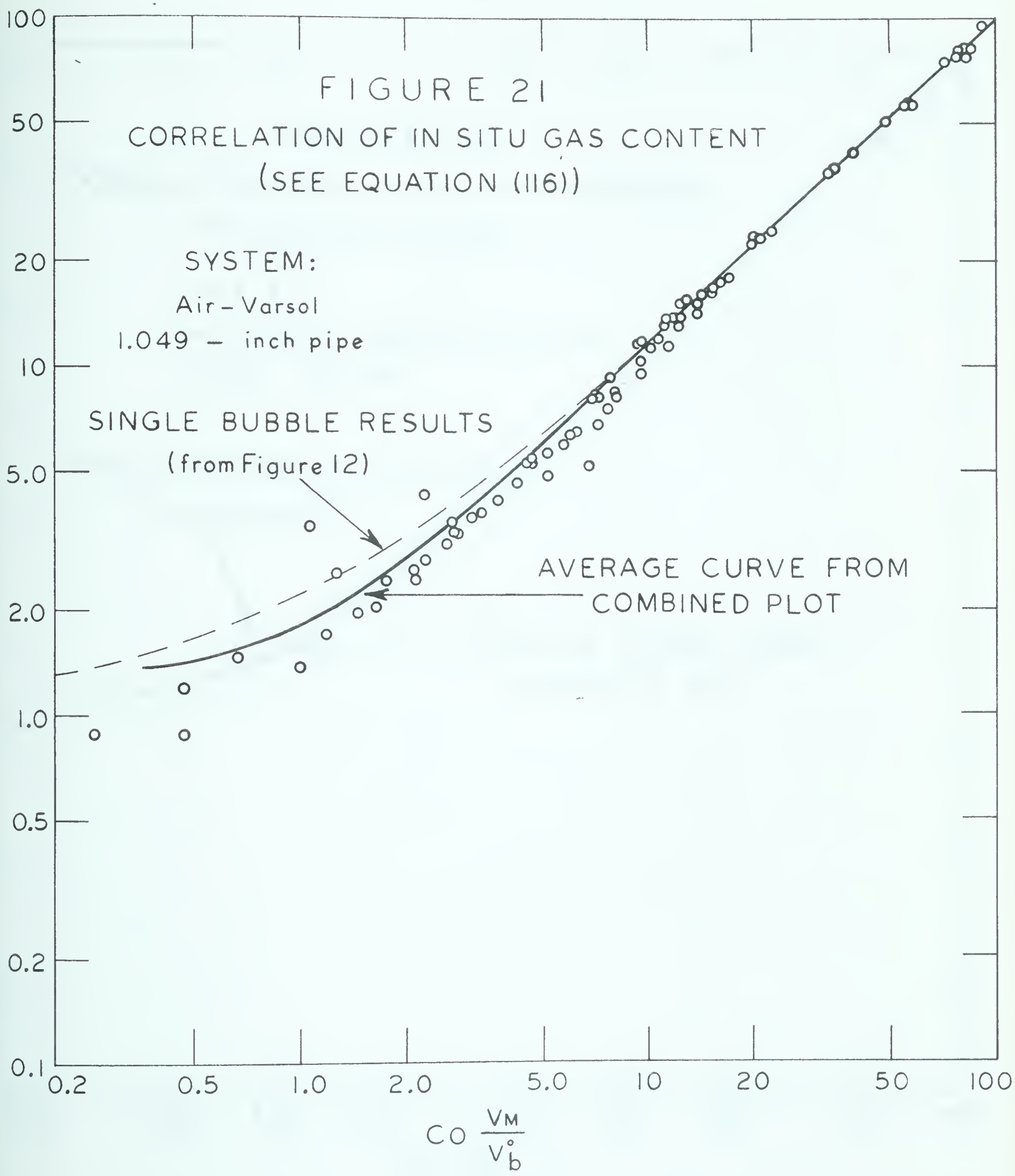
FIGURE 21
CORRELATION OF IN SITU GAS CONTENT
(SEE EQUATION (116))
SYSTEM:
Air – Varsol
1.049 – inch pipe
SINGLE BUBBLE RESULTS
(from Figure 12)
AVERAGE CURVE FROM
COMBINED PLOT
100
50
20
10
5.0
2.0
1.0
0.5
0.2
0.1
0.2
0.5
1.0
2.0
5.0
10
20
50
100
V_b/V_b°
$C_O \frac{V_M}{V_b^\circ}$

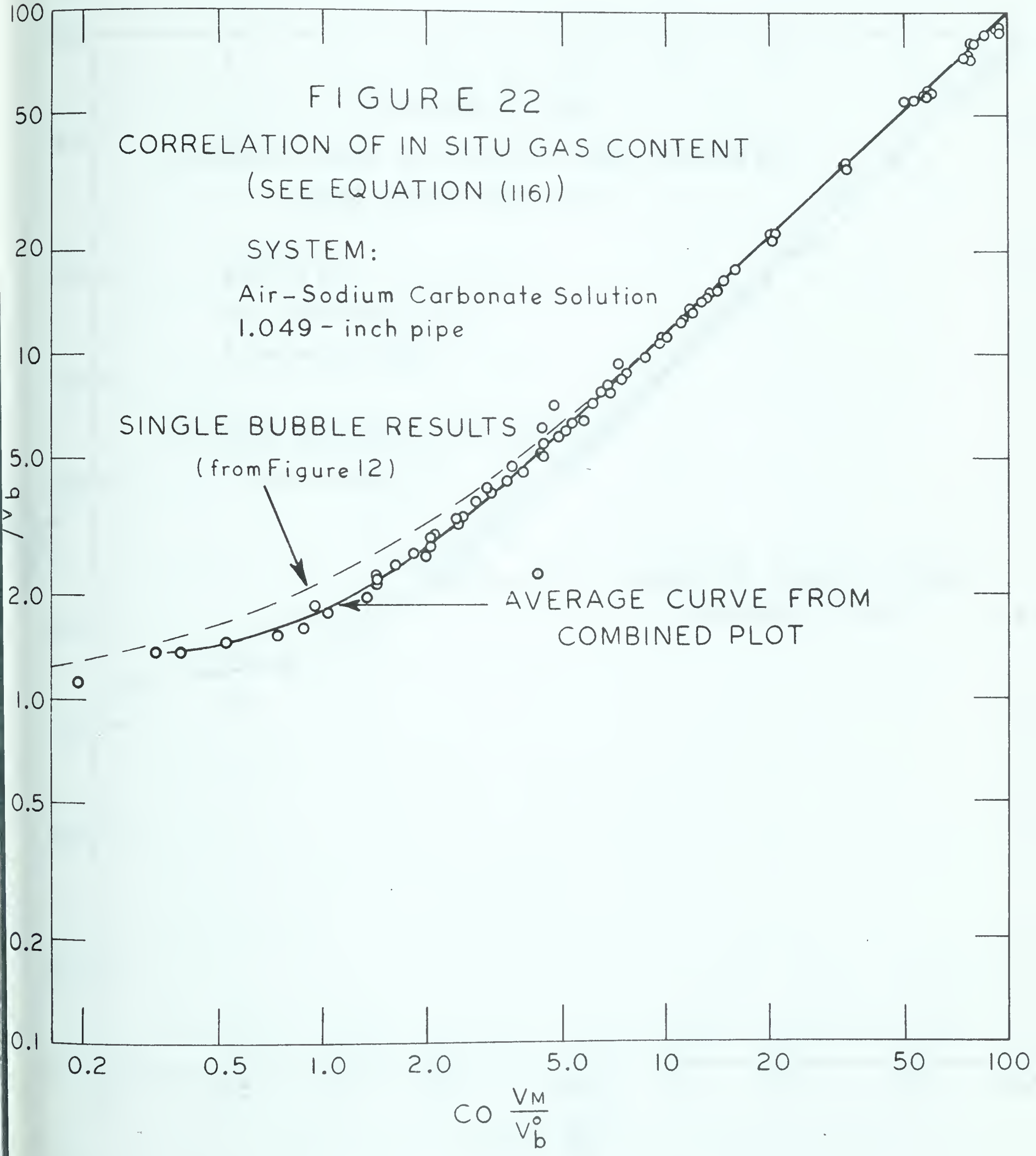
FIGURE 22
CORRELATION OF IN SITU GAS CONTENT
(SEE EQUATION (116))
SYSTEM:
Air–Sodium Carbonate Solution
1.049 – inch pipe
SINGLE BUBBLE RESULTS
(from Figure 12)
AVERAGE CURVE FROM
COMBINED PLOT
100
50
20
10
5.0
2.0
1.0
0.5
0.2
0.1
0.2
0.5
1.0
2.0
5.0
10
20
50
100
$C_O \frac{V_M}{V_b^o}$

FIGURE 23

CORRELATION OF IN SITU GAS CONTENT

(SEE EQUATION (116))

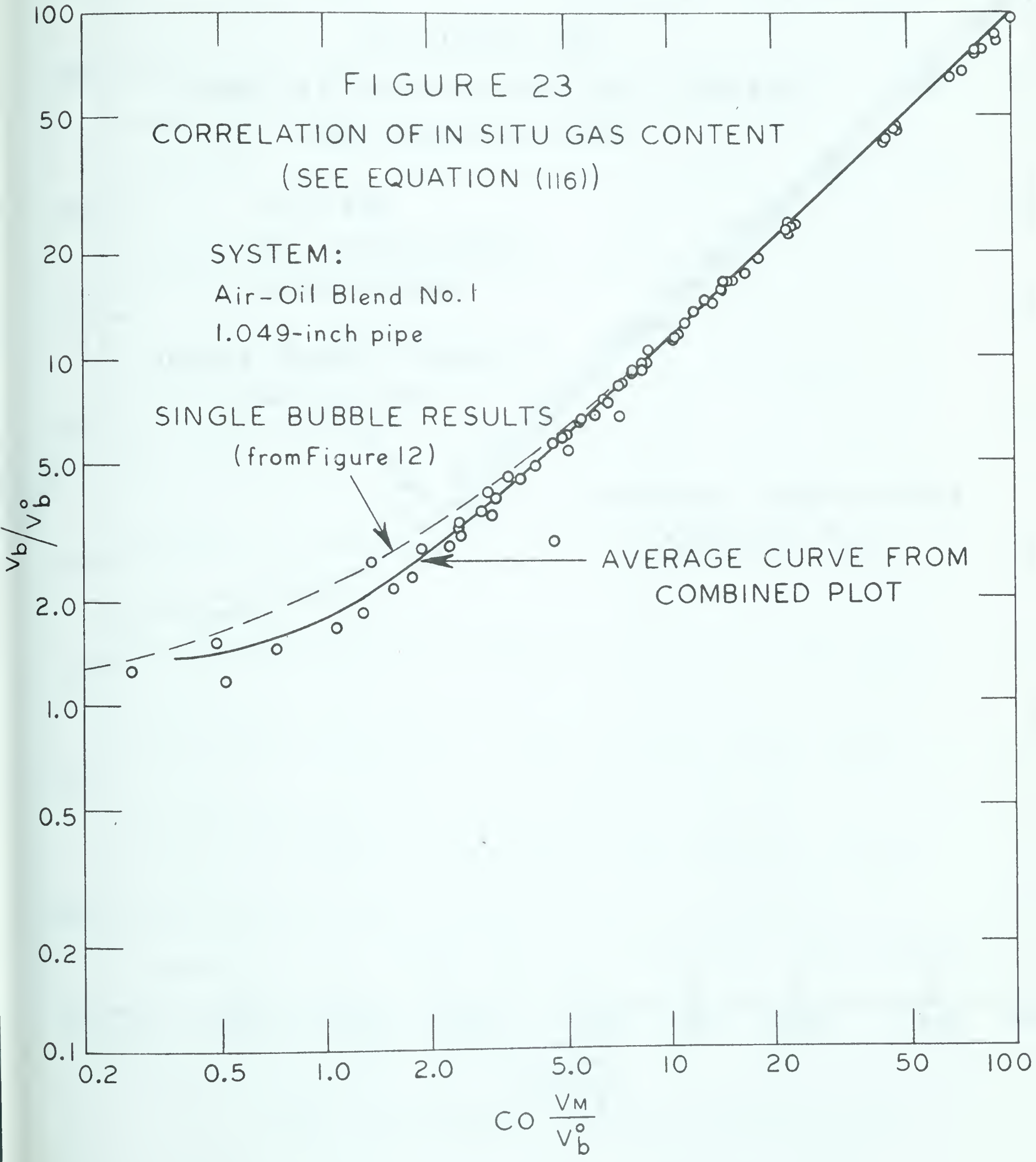

FIGURE 24

CORRELATION OF IN SITU GAS CONTENT
(SEE EQUATION (116))

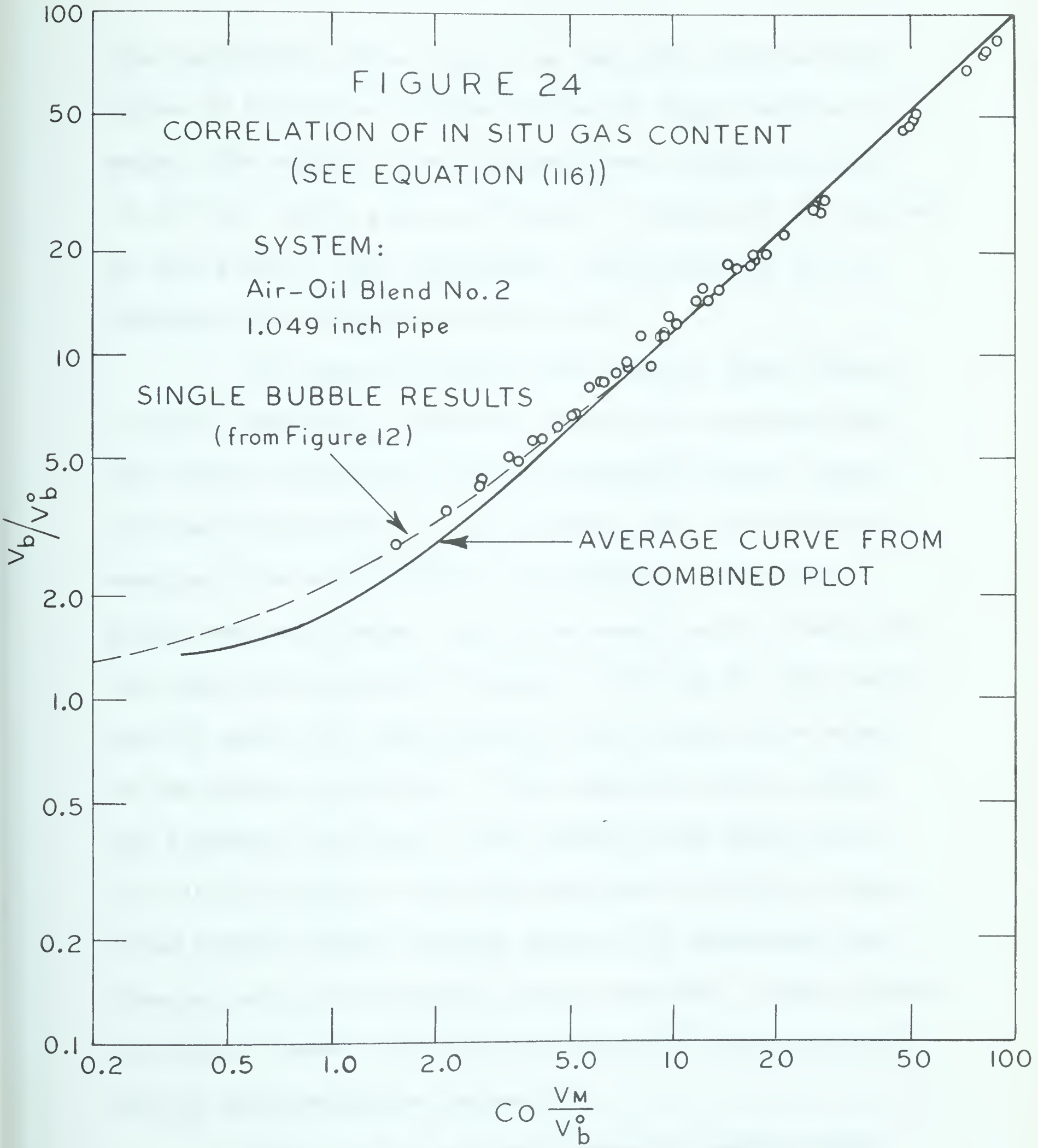

Also included in these figures is the curve obtained from Figure 12 for the velocities of rise of single bubbles in water. The average curve obtained from a large scale plot of all the results given in Figures 15 through 24 is included in each figure. For convenience, the coordinates of the average curve are given in Table VIII.

The degree of correlation shown in these figures is quite remarkable, especially when it is considered that the results include all the data available without regard for the flow pattern. In the combined plot from which the average curve was obtained, over thirteen hundred data points were considered. As can be seen from the results for the individual systems in Figures 15 through 24, the results are all quite well represented by the average curve except at low mixture velocities. There appeared to be a slight but systematic increase in the ordinate with mass rate of flow at high mixture velocities and there is also a slight trend towards higher ordinate values with increasing tube diameter and with increasing liquid viscosity. These effects are minor, however, and could be due to the approximations made in calculating the parameters.

There are two general classes of results which

TABLE VIII

CORRELATION OF GAS CONTENT - COORDINATES OF AVERAGE CURVE

$\frac{V_b}{V_b^\circ}$	$\frac{V_M}{V_b^\circ}$
1.35	.36
1.4	.44
1.7	.89
1.9	1.13
2.0	1.24
2.5	1.73
3.0	2.19
3.5	2.65
4.0	3.11
5.0	4.03
6.0	4.96
8.0	6.75
10.0	8.65
15.0	13.2
20.0	17.7
25.0	22.3
30.0	27.3
50.0	47.5
70.0	68.7
100.0	101.0
150	158
200	217
300	339

differ most frequently from the correlating curve. At low gas velocities for a given low liquid velocity, low ordinate values occur occasionally, indicating, presumably, that bubble flow occurs. At high liquid velocities, deviations to either side seem to occur at relatively low air rates. This could also be a bubble flow phenomenon or, since high pressure drops are usually associated with the flow at high liquid velocities, the behavior could be due to neglecting the expansion of the gas. The greatest deviations from the correlating curve for a system as a whole are for the flow of air-water mixtures in a 2.50-inch diameter tube. The character of the deviations in this case indicates that the majority of the results which differ from the average curve are for bubble flow and not for fully developed slug flow.

The bubble velocities calculated from holdup data for gas-liquid slug flow agree with those for single bubbles in moving liquid at the upper ranges of the latter results but fall below them with decreasing mixture velocity. This type of behavior, which is qualitatively in agreement with the observations of Nicklin (24) for actual bubble velocities in slug flow, may be due to the modifying effect of small

entrained bubbles on the flow around the Taylor bubble, as he has suggested, or it may be due to the fact that the film is not in laminar flow as has been assumed. There did not seem to be any systematic deviation from the curve for single bubbles with increasing gas rate, however, since the range of values is so narrow, it is quite possible that any such trends could be masked by the experimental scatter. The curve would be expected to fall below the slug flow results for very low gas flow rates in the bubble flow region because the bubble velocities would generally be lower.

The behavior of the experimental results indicates that there is a change in behavior at an abscissa value of about 25. For lower abscissa values, the results show the same behavior qualitatively as occurs for the single bubble results, a slight curvature upward being obtained. For greater values of the abscissa, the ordinate values are practically linear in the abscissa. A superficial examination indicated that this change in behavior might be related to the transition from slug flow to froth or annular flow. Since flow patterns have been observed for the flow of air-water mixtures in 0.630 and 1.025-inch diameter tubes (9, 10),

these results can be used to indicate the degree of correlation of the transition obtained on the coordinates of Figures 15 and 16. Accordingly, Figure 25 shows the results for the tests in which slug flow was observed. It can be seen that the slug flow results are grouped at low abscissa values, however the transition from slug to froth flow was found to depend also on the mass rate of flow, slug flow persisting to higher abscissa values at higher mass flow rates. The observed transition points ranged from abscissa values of slightly greater than 10 up to about 40. Therefore, the coordinates are not too suitable for correlating the transition from slug to froth or annular flow although they do afford a rough estimate of the transition.

For high mixture velocities, froth, annular and mist flow patterns occur and the 'bubble' velocity loses its physical significance as such. As was noted earlier, however, the calculations leading to this 'bubble' velocity apply to any flow pattern in which the gas rises at a constant average velocity in the tube. For these other flow patterns, then, V_b signifies the average velocity of the gas in the tube. For these other flow patterns also, the equilibrium film thickness as calculated has no physical significance

FIGURE 25

CORRELATION OF IN SITU GAS CONTENT

(SEE EQUATION (116))

EXPERIMENTAL DATA FOR SLUG FLOW

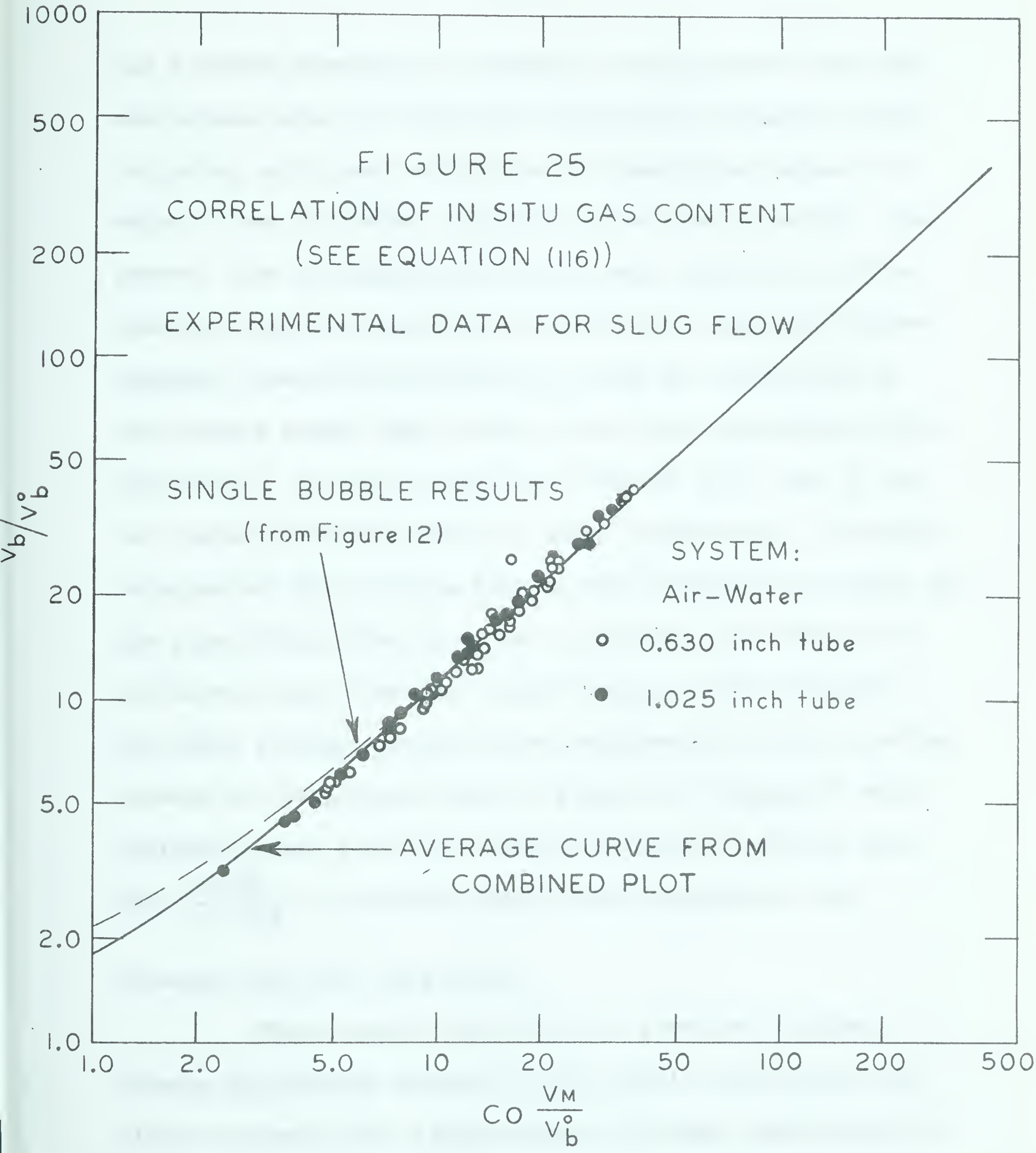

and a rather paradoxical situation is encountered since the approximate abscissa which was introduced in Equation (124) is giving quite good correlation of results in regions for which it has no obvious relation to the flow occurring. The general form of Equation (93) still must describe the flow, however, since it is merely one form of the material balance equation; however, the coefficients must be interpreted as area ratios rather than as functions of an 'equilibrium film thickness'. As can be seen from Equation (90), this is the more general interpretation of their significance. As would be expected, the relation between the parameters no longer has the significance that is given in Equation (107) where the difference was a function of the change in film thickness. This fact is also apparent from consideration of the relation between the parameters shown in Figures 15 through 24 which indicates that, for high mixture velocities, V_b/V_b° is less than $\frac{V_M/V_b^\circ}{(1-\zeta^\circ)^2}$, a situation which is not consistent with Equation (107) for slug flow.

These results show there is a marked relation between the average velocity of the gas in the tube and the mixture velocity for a given system, thereby emphasizing the

importance of the mixture velocity. It is rather surprising that the effects of viscosity and tube size on this relation should be substantially the same for all flow patterns; however, this is what the results indicate.

The good agreement between the University of Alberta results for smooth tubes and those of Hughmark for a commercial steel pipe (relative roughness, $\varepsilon/R = 0.004$) indicates that the tube roughness has relatively little effect on the flow geometry.

In this section, it has been demonstrated that the proposed model for bubble movement in gas-liquid slug flow leads to a form of correlation of gas content which applies not only in the region of slug flow, but to the behavior in the other regions of flow as well. The results for very low gas flows, which would probably be in the bubble flow region, are the only results that are not represented quite well by the empirical relation developed.

5. Pressure Drop in Slug Flow

For the model of gas-liquid slug flow that has been proposed, the pressure drop is given by Equation (122) which becomes, upon substitution of Equation (116),

$$\frac{\Delta P}{H} = \left(-\frac{2}{R}\tau_w + \frac{\rho g}{g_c}\right)\left(1 - \frac{x_G}{(1-\varepsilon)^2}\right) \qquad (125)$$

On the basis of the earlier discussion of the pressure drop across a single bubble, the first term in brackets on the right is seen to be the pressure drop for single-phase liquid flow at the mixture velocity. Writing this as $(\Delta P/H)_{sp}$ and rearranging gives

$$\frac{\Delta P/H}{(\Delta P/H)_{sp}} = 1 - \frac{x_G}{(1-\varepsilon)^2} \qquad (126)$$

which indicates that the ratio of the two-phase pressure drop to the pressure drop for liquid flowing alone at the mixture velocity should be predictable from the gas content, x_G, and the film thickness for the mixture velocity being considered. Once again, the film thickness should not change sufficiently in the region of slug flow to affect appreciably the factor $(1-\varepsilon)^2$ and the slug flow results should be represented by the equation

$$\frac{\Delta P/H}{(\Delta P/H)_{sp}} = 1 - C_o\, x_G \qquad (127)$$

where the parameter C_o, as defined by Equation (92), is constant for a given system.

In the previous treatments of gas-liquid slug flow in the literature, those of Griffith and Wallis (12) and of Nicklin (24), equations somewhat similar to Equation (125) have been proposed for the prediction of pressure drop. Griffith and Wallis proposed the relation

$$\frac{\Delta P}{H} = -\frac{2}{R}\tau_w \frac{V_L^*}{V_L^* + V_G^*} + \frac{\rho g}{g_c}(1 - x_G) \qquad (128)$$

while Nicklin's equation for the prediction of pressure drops is

$$\frac{\Delta P}{H} = \left(-\frac{2}{R}\tau_w + \frac{\rho g}{g_c}\right)(1 - x_G) \qquad (129)$$

Equations (128) and (129) differ from each other only in the evaluation of the frictional component of pressure drop from the value for single-phase liquid flow while both equations differ in addition from Equation (125) in the evaluation of the static component. In Griffith and Wallis' development, the liquid content or fraction of liquid in the tube is used to represent the static pressure drop while the frictional component is given by the pressure drop for liquid flowing at the mixture velocity multiplied by the flowing volume fraction of liquid. Nicklin's proposal is to use the liquid content as the multiplier of the single-phase pressure drop

to obtain the frictional component in addition to using it to represent the static pressure drop. The scheme proposed in the present study entails the use of the liquid length fraction in the evaluation of both the static and frictional components of pressure drop, thereby allowing for the liquid in the film surrounding the bubble which is supported by wall shear and contributes neither to the static nor frictional pressure drops. Comparison of Equations (125) and (129) shows that Equation (129) is the special case for which the film thickness is zero.

Equations (125), (128), and (129) all represent various degrees of approximation to the prediction of pressure drop in the model. They will all be in error, however, insofar as the model does not describe the actual physical situation. Thus, none of the proposals accounts for the effect of gas entrained in the liquid slug on either the static or frictional components of the pressure drop or for the different velocity distribution in the immediate wake of the bubble. Equation (128) will not be considered further as it is simply a modification of Equation (129) and there does not appear to be any justification on theoretical grounds for using the flowing fraction of liquid in evaluating the frictional resistance to flow.

To test the applicability of Equations (125) and (129) for the prediction of pressure drops in gas-liquid slug flow, the pressure drop ratio of Equation (126) can be calculated from experimental results and its variation with the gas content, x_G, compared with the theoretical relations arising from Equations (125) and (129). For this purpose, the experimental results of Govier (9, 10), previously referred to in connection with Figure 25, for tests in which slug flow was observed were used. In the calculation of the single-phase pressure drops for these results, the von Karman equation for the friction factor in smooth tubes was used. Figures 26 and 27 show the points calculated from these experimental results as well as the predictions afforded by Equation (129) and by Equation (125) for the systems being considered, the values of C_o for Equation (125) being obtained from Table VII.

Two facts are at once apparent from Figures 26 and 27. The first is that a good degree of correlation of the results is obtained on these coordinates which arose from consideration of the proposed model for slug flow. The second fact is that neither Equation (129), which is based on the potential flow model, nor Equation (125), which is

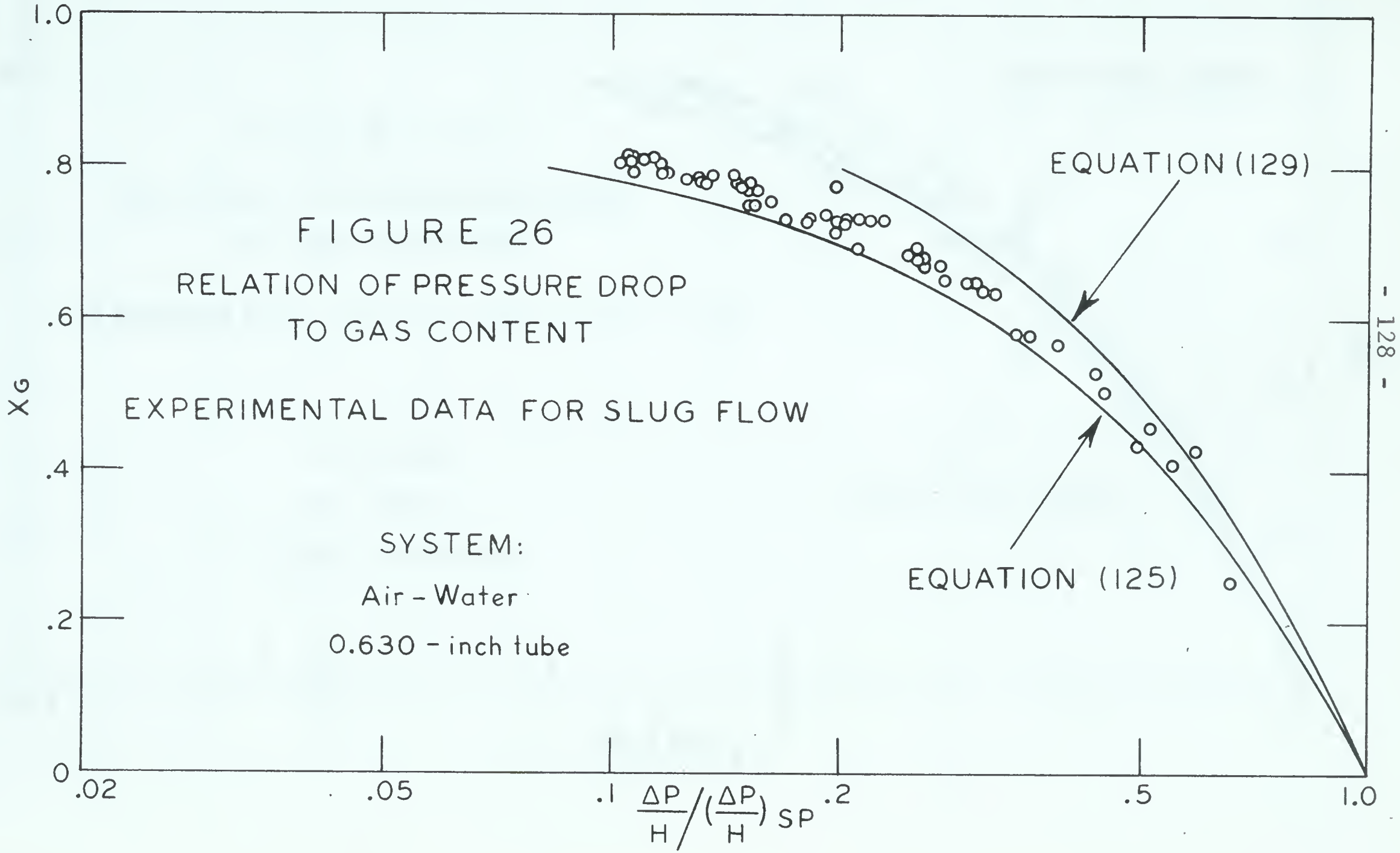

FIGURE 26

RELATION OF PRESSURE DROP TO GAS CONTENT

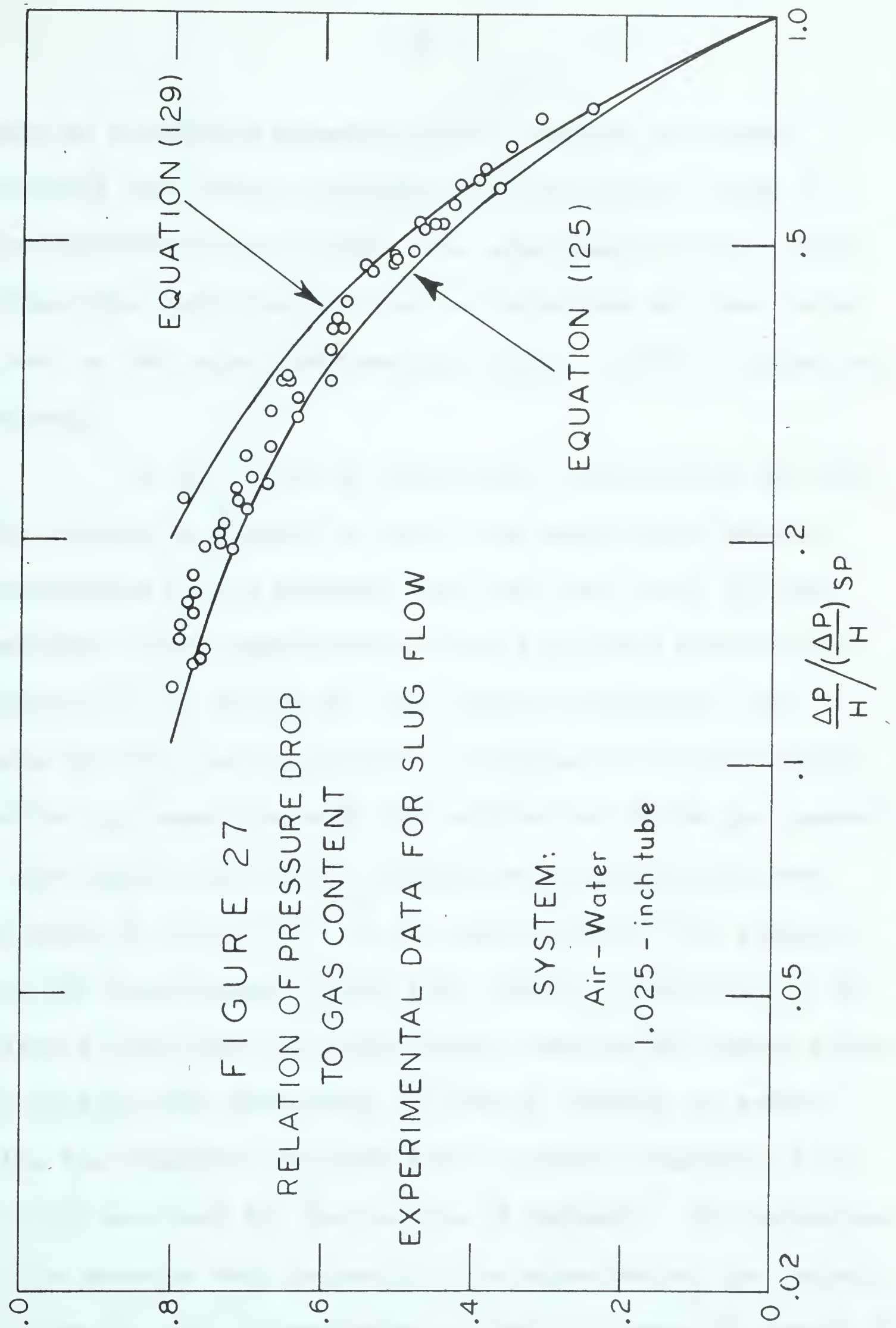
EQUATION (129)
EQUATION (125)
EXPERIMENTAL DATA FOR SLUG FLOW
RELATION OF PRESSURE DROP
TO GAS CONTENT
SYSTEM:
Air – Water
1.025 – inch tube
X_G
$\frac{\Delta P}{H} / (\frac{\Delta P}{H})_{SP}$
1.0
.8
.6
.4
.2
0
.02
.05
.1
.2
.5
1.0

FIGURE 27

based on a combined potential flow - viscous flow model, describes the results accurately over the entire range of flow conditions encountered. The experimental results fall between the predictions of the two equations and tend to be closer to the curve representing Equation (125) at higher gas contents.

As the degree of correlation obtained for the slug flow results in Figures 26 and 27 was quite good, similar calculations of the pressure drop ratio were made for the remainder of the experimental results from the University of Alberta (9, 10, 4) and for the results of Hughmark (17). These are the results previously referred to in the previous section in connection with the correlation of the gas content in gas-liquid flow and the properties of the liquids used are given in Table VII. In the calculation of the pressure drop for single-phase liquid flow, which is required for the pressure drop ratio, the von Karman equation for smooth pipes was used for the University of Alberta results, as before, while the Colebrook equation for a relative roughness, ε/R, of 0.004 was used for the results of Hughmark. The variation of the pressure drop ratios with the experimental gas content is shown for the systems investigated in Figures 28 through 37.

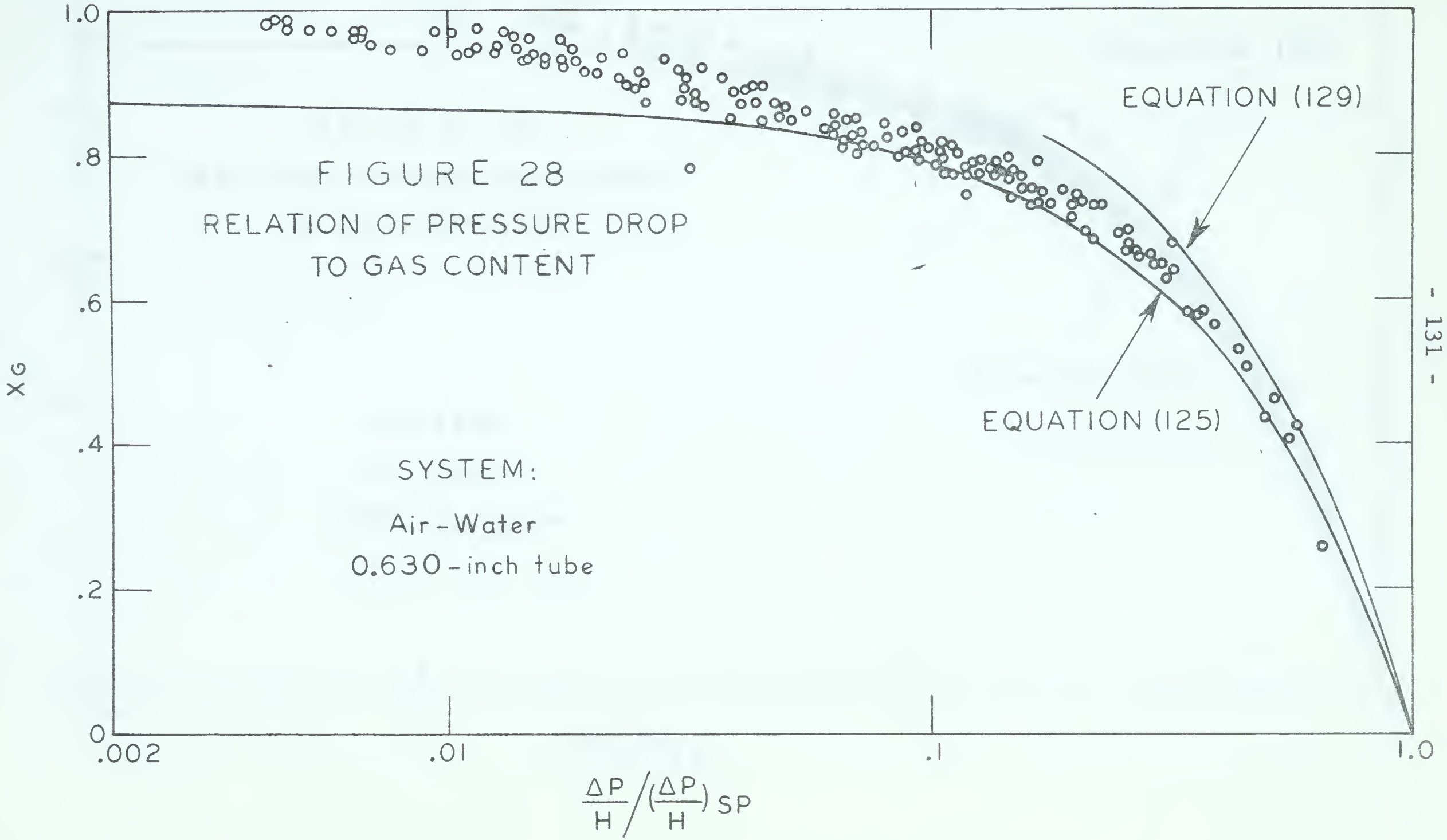
FIGURE 28
RELATION OF PRESSURE DROP
TO GAS CONTENT
SYSTEM:
Air-Water
0.630-inch tube
EQUATION (129)
EQUATION (125)
x_g
1.0
.8
.6
.4
.2
0
.002
.01
.1
1.0
$\frac{\Delta P}{H} \Big/ \left(\frac{\Delta P}{H}\right)_{SP}$

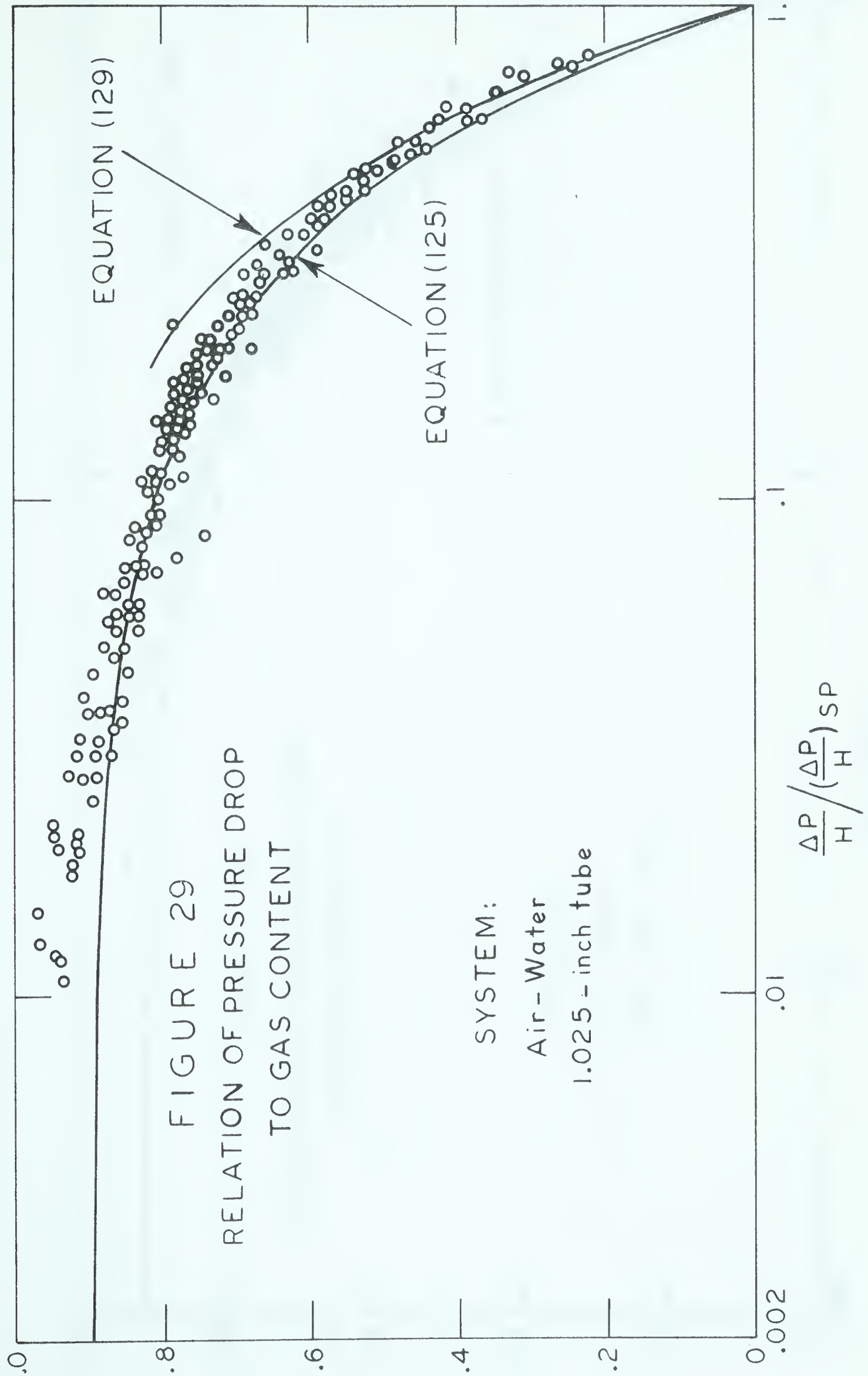

FIGURE 29

RELATION OF PRESSURE DROP TO GAS CONTENT

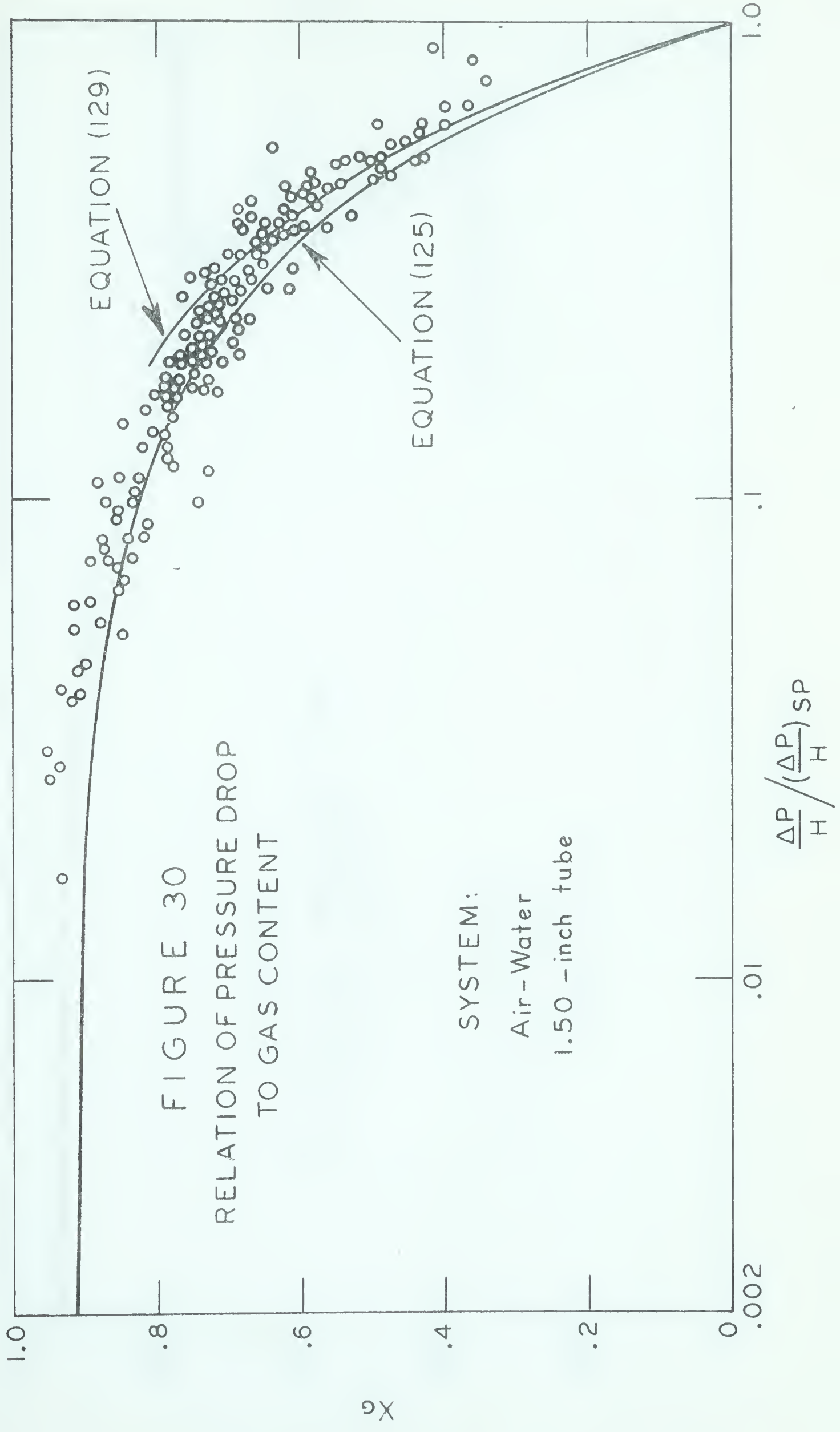

FIGURE 30

RELATION OF PRESSURE DROP TO GAS CONTENT

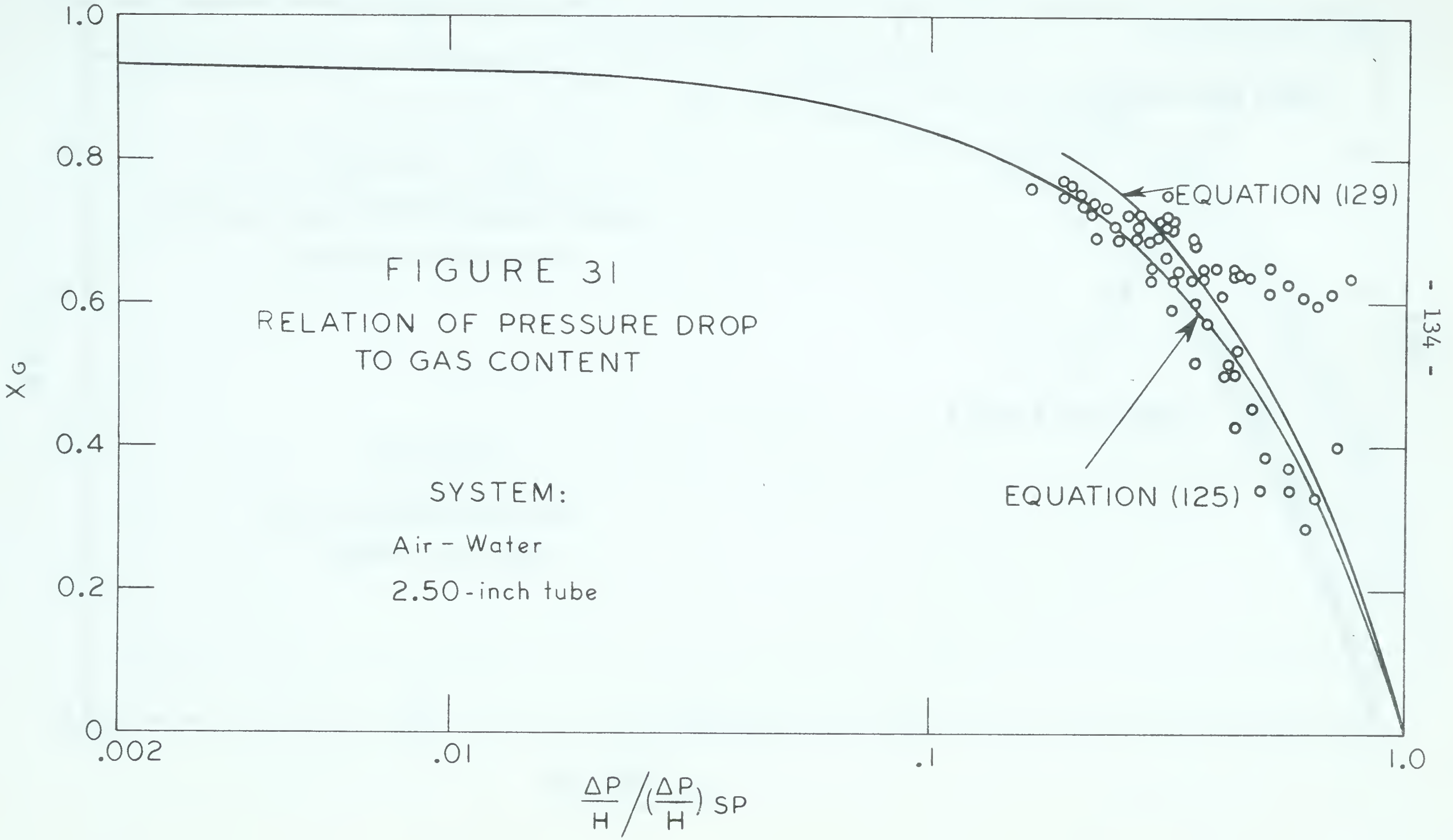

FIGURE 31

RELATION OF PRESSURE DROP TO GAS CONTENT

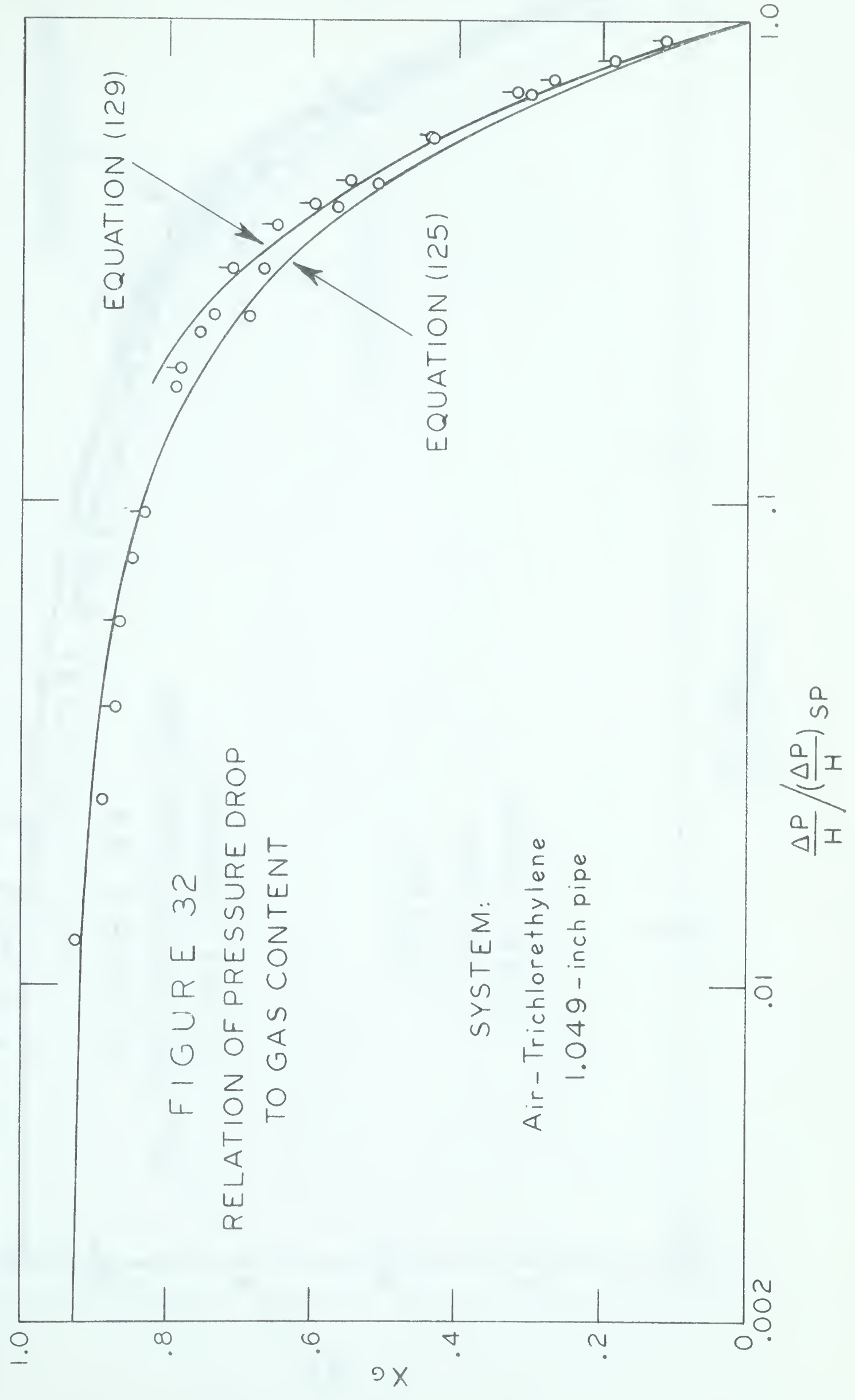

FIGURE 32

RELATION OF PRESSURE DROP TO GAS CONTENT

SYSTEM:

Air – Trichlorethylene

1.049 – inch pipe

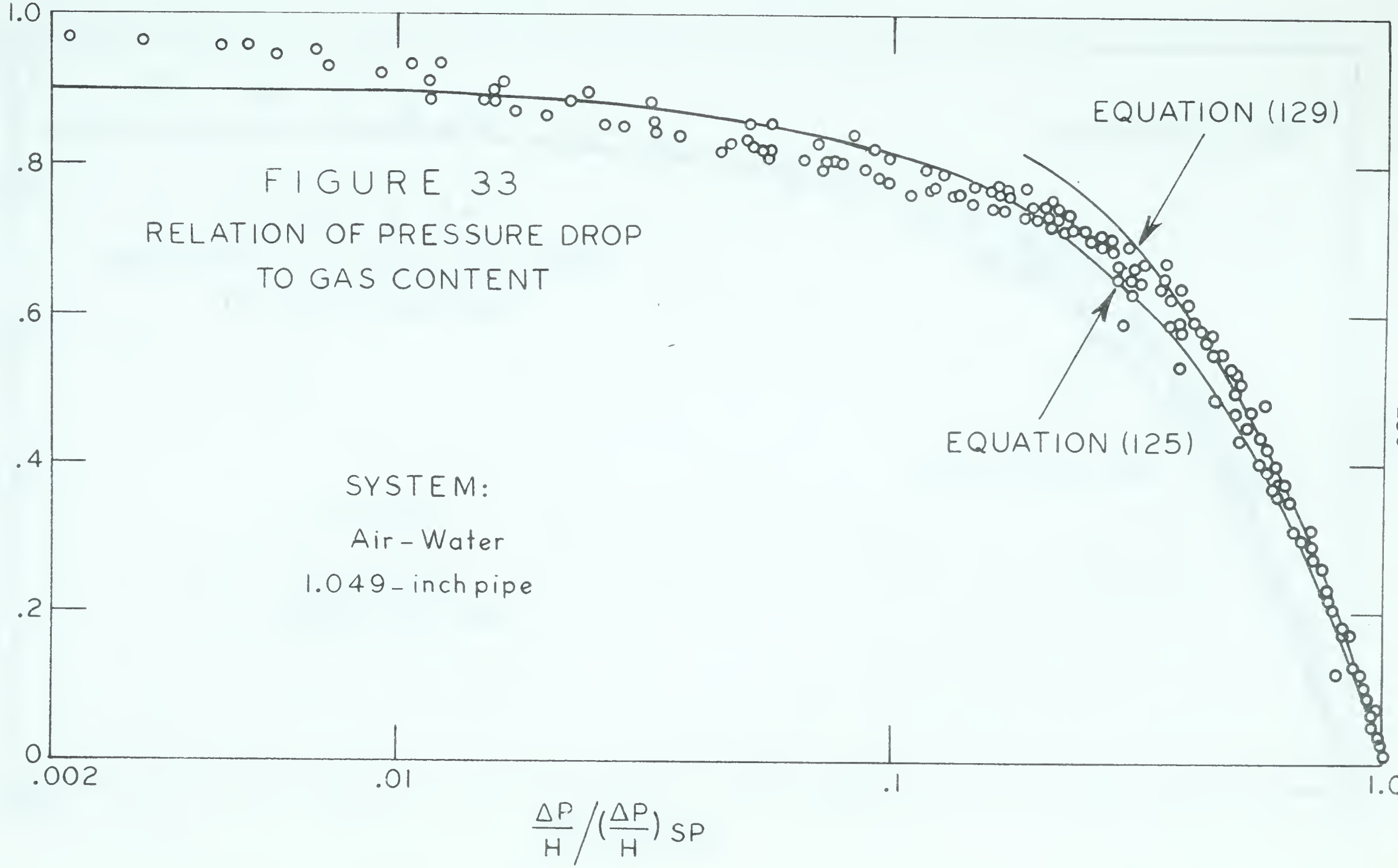

FIGURE 33

RELATION OF PRESSURE DROP TO GAS CONTENT

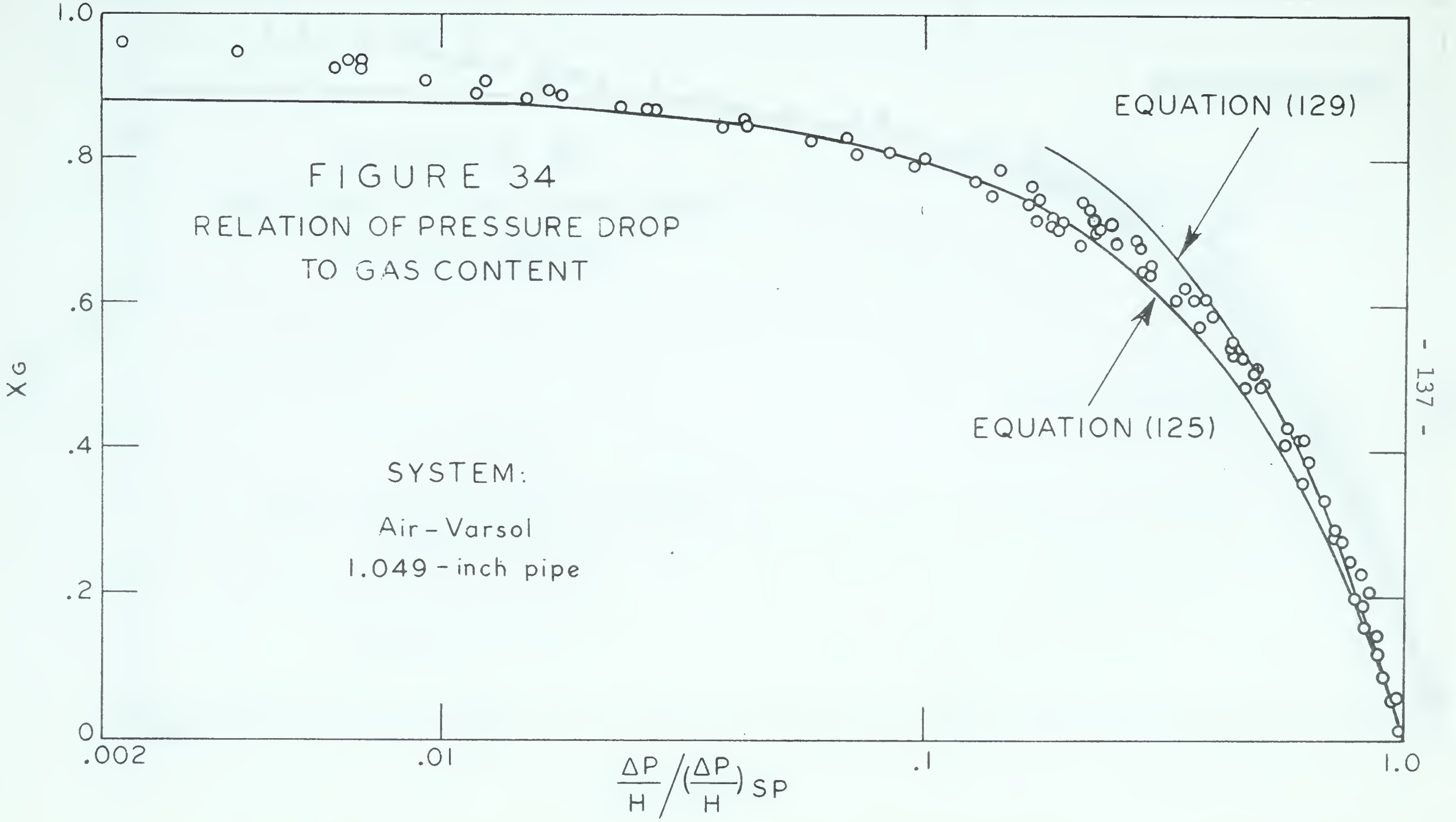

FIGURE 34

RELATION OF PRESSURE DROP TO GAS CONTENT

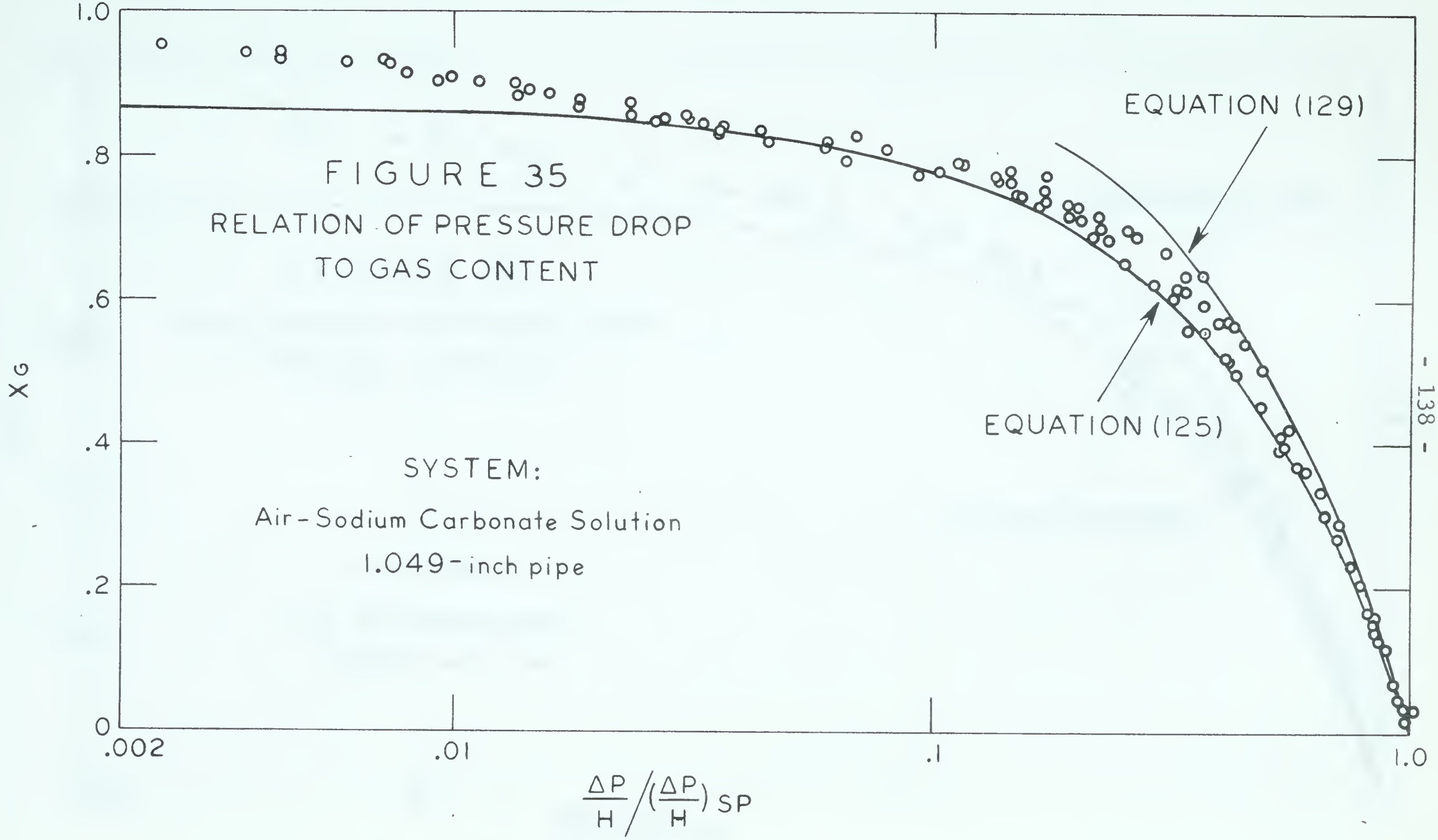

FIGURE 35

RELATION OF PRESSURE DROP TO GAS CONTENT

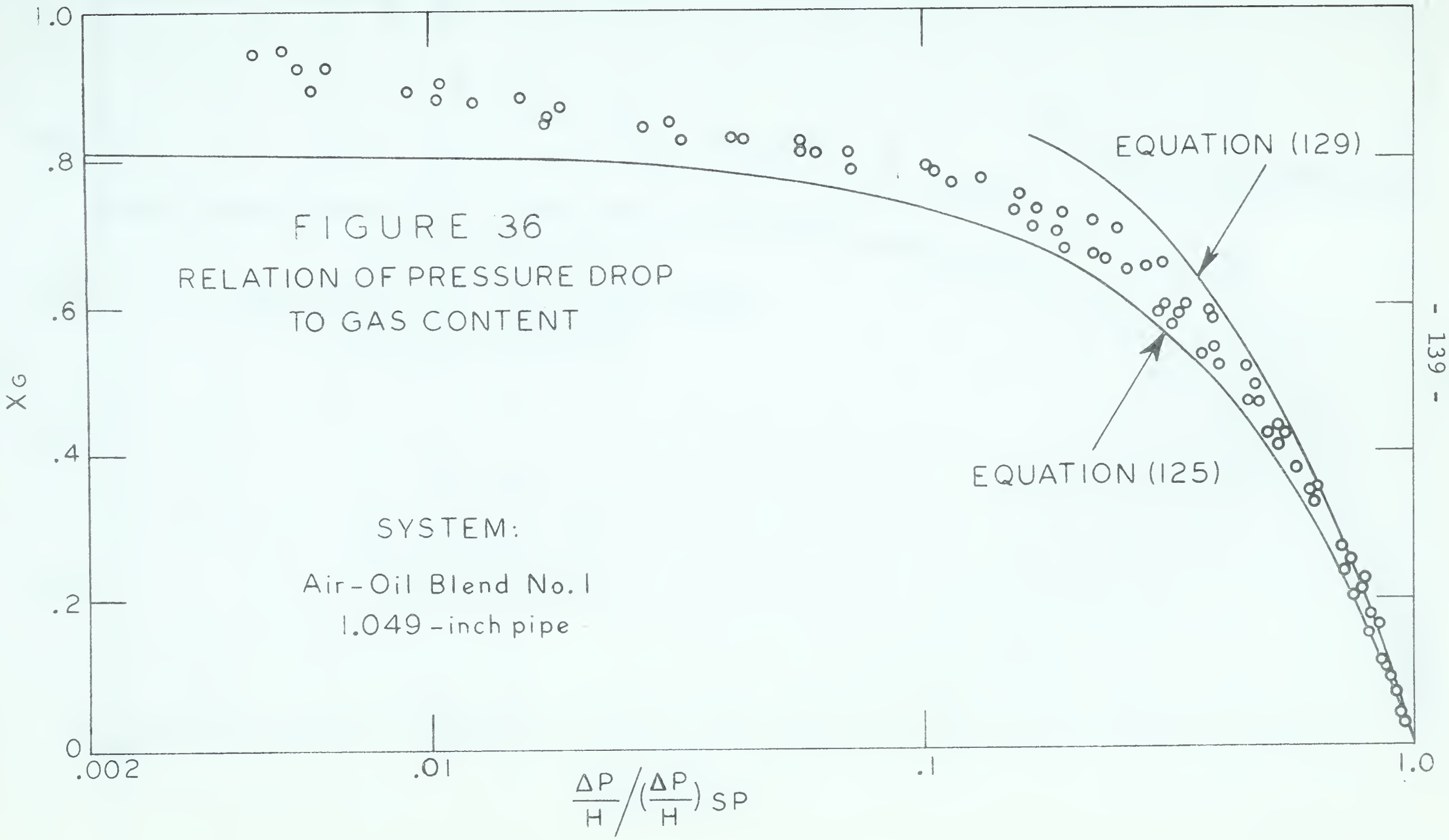

FIGURE 36

RELATION OF PRESSURE DROP TO GAS CONTENT

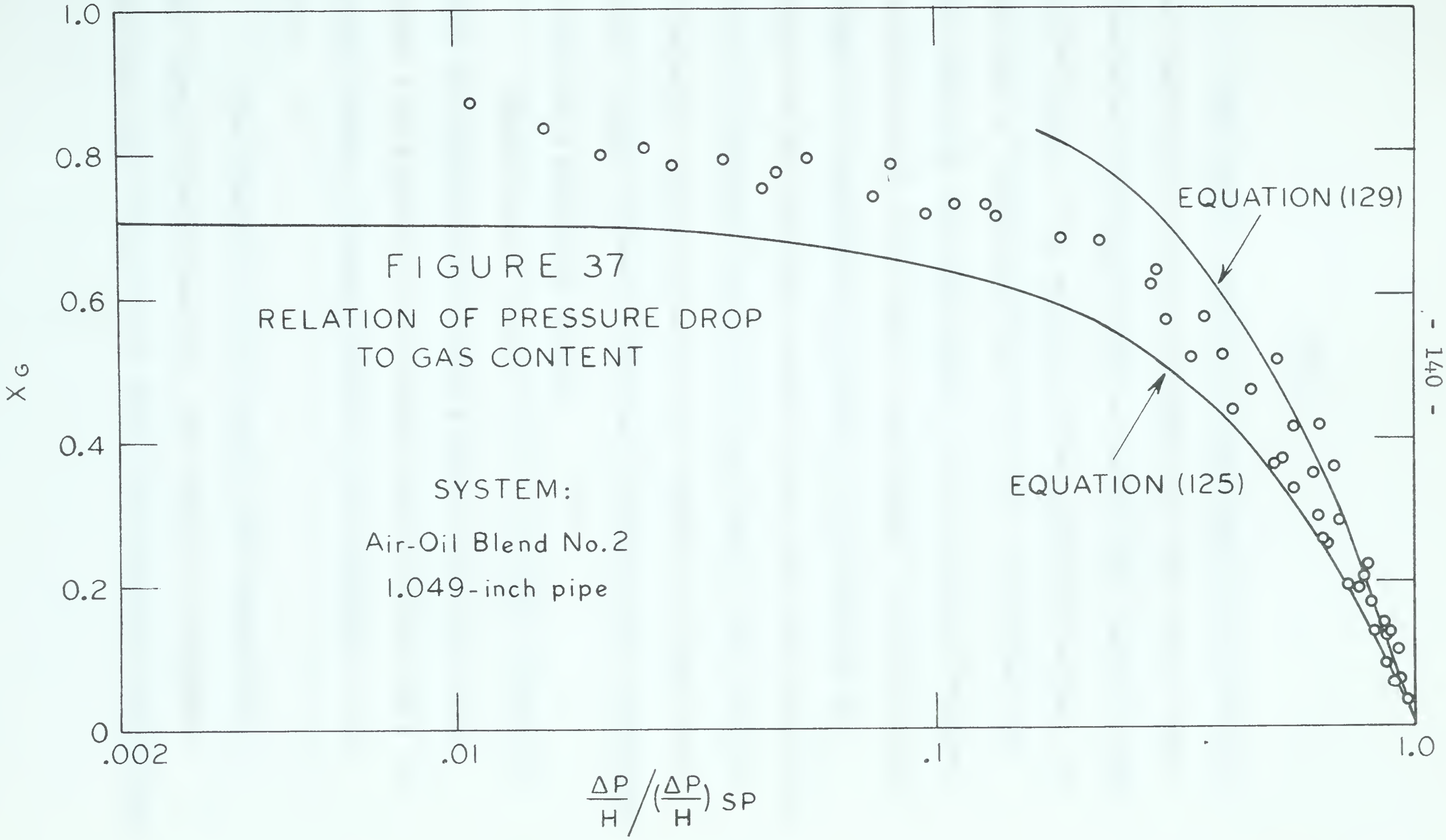

FIGURE 37

RELATION OF PRESSURE DROP TO GAS CONTENT

Once again, quite good correlation of the results for an individual system is obtained over the entire range of flow rates investigated and not solely for results in the slug flow region. The majority of results fall between the predictions of Equations (125) and (129). The effect of liquid viscosity and tube diameter on the relation between the pressure drop ratio and the gas content is qualitatively the same as is predicted by Equation (125) although the magnitude of the viscosity effect is less than that predicted. There is no definable trend with mass rate of flow for the low viscosity liquids while for the liquids of higher viscosities, higher pressure drops were obtained with increasing mass rate at a given gas content.

There does not appear to be any marked difference between the University of Alberta results and the results obtained from Hughmark's data which would indicate that the abscissa accounts satisfactorily for the roughness of the conduit.

The behavior of the results with successively larger liquid viscosities (i.e. the results of Hughmark progressing from Figure 32 to Figure 37) provides experimental

justification for consideration of the length fraction of liquid in calculating pressure drops for slug flow. For a given volume fraction of liquid, the relative pressure drop becomes lower with increasing liquid viscosity which is consistent with the hypothesis since a greater film thickness would occur with the more viscous liquids. The observed trend with mass rate of flow for the results with higher viscosity liquids could be due to a difference in behavior for these liquids although it is more likely due to the fact that the pressure drop measurements were made over the entire pipe including the region of developing slug flow. This hypothesis is supported in part by the results in the previous section where slightly higher average gas velocities (corresponding to lower gas contents) were noted for the higher viscosity liquids. This effect would be magnified in the pressure drop due to the dual role that the gas content plays in determining the static and frictional components.

That the experimental results for slug flow should fall between the predictions based on the two models is not surprising when the assumptions involved are considered. The potential flow model which is described by Equation (129)

assumes that the entire mass of liquid in the tube contributes to the pressure drop. The combined potential flow - viscous flow model which is described by Equation (125), on the other hand, assumes that there is a mass of liquid equivalent to a film of equilibrium thickness around the total volume of gas in the tube which does not contribute at all to the pressure drop. This latter proposal in effect over-corrects the deficiency of the potential flow model; however, it should provide a better approximation and this seems to be borne out by the results in Figures 28 to 37. It can be seen, therefore, that the qualitative behavior of the results shown in Figures 28 through 37 with respect to the theoretical relation, Equation (125), could arise from failure to analyze the bubble model with sufficient accuracy. For the region of slug flow, however, Equations (125) and (129) should give the lower and upper limits, respectively, for the pressure drop corresponding to a given gas content.

Outside the limits of slug flow, a fairly good correlation of pressure drop is obtained on the coordinates of Figures 28 to 37 for each of the systems; however, the nature of the relationship for these regions is not suitable for a practical correlation. For high gas contents, the

relative pressure drop changes rapidly with gas content and both the pressure drop relation and the prediction of gas content would have to be considerably more precise than is possible at the present time.

For the region of low gas contents, however, say below x_G values of about 0.8, refinement of the relationships presented here should permit quite accurate prediction of pressure drops in gas-liquid systems. In their present form, Equations (125) and (129) should give satisfactory predictions of minimum and maximum pressure drops for gas-liquid flow with low viscosity liquids (say below about 8.0×10^{-5} ft^2/sec kinematic viscosity) at low gas contents when used in conjunction with the correlation of gas contents presented in the preceding section. The procedure would involve calculating the values of V_b° and C_o from Equations (68) and (66), obtaining the bubble velocity from the average curve of Figures 15 to 24 (i.e. from the curve defined in Table VIII) and obtaining the gas content, x_G, from Equation (116). With the gas content known, the limits of pressure drop could be obtained from Equations (125) and (129) for the mixture velocity being considered.

While this consideration of bubble mechanics has led to an acceptable correlation of pressure drops for a limited range of flow rates, it is believed that greater significance must be attached to the development of the parameters for correlating the gas content and the pressure drop. In its present form, the gas content correlation appears capable of predicting gas contents for most regions of gas-liquid flow within about ten percent and, if modified empirically through a statistical treatment of the existing gas-liquid flow results in the literature, should be able to provide even more accurate predictions. Similarly, the experimental results considered here for pressure drops in gas-liquid flow are correlated quite well on the parameters of Figure 28 through 37 in their present form and these should be capable of better correlation through empirical modification of the relations which were deduced here from theory. It is unlikely, however, that this form of correlation will prove suitable for flows with high gas contents.

6. Summary

Consideration of the material balance equation for the liquid flowing around a Taylor bubble in a moving liquid

stream leads to the dimensionless parameters V_b/V_b° and $C_o V_M/V_b^\circ$ for correlating the gas content in gas-liquid slug flow. Comparison of results from the literature on these coordinates indicates that they correlate the gas content, not only for the region of slug flow, but over the entire range of flow rates encountered in gas-liquid flow with the exception of very low gas flow rates in the bubble flow region.

From the force balance around a single Taylor bubble, a general expression for the pressure drop in gas-liquid slug flow is developed. This relation is

$$\frac{\Delta P/H}{(\Delta P/H)_{sp}} = 1 - C_o\, x_G \qquad (127)$$

This equation is shown to form a lower limit for the pressure drop in gas-liquid slug flow. While the experimental results for all flow patterns are correlated to some degree on the coordinates indicated by this equation, $\Delta P/H/(\Delta P/H)_{sp}$ and x_G, it is unlikely that it will be useful for high gas contents because of the nature of the relationship in these regions.

As the relations developed were obtained from a proposed model for gas-liquid slug flow, the agreement obtained indicates that this model provides a satisfactory description

of the bubble for estimating gas contents and pressure drops. The agreement obtained outside the limits of slug flow indicates that the average velocity of the gas in the tube is related to the mixture velocity in much the same manner regardless of the flow pattern.

CONCLUSIONS

A model has been proposed for the mechanism of flow associated with the movement of a large gas bubble through stagnant liquid in a tube which accounts for the viscous flow in the annular film around the rear of the bubble as well as the potential flow at the nose. This model, in conjunction with experimental observation of bubble shapes in different liquids, has led to the equation

$$V_b^\circ = 0.496\sqrt{gR}\sqrt{1 - \frac{-1 + \sqrt{1 + 2CR}}{CR}} \qquad (68)$$

where

$$C = \sqrt[3]{14.5\,\frac{\rho^2 g}{\mu^2}} \qquad (67)$$

for the correlation of bubble velocities. It has also been demonstrated that surface tension effects are negligible if

$$\frac{\rho g R^2}{\sigma}\left(1 - \frac{-1 + \sqrt{1 + 2CR}}{CR}\right)^2 > 5.0 \qquad (75)$$

The minimum size of bubble which behaves according to Equation (68) has been considered and it is shown that all bubbles for which the condition

$$r_e > 0.75R\left(1 - \frac{-1 + \sqrt{1 + 2CR}}{CR}\right) \qquad (76)$$

is satisfied do so behave, however smaller bubbles may also, especially in large diameter tubes.

Consideration of this model for the case of a bubble rising in a moving stream of liquid in a tube has led to a form of empirical correlation of the average gas velocity (or of the gas content) in gas-liquid flow which appears to apply not only for the slug flow pattern but for all flow rates with the exception of the low gas flows associated with the bubble flow pattern. The coordinates of the correlating curve are given in Table VIII in the text.

Consideration of the force balance for a single bubble has led to the development of the following expression for the pressure drop in gas-liquid slug flow.

$$\frac{\Delta P/H}{(\Delta P/H)_{sp}} = 1 - \frac{x_G}{(1 - \zeta)^2} \qquad (126)$$

It has been shown both on theoretical and experimental grounds that the value of the parameter $\frac{1}{(1 - \zeta)^2}$ in Equation (126) lies between one and the value corresponding to a bubble rising in stagnant liquid, $C_o = \frac{1}{(1 - \zeta_o)^2}$.

The improved understanding of the mechanism of gas-liquid slug flow developed here has led to the development of empirical correlations for gas content and pressure drop which show a marked improvement over existing methods in the systemization of results for all flow patterns except bubble flow. While these correlations permit quite good prediction of gas contents and pressure drops in their present form, it is believed that empirical correlation of results within the framework of the correlations developed here by semi-empirical means will permit even more accurate predictions of the behavior of flowing gas-liquid mixtures. It is not believed, however, that the form of correlation of pressure drop developed here is suitable for use with systems having high gas contents.

NOMENCLATURE[a]

A	Cross-sectional area of tube, ft^2
C	Property parameter defined by Equation (67), ft^{-1}
C_o	Coefficient of V_L in Equation (92), $\frac{1}{(1-\zeta_o)^2}$.
C_4	Coefficient of V_L in Equation (96).
E	Total energy, ft lb_f/lb_m
Eo	Eotvos number, $\frac{\rho g L^2}{\sigma}$
F	Drag force, lb_f
g	Acceleration of gravity, ft/sec^2
$\bar{g}$	Gravity vector, ft/sec^2
g_c	Conversion factor, lb_m ft/lb_f sec^2
H	Length of tube, ft
ℓ_b	Length of bubble, ft
ℓ_s	Length of slug, ft
L	Characteristic length, ft
m	Distance from wall, R - r, ft
$\mathring{M}$	Momentum flux, lb_f
P	Pressure, lb_f/ft^2

a Various other special symbols are defined in the text where they occur.

ΔP_R	Pressure recovery in the wake of a Taylor bubble, lb_f/ft^2
$\bar{q}$	Heat flux, $lb_f/ft\ sec$
Q	Volumetric rate of flow, ft^3/sec
r	Radial position, ft
r'	Radial position normalized with respect to R_C, $\frac{r}{R_C}$
r_e	Equivalent spherical radius defined by Equation (13), ft
r_o	Frontal radius of bubble, ft
R	Radius of tube or pipe, ft
R_C	Equilibrium cylindrical radius at rear of Taylor bubble, ft
t	Time, sec
u	Radial component of velocity - cylindrical coordinates, ft/sec
v	Axial component of velocity - cylindrical coordinates, ft/sec
$\bar{V}$	Velocity vector, ft/sec
V	Magnitude of velocity vector, ft/sec
$\underline{V}$	Average velocity of liquid relative to bubble, ft/sec
V_b°	Bubble velocity in stagnant liquid, ft/sec
V_b	Bubble velocity, ft/sec
V_F	Average velocity in film relative to tube, ft/sec
V_L	Average liquid velocity relative to tube - single bubble case, ft/sec

V_M Mixture velocity, $V_L^* + V_G^*$, ft/sec

V^* Superficial velocity, $\frac{Q}{A}$, ft/sec

$\mathcal{V}'$ Volume of liquid in film supported by wall shear, ft^3

$\mathcal{V}''$ Volume of liquid in film accelerating freely, ft^3

$\mathcal{V}_b$ Volume of bubble, ft^3

$\mathcal{V}_L$ Volume of liquid in tube, ft^3

x Axial position, ft

x_G Volume fraction of gas in tube (gas content)

x' Axial position normalized with respect to R_C, $\frac{x}{R_C}$

x_e Transition length for a Taylor bubble, ft

Greek Symbols

γ Normalized radial position, $\frac{r}{R}$

Γ Square root of bubble Froude number, $\frac{V_b^\circ}{\sqrt{gL}}$

δ Film thickness, $R - r_i$, ft

ζ Normalized film thickness, $\frac{\delta}{R}$

ζ_o Normalized film thickness for a Taylor bubble in stagnant liquid

η Normalized axial position, $\frac{x}{R}$

θ Angle from stagnation point - spherical coordinates

μ Viscosity of liquid, $lb_m/ft\ sec$

ρ Density of liquid, lb_m/ft^3

ρ' Density of bubble fluid, lb_m/ft^3

ρ_a Average density of gas-liquid mixture in tube, lb_m/ft^3

σ Surface tension, lb_m/sec^2

$\bar{\tau}$ Shear stress tensor, lb_f/ft^2

τ Shear stress, lb_f/ft^2

$\underline{\tau}$ Shear stress in fully-developed, single-phase flow lb_f/ft^2

Φ Potential function

χ Normalized frontal radius of bubble, $\frac{r_o}{R}$

Ψ Stream function

ω Normalized distance from the wall, $\frac{m}{R}$

Subscripts

A Refers to liquid approaching bubble (approach flow)

F Refers to film

G Refers to gas phase

i Refers to gas-liquid interface

L Refers to liquid phase

sp Denotes single-phase liquid

w Refers to tube wall

LIST OF REFERENCES

1. Anderson, G. H. and B. G. Mantzouranis; "Two-Phase (Gas-Liquid) Flow Phenomena - I", Chem. Eng. Sci., 12, 109-126 (1960).

2. Bennett, J.A.R.; "Two-Phase Flow in Gas-Liquid Systems - A Literature Survey", At. Energy Res. Est. (Gt. Brit.) Report CE/R 2497 (1958).

3. Brown, R.A.S. and G. W. Govier; "High-Speed Photography in the Study of Two-Phase Flow", Can. J. Chem. Eng., 39, 159-164 (1961).

4. Brown, R.A.S., G. A. Sullivan and G. W. Govier; "The Upward Vertical Flow of Air-Water Mixtures. III. Effect of Gas Phase Density on Flow Pattern, Holdup and Pressure Drop", Can. J. Chem. Eng., 38, 62-66 (1960).

5. Cromer, S. and R. L. Huntington; "Visual Studies of the Flow of Air-Water Mixtures in a Vertical Pipe", Trans. Am. Inst. Min. Engrs., 136, 79-90 (1940).

6. Davies, R. M. and Sir Geoffrey Taylor; "The Mechanics of Large Bubbles Rising Through Extended Liquids and Through Liquids in Tubes", Proc. Roy. Soc. (London), 200A, 375-390 (1950).

7. Dumitrescu, D. T.; "Stromung an einer Luftblase im Senkrechten Rohr", Z. Ang. Math. u. Mech., 23, 139-149 (1943).

8. Goldsmith, H. L. and S. G. Mason; "The Movement of Single Large Bubbles in Closed Vertical Tubes", J. Fluid Mech., 14, 42-58 (1962).

9. Govier, G. W., B. A. Radford and J.S.C. Dunn; "The Upwards Vertical Flow of Air-Water Mixtures. I. Effect of Air and Water Rates on Flow Pattern, Holdup and Pressure Drop", Can. J. Chem. Eng., 35, 58-70 (1957).

10. Govier, G. W. and W. L. Short; "The Upward Vertical Flow of Air-Water Mixtures. II. Effect of Tubing Diameter on Flow Pattern, Holdup and Pressure Drop", Can. J. Chem. Eng., 36, 195-202 (1958).

11. Govier, G. W., G. A. Sullivan and R. K. Wood; "The Upward Vertical Flow of Oil-Water Mixtures", Can. J. Chem. Eng., 39, 67-75 (1961).

12. Griffith, P. and G. B. Wallis; "Two-Phase Slug Flow", Trans. Am. Soc. Mech. Engrs., 83C, 307-320 (1961).

13. Haberman, W. L. and R. K. Morton; "An Experimental Study of Bubbles Moving in Liquids", Proc. Am. Soc. Civil Engrs., 80, 387-412 (1954).

14. Harmathy, T. Z.; "Velocity of Large Drops and Bubbles in Media of Infinite or Restricted Extent", Am. Inst. Chem. Engrs. Jour., 6, 281-288 (1960).

15. Hattori, Sin-iti; "On the Motion of a Cylindrical Bubble in a Tube and Its Application to the Measurement of the Surface Tension of a Liquid", Tokyo Imperial University, Aeronautical Research Institute, 1935, No. 115, 163-195.

16. Hewitt, G. F.; "Analysis of Annular Two-Phase Flow: Application of the Dukler Analysis to Vertical Upward Flow in a Tube", At. Energy Res. Est. (Gt. Brit.) Report AERE - R3680 (1961).

17. Hughmark, G. A.; "Holdup and Pressure Drop with Gas-Liquid Flow in a Vertical Pipe", Ph.D. Thesis, Louisiana State University, 1959.
(See also: Hughmark, G. A. and B. Pressburg; Am. Inst. Chem. Engrs. Jour., 7, 677-682 (1961).)

18. Isbin, H. S., R. H. Moen and D. R. Mosher; "Two-Phase Pressure Drops", At. Energy Com. (USA) Report AECU-2994 (1954).

19. Kozlov, B. K.; "Forms of Flow of Gas-Liquid Mixtures and Their Stability Limits in Vertical Tubes", Zhur. Tekh. Fiz., 24, 2285-2288 (1954) (Translation: ATS-RJ-418).

20. Laird, A.D.K. and D. Chisholm; "Pressure and Forces Along Cylindrical Bubbles in a Vertical Tube", Ind. Eng. Chem., 48, 1361-1364 (1956).

21. Lamb, Sir Horace; "Hydrodynamics", Sixth Ed., Dover Publications, New York, 1945, Sect. 337.

22. Milne-Thomson, L. M.; "Theoretical Hydrodynamics", Fourth Ed., Macmillan and Co. Ltd., London, 1960, P464.

23. Moissis, R. and P. Griffith; "Entrance Effects in a Developing Slug Flow", Trans. Am. Soc. Mech. Engrs., 84C, 29-39 (1962).

24. Nicklin, D. J.; "Two-Phase Flow in Vertical Tubes", Ph.D. Thesis, Cambridge.
(See also: Nicklin, D. J., J. O. Wilkes and J. F. Davidson; Trans. Inst. Chem. Engrs., 40, 61-68 (1962).

25. O'Brien, M. P. and J. E. Gosline; "Velocity of Large Bubbles in Vertical Tubes", Ind. Eng. Chem., 27, 1436-1440 (1935).

26. Prandtl, L. and O. G. Tietjens; "Fundamentals of Hydro- and Aeromechanics", Dover Publications, New York, 1957, P. 151.

27. Rosenberg, B., "The Drag and Shape of Air Bubbles Moving in Liquids", David Taylor Model Basin Report 727, September 1950.

28. Uno, S. and R. C. Kintner; "Effect of Wall Proximity on the Rate of Rise of Single Air Bubbles in a Quiescent Liquid", Am. Inst. Chem. Engrs. Jour., 2, 420-425 (1956).

29. White, E. T.; Private communication.

30. White, E. T. and R. H. Beardmore; "The Velocity of Rise of Single Cylindrical Air Bubbles Through Liquid Contained in Vertical Tubes", Chem. Eng. Sci., 17, 351-356 (1962).

APPENDICES

APPENDIX I

EXPERIMENTAL EQUIPMENT AND PROCEDURE

The experimental work available on the velocities of rise of Taylor bubbles through stagnant liquids has indicated that the potential flow analysis which gives quite good results for gas bubbles in water and in other liquids of low viscosity does not adequately predict the velocities of bubbles in more viscous liquids. Accordingly, a study was made of the velocities of rise of single bubbles of air in water and in three petroleum oils. The properties of these liquids are given in Table I in the text. The properties of water have been obtained from standard tables while the densities and viscosities of the oils were obtained by the Oil and Gas Conservation Board Laboratory of the Province of Alberta. The values of the surface tension were obtained by the Standards Laboratory of the Department of Chemical and Petroleum Engineering of the University of Alberta.

The cylindrical tube used has been described in the literature (11) and consists of two coupled sections of cellulose-acetate-butyrate tubing to give a length of 37 feet. The tube diameter is 1.038 inches and the wall thickness 0.141 inches. The end closures of the tube are full-flow

plug valves. Air bubbles were introduced at the lower end of the tube from a reservoir of 1 1/2-inch pipe, the actual introduction being effected by opening the lower plug valve.

As photographs of the bubbles were required to determine the bubble shapes, a one-foot long section of the tube located approximately 25 feet above the lower plug valve was enclosed in a view-box to minimize distortion of bubble image. The view-box was fabricated from lucite sheet and fitted onto the tube with O-ring seals. In operation, the view-box was filled with the tube liquid. In the viewing section, the tube was inscribed with several reference lines to aid the quantitative determination of the bubble shape.

Two methods were used to introduce a bubble of known volume into the tube. Most frequently, a known volume of air at atmospheric pressure was obtained in a glass gas bomb over the liquid being studied. The bottom reservoir (see Figure I-1) was filled with the liquid and the lower plug cock closed. The gas was then displaced by the test liquid into the reservoir through valve 2, liquid being removed simultaneously from valve 3. When all the gas had been transferred to the reservoir, valves 2 and 3 were closed and the gas bomb disconnected. With the tube full of test liquid, the bubble was then pressured by connecting valves 1

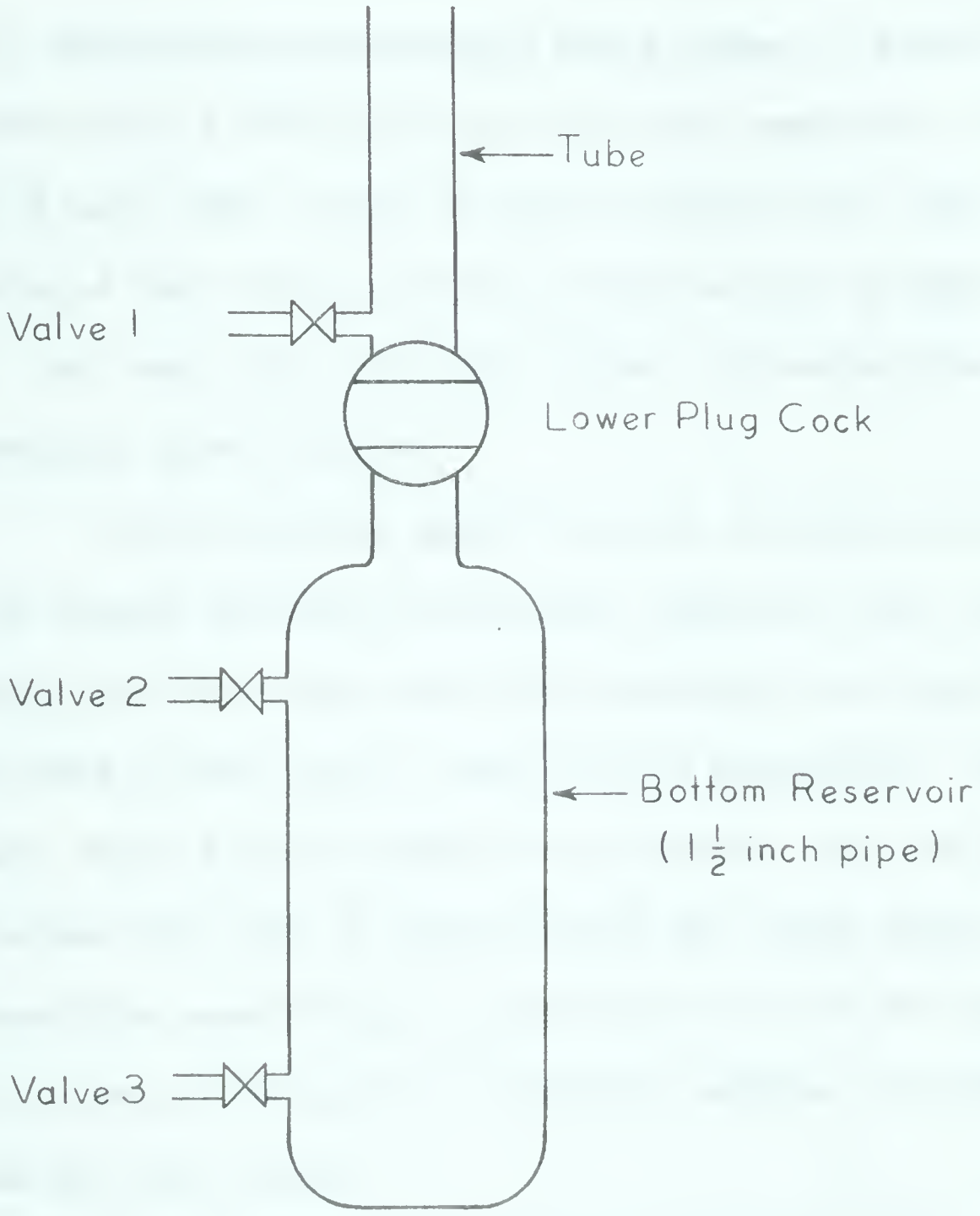

FIGURE I-1

SCHEMATIC DIAGRAM OF BUBBLE INTRODUCTION SYSTEM

and 3, appropriate precautions being taken to avoid the introduction of additional air into the reservoir. Valves 1 and 3 were then closed as was the upper plug cock. After allowing a few minutes for the liquid motion in the tube to stop, the lower plug cock was opened, releasing the bubble at essentially tube pressure.

The alternate method used to introduce the bubble to the system involved filling the reservoir with test liquid, closing the lower plug cock and measuring the liquid drained from valve 3 with valve 2 open to the atmosphere. This method, while equally useful in principle, was not used very much since the lack of space around the lower plug cock enhanced the possibility of error due to loss of liquid. It was also more difficult to introduce bubbles of predetermined volume by this method.

Bubble velocities were obtained by using three stopwatches to time the rise of the bubbles over two successive intervals. The three timing levels are shown in Figure I-2 and correspond to test lengths of 9.27 feet and 10.40 feet. In operation, the three stopwatches were started simultaneously and then taken to the appropriate timing levels. The watches were then stopped when the bubbles passed the respective timing stations. The lower timing station was

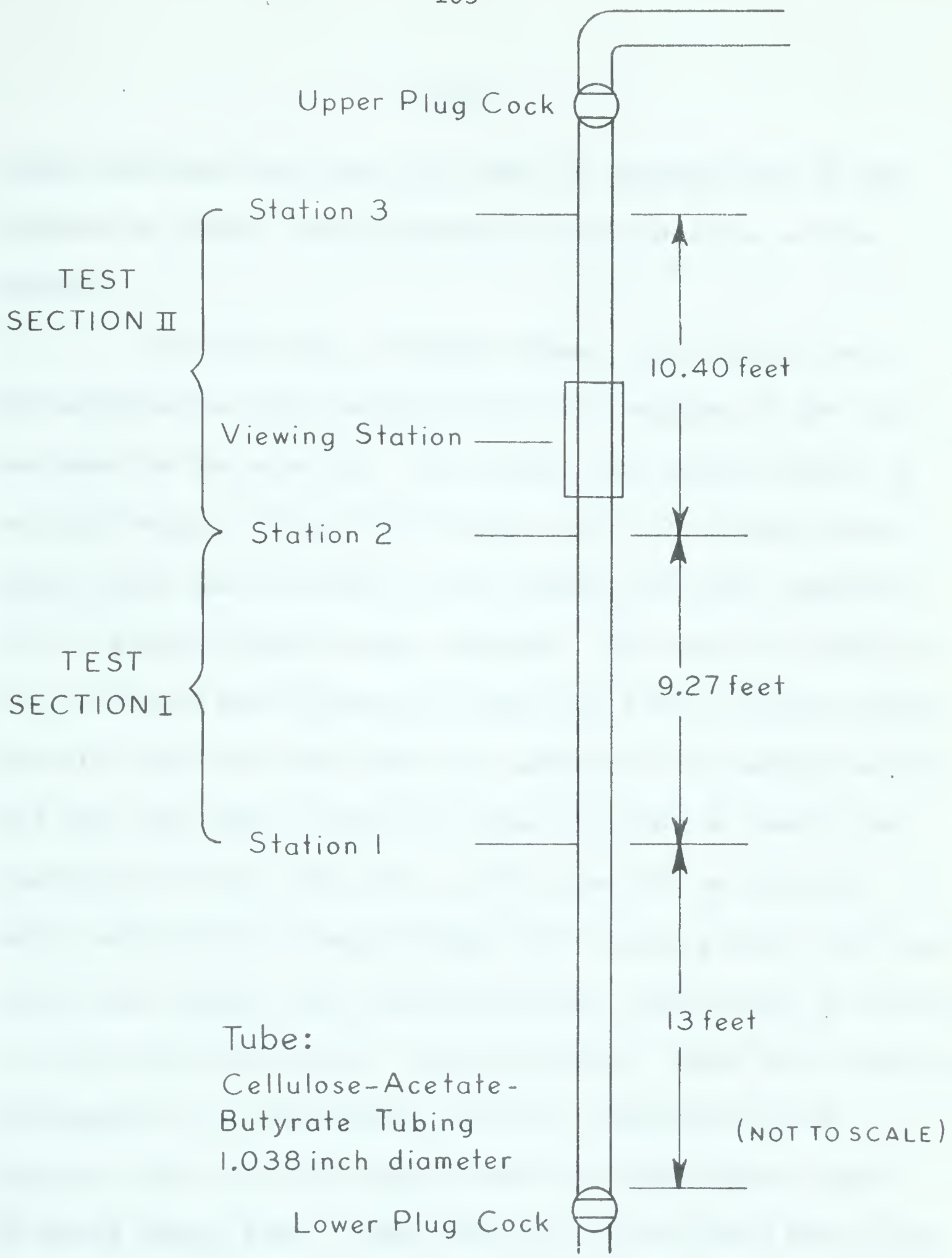

FIGURE I-2

SCHEMATIC DIAGRAM OF TUBE

about thirteen feet above the point of introduction of the bubbles to permit stabilization of the velocities of the bubbles.

In the study of bubble shapes, the bubbles were photographed as they passed through the section of the tube enclosed in the view box. The camera used was an Exacta II equipped with a 50-mm, f-3.5 Tessar lens and it was located about three feet in front of the viewing section, depending on the size of bubble being measured. The vertical position of the camera was adjusted to bring the line of sight approximately level with the reference marks on the viewing section and care was taken to have the line of sight as nearly perpendicular to the front face of the view box as possible. A white matte board located behind the viewing section and about three feet distant was illuminated with flood lamps to provide an even back-lighting for the photographs. With this lighting arrangement, the photographs could be obtained with an exposure time of 1/500 second which was sufficiently short to avoid motion blur. Both Kodak Tri-X and Ilford HPS films were used with equal success. As manual triggering of the shutter was used, it was not always possible to 'catch' the entire bubble or to have the bubble nose at a level to

minimize distortion, however sufficient tests were made to obtain the information required.

The analysis of the bubble shapes was carried out by projecting the image of the bubble nose onto a rear-projection screen with a superimposed arithmetic grid. This procedure and equipment have been described previously (3). After the projected image had been adjusted on the basis of the outer tube diameter and the vertical reference lines to obtain an undistorted view, the coordinates of the bubble image were obtained for a series of horizontal levels. This procedure was followed because it permitted easy calculation of the bubble axis for each level which indicated whether or not the bubble was distorted. When a number of bubbles in a given liquid had been tested in this way, the results were plotted to determine whether the bubble size had any effect on the shape of the nose. When no effect was found for any of the liquids, a detailed analysis of the shape was made for one bubble in each set of measurements by photographing the image of the bubble on the rear-projection screen and obtaining a positive copy of the bubble image with the superimposed grid lines. This method was preferable to carrying out the detailed analysis on the screen as there was a slight drift

with time in the image size, presumably due to heat effects in the projector.

Experimental Results

The results of the determinations of velocities of air bubbles of the Taylor type rising through liquids in the 1.038-inch diameter tube are tabulated in Tables I-1 through I-4. In each of the Tables, the bubble volume, the velocities obtained over the two test intervals and the average velocity of the bubble are given along with the approximate bubble length. There did not appear to be any systematic difference between the bubble velocities obtained over the two timing intervals or between bubbles of different sizes. The average velocities of air bubbles in the liquids tested are given in Tables II and III in the text.

The bubble shapes obtained from the analysis outlined above are shown in Figures I-3 through I-6. No effect of bubble size on bubble shape was observed. The bubble shapes shown in Figures I-3 through I-6 have been combined in Figure 5 in the text to illustrate better the differences in bubble shapes in the different liquids.

TABLE I-1

EXPERIMENTAL BUBBLE VELOCITIES

Air-Water System

Bubble Volume cc.	Bubble Velocity, ft/sec			Approximate Bubble Length[a]
	Test Section I	Test Section II	Average	
162	0.569	0.580	0.574[5]	6.6
62	0.580	0.580	0.580	3.0
37	0.576	0.578	0.577	1.9
162	0.580	0.578	0.579	6.8
212	0.569	0.580	0.574[5]	8.2
262	0.576	0.578	0.577	9.8
112	0.580	0.578	0.579	4.9

a Estimated from bubble photograph, inches

TABLE I-2

EXPERIMENTAL BUBBLE VELOCITIES

Air-Varsol System

Bubble Volume cc.	Bubble Velocity, ft/sec			Approximate Bubble Length[a]
	Test Section I	Test Section II	Average	
107	0.580	0.571	0.575[5]	5.5
205	0.576	0.580	0.578	-
205	0.565	0.571	0.568	8.5
167	0.576	0.562	0.569	7.3
128	0.565	0.571	0.568	5.7
88.5	0.576	0.568	0.572	4.4
49	0.576	0.565	0.570[5]	2.5
29	0.576	0.565	0.570[5]	1.8
128	0.583	0.562	0.572[5]	5.9
205	0.572	0.571	0.571[5]	8.9
167	0.572	0.562	0.567	7.2
128	0.572	0.568	0.570	5.8
88	0.572	0.568	0.570	4.1
49	0.572	0.571	0.571[5]	2.6
29	0.576	0.568	0.572	1.7
88.5	0.576	0.574	0.575	4.1
17.8	0.569	0.568	0.568[5]	0.64

a Estimated from bubble photograph, inches

TABLE I-3

EXPERIMENTAL BUBBLE VELOCITIES

Air-Marcol System

Bubble Volume cc.	Bubble Velocity, ft/sec			Approximate Bubble Length [a]
	Test Section I	Test Section II	Average	
32	0.559	0.555	0.557	-
54	0.562	0.555	0.558[5]	-
32	0.552	0.562	0.557	2.0
54	0.565	0.555	0.560	3.0
97	0.555	0.559	0.557	5.2
140	0.555	0.562	0.558[5]	6.9
183.5	0.562	0.553	0.557[5]	9.1
224.5	0.562	0.553	0.557[5]	-
224.5	0.562	0.553	0.557[5]	-

a Estimated from bubble photograph, inches

TABLE I-4

EXPERIMENTAL BUBBLE VELOCITIES

Air-Primol System

Bubble Volume cc.	Bubble Velocity, ft/sec			Approximate Bubble Length [a]
	Test Section I	Test Section II	Average	
229	0.488	0.498	0.493	-
187	0.495	0.486	0.490[5]	-
143	0.495	0.486	0.490[5]	6.5
99	0.495	0.495	0.495	6.5
55	0.501	0.493	0.497	3.7
32.7	0.493	0.498	0.495[5]	2.4
187	0.499	0.493	0.496	11.8

a Estimated from bubble photograph, inches

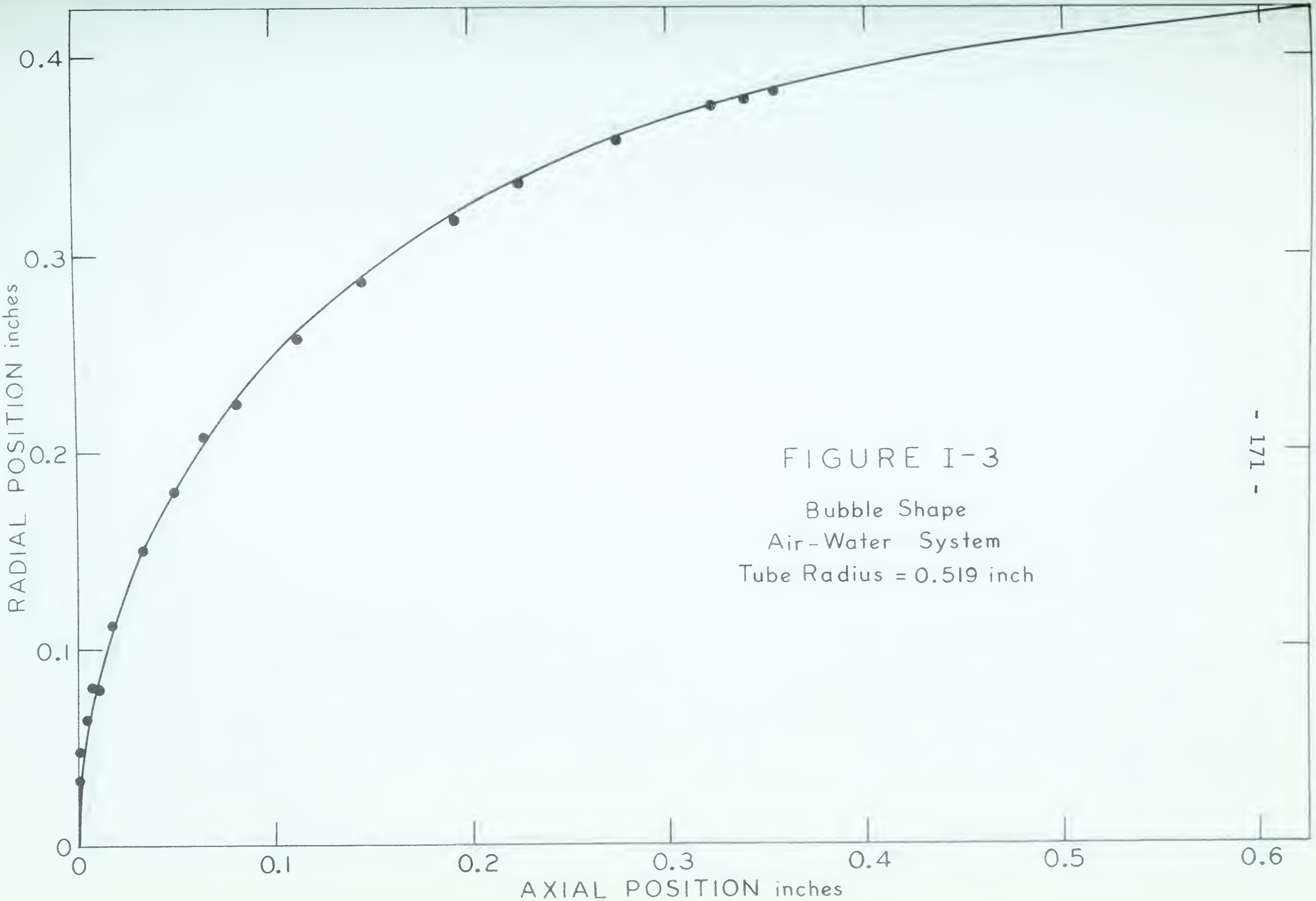

FIGURE I-3

Bubble Shape
Air-Water System
Tube Radius = 0.519 inch

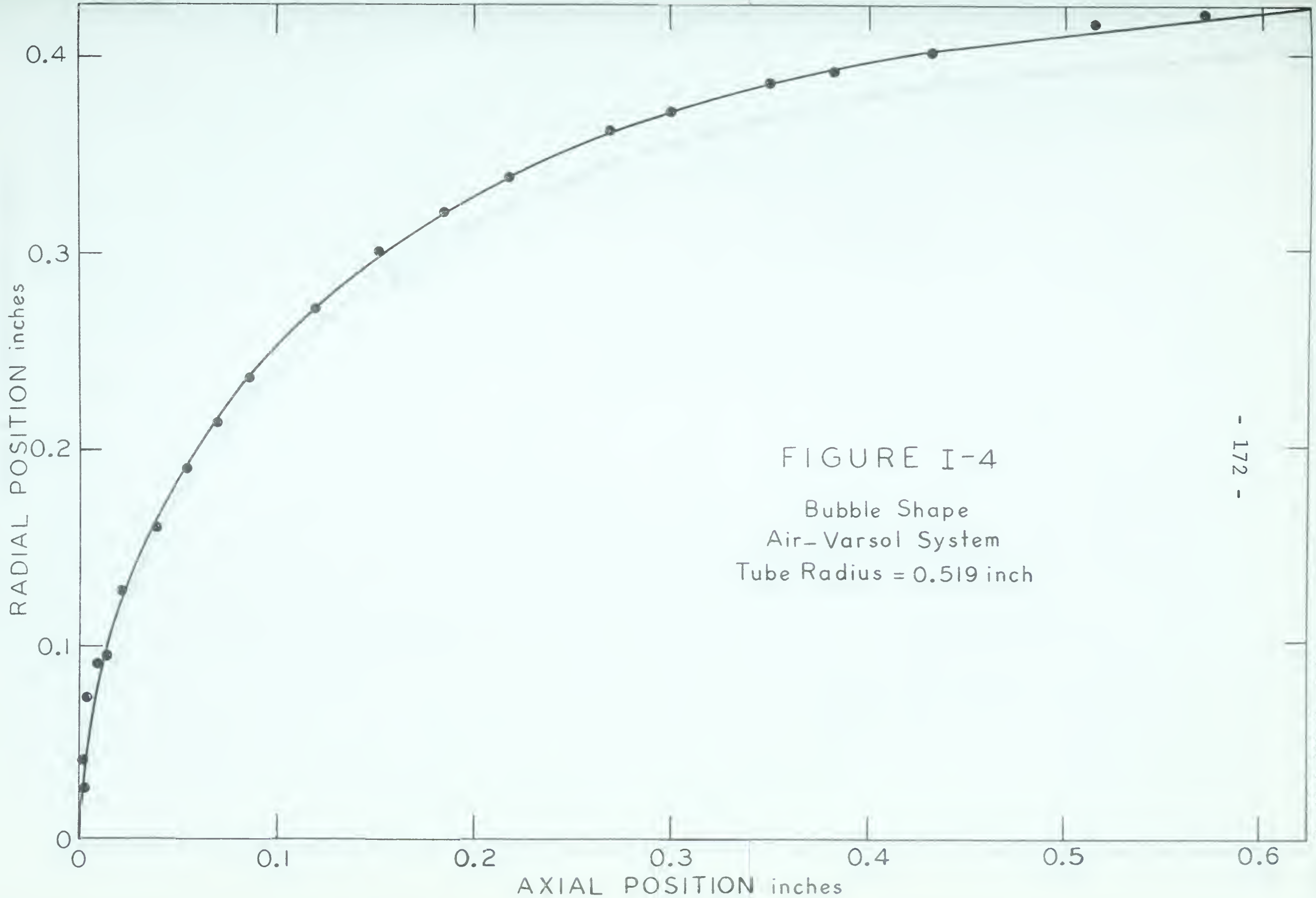

FIGURE I-4

Bubble Shape
Air–Varsol System
Tube Radius = 0.519 inch

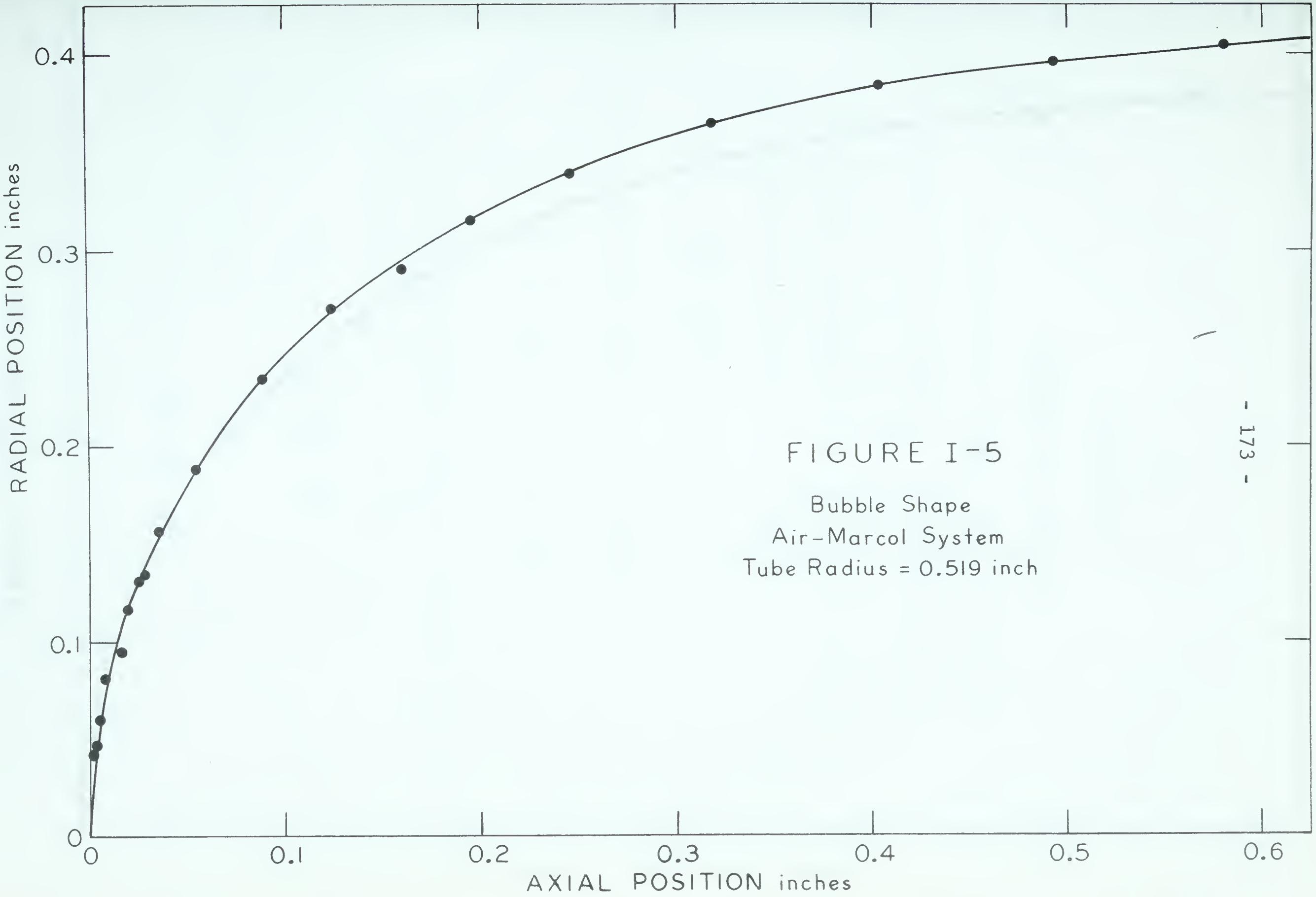

FIGURE I-5

Bubble Shape
Air-Marcol System
Tube Radius = 0.519 inch

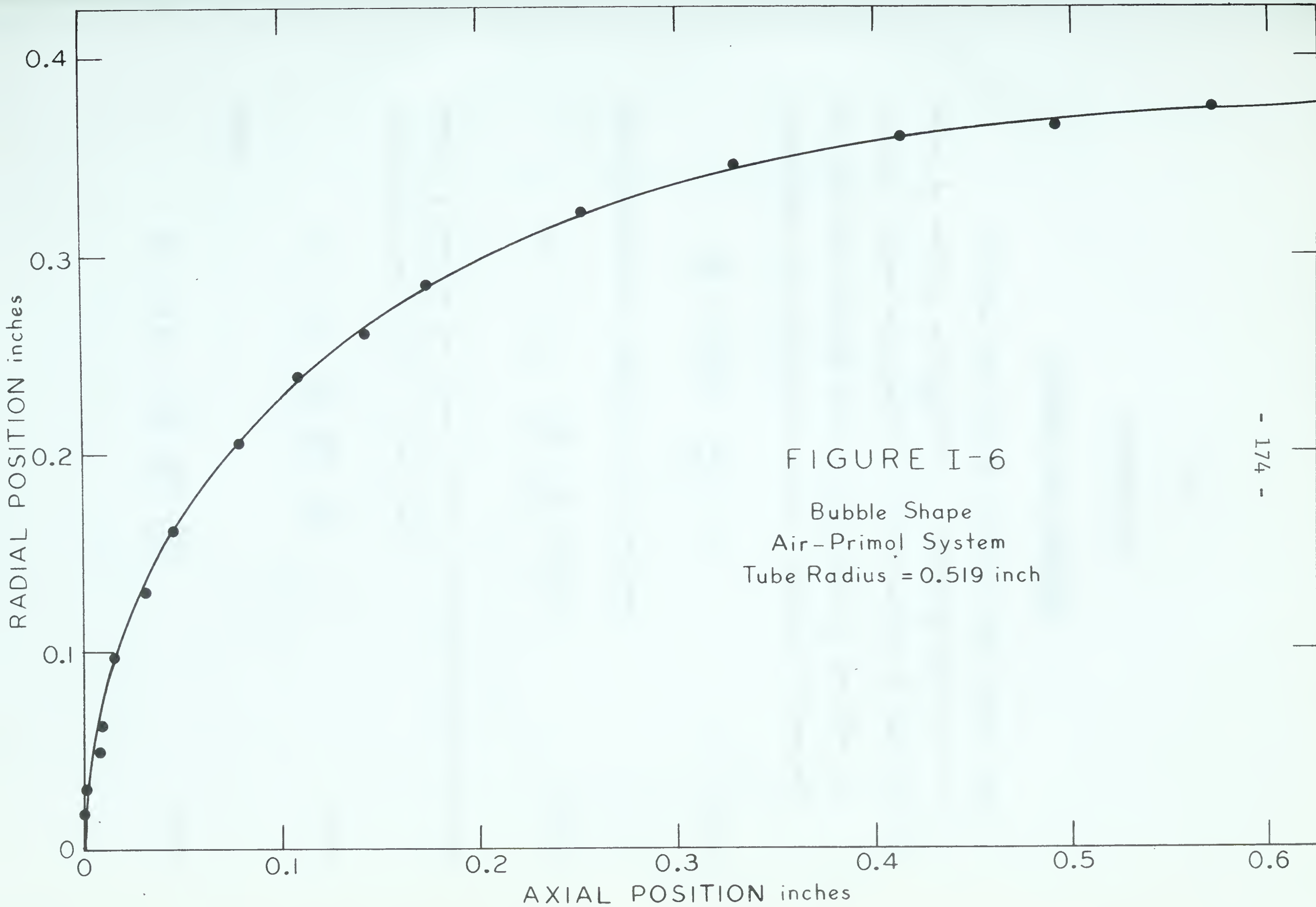

FIGURE I-6

Bubble Shape
Air-Primol System
Tube Radius = 0.519 inch

APPENDIX II

LAMINAR FILM ANALYSIS

Consider the flow of liquid in the annular film shown in section in Figure II-1. Assuming the flow to be steady, uniform and symmetrical with respect to the axis of the tube and assuming also that the axis of the tube is coincident with the gravity vector, Equation (2) becomes

$$-\frac{\partial P}{\partial x} + \frac{1}{r}\frac{\partial(\tau r)}{\partial r} - \frac{\rho g}{g_c} = 0 \qquad \text{(II-1)}$$

Upon integration, Equation (II-1) becomes

$$\tau r = \tau_i r_i + \left(\frac{\rho g}{g_c} + \frac{\partial P}{\partial x}\right)\frac{r^2 - r_i^2}{2} \qquad \text{(II-2)}$$

where τ_i denotes the shear stress at the gas-liquid interface. Separating the constant terms gives

$$\tau r = B_1 + \frac{r^2}{2}\left(\frac{\rho g}{g_c} + \frac{\partial P}{\partial x}\right) \qquad \text{(II-3)}$$

where

$$B_1 = \tau_i r_i - \frac{r_i^2}{2}\left(\frac{\rho g}{g_c} + \frac{\partial P}{\partial x}\right) \qquad \text{(II-4)}$$

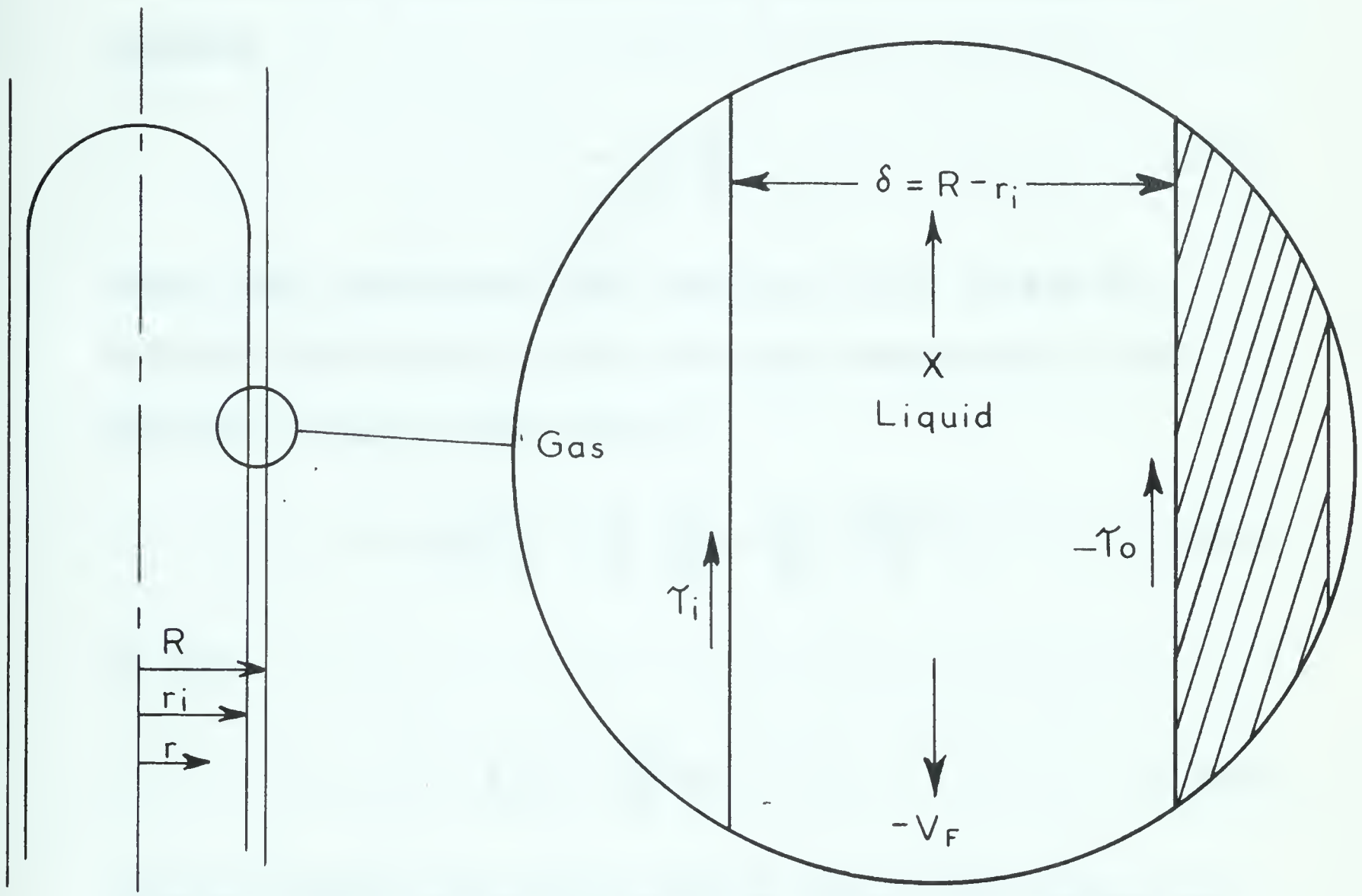

FIGURE II-1

THE EQUILIBRIUM FILM

If the flow in the film is laminar and the liquid Newtonian, the shear stress can be expressed through the relation

$$\tau = \frac{\mu}{g_c} \frac{dv}{dr} \qquad \text{(II-5)}$$

which, when substituted into Equation (II-3) yields the velocity distribution in the film upon integration. This procedure leads to the equation

$$v = -B_2 \ln\frac{R}{r} - \frac{g_c}{2\mu} \left(\frac{\rho g}{g_c} + \frac{\partial P}{\partial x}\right) \frac{R^2-r^2}{2} \qquad \text{(II-6)}$$

in which

$$B_2 = \frac{g_c}{\mu} B_1 \qquad \text{(II-7)}$$

Equation (II-6) can be expressed in terms of the normalized distance from the wall, $\omega = m/R$, where

$$m = R - r \qquad \text{(II-8)}$$

by expanding the logarithmic term as a power series and neglecting terms of higher order in ω. In this form, Equation (II-6) is

$$-v = B_2\left(\omega + \frac{1}{2}\omega^2 + \frac{1}{3}\omega^3 + \text{---}\right) + \frac{R^2 g_c}{4\mu}\left(\frac{\rho g}{g_c} + \frac{\partial P}{\partial x}\right)\omega(2-\omega) \qquad \text{(II-9)}$$

The average velocity of the liquid in the film relative to the wall of the tube can be obtained from the velocity distribution by integrating across the film as shown by the following equation

$$V_F = \frac{2}{R^2-r_i^2}\int_{r_i}^{R} vr\, dr \qquad \text{(II-10)}$$

From Equations (II-6) and (II-10), the average velocity in the film is obtained as

$$V_F = -B_2\left(\frac{r_i^2}{R^2-r_i^2}\ln\frac{r_i}{R} + \frac{1}{2}\right) - \frac{g_c}{8\mu}\left(\frac{\rho g}{g_c} + \frac{\partial P}{\partial x}\right)(R^2-r_i^2) \qquad \text{(II-11)}$$

Equation (II-11) can be expressed in terms of the relative film thickness, $\zeta = \delta/R$, in the same way that the velocity distribution was obtained in terms of the relative position in the film in the foregoing paragraph. Making the substitution

$$\delta = R - r_i \qquad \text{(II-12)}$$

and expanding the logarithmic term leads to the equation

$$V_F = -\frac{\left(\frac{\rho g}{g_c} + \frac{\partial P}{\partial x}\right)g_c R^4}{\mu(R^2-r_i^2)}\, Y_1 + \frac{g_c \tau_i R^3}{\mu}\,\frac{(1-\zeta)}{R^2-r_i^2}\, Y_2 \qquad \text{(II-13)}$$

where Y_1 represents the series

$$Y_1 = \frac{2}{3}\zeta^3(1-\zeta) + \frac{1}{10}\zeta^5 + \frac{1}{60}\zeta^6 + \text{---} \qquad \text{(II-14)}$$

and Y_2 the series

$$Y_2 = \zeta^2 - \frac{1}{3}\zeta^3 - \frac{1}{12}\zeta^4 - \text{----} \qquad \text{(II-15)}$$

If the flow in the core is analyzed similarly, through application of Equation (II-1) to the situation shown in Figure II-2, the following equation analogous to Equation (II-2) results

$$\frac{\partial P}{\partial x} = \left(\frac{2\tau_i}{r_i} - \frac{\rho' g}{g_c}\right) \qquad \text{(II-16)}$$

Equation (II-16) can be solved simultaneously with Equation (II-2) to eliminate the interfacial shear term, giving

$$\tau r = -\frac{r_i^2}{2}\left(\frac{\rho g}{g_c} - \frac{\rho' g}{g_c}\right) + \frac{r^2}{2}\left(\frac{\rho g}{g_c} + \frac{\partial P}{\partial x}\right) \qquad \text{(II-17)}$$

The velocity distribution in the film and the average velocity in the film can be obtained from Equation (II-17) by the same methods used above with Equation (II-3).

In the case being considered in the body of this work, the density and viscosity of the bubble fluid are small with respect to the corresponding properties of the liquid in the film with the result that the interfacial shear and the pressure gradient along the bubble are negligible. Under these conditions, then, the velocity distribution becomes, from Equation (II-6),

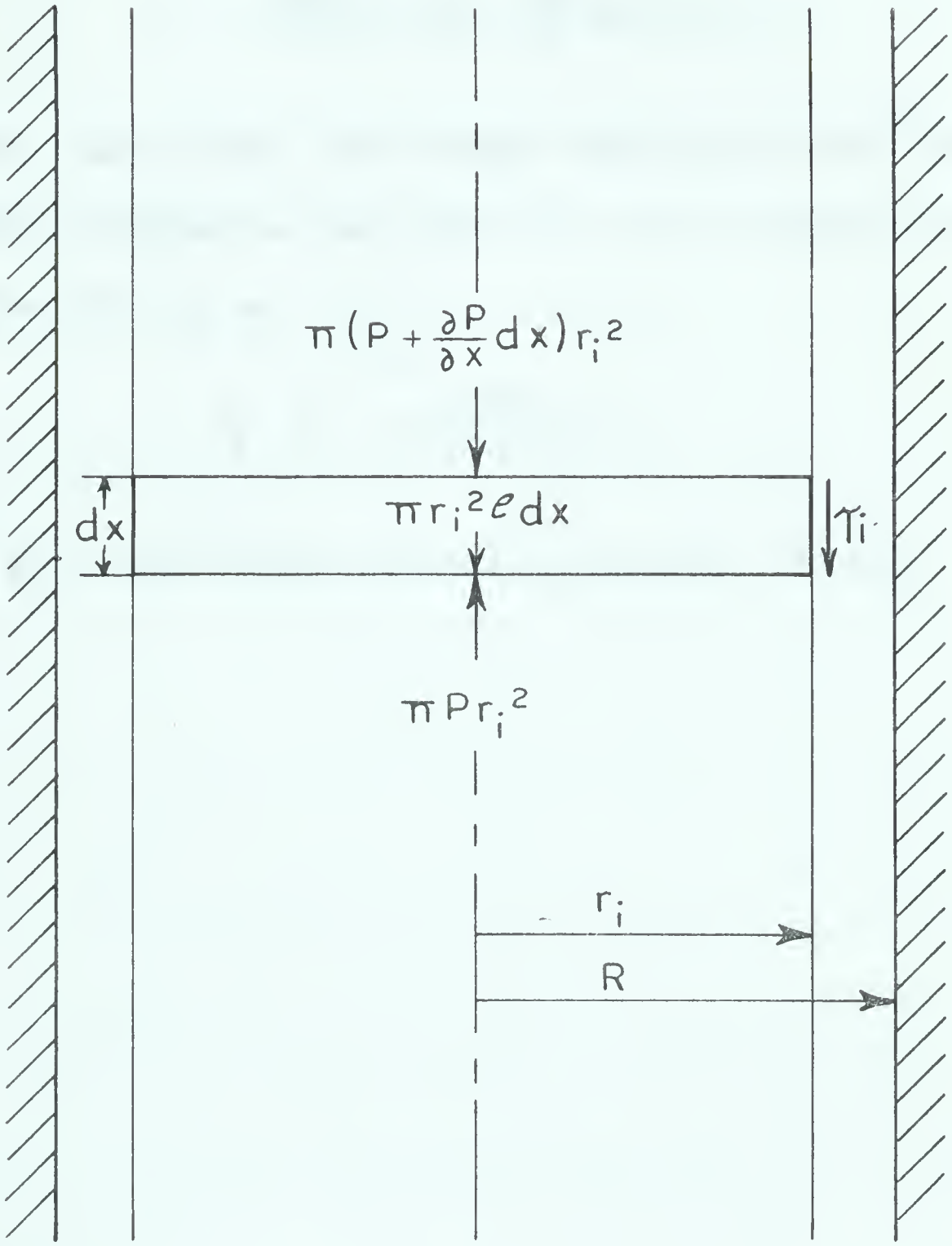

FIGURE II-2

FORCES ACTING ON AN ELEMENT OF A BUBBLE

$$v = \frac{\rho g r_i^2}{2\mu} \ln\frac{R}{r} - \frac{\rho g}{4\mu}(R^2-r^2) \qquad \text{(II-18)}$$

For this case, also, the average velocity of the liquid in the film relative to the tube wall can be obtained from Equation (II-13) as

$$V_F = -\frac{\rho g R^4}{\mu(R^2-r_i^2)} Y_1 \qquad \text{(II-19)}$$

where Y_1 is the series defined by Equation (II-14).

APPENDIX III

CALCULATION OF MOMENTUM FLUX

The flux of momentum relative to the bubble at a section is given by the relation

$$\mathring{M} = \frac{2\pi\rho}{g_c}\int_{r_i}^{R}(V_b - v)^2 r\, dr \qquad \text{(III-1)}$$

as was indicated in Equation (43) in the text. (It will be noted that Equation (III-1) refers to the physical coordinates and not the transformed coordinates previously used. The axial component of velocity, v, is, therefore, the absolute velocity.) The momentum flux is to be evaluated for the liquid ahead of the bubble under plug flow and laminar flow conditions and for the liquid in the annular film in laminar flow. The flow is being considered, then, at sections 1 or 4 and at section 3 of Figure 8 although, as has been noted above, the coordinates are not as indicated in this figure.

The momentum flux associated with the liquid ahead of the bubble, that is, with the approach flow, will be evaluated first. For plug flow, the axial velocity v in Equation (III-1) is simply V_L, the average liquid velocity

relative to the tube, and the velocity term is constant and can be removed from the integral, giving

$$\mathring{M}_A = \frac{2\pi\rho}{g_c} (V_b - V_L)^2 \frac{R^2}{2}$$

or

$$\mathring{M}_A = \frac{\pi R^2 \rho}{g_c}\left[(V_b - V_L)^2 \right] \qquad \text{(III-2)}$$

If the approach flow is laminar, the axial velocity in Equation (III-1) is given by the equation

$$v = 2V_L\left(1 - \frac{r^2}{R^2}\right) \qquad \text{(III-3)}$$

Substituting Equation (III-3) into Equation (III-1) gives

$$\mathring{M}_A = \frac{2\pi\rho}{g_c}\int_0^R \left(V_b - 2V_L\left(1 - \frac{r^2}{R^2}\right)\right)^2 r\, dr$$

$$= \frac{2\pi\rho}{g_c}\left[\frac{(V_b - V_L)^2}{2} + \frac{V_L^2}{6} \right] \qquad \text{(III-4)}$$

The axial velocity in Equation (III-1) for laminar flow in the annular film when the pressure gradient along the bubble and the shear stress at the gas-liquid interface can be neglected is obtained from Equation (II-9) as

$$-v = \frac{\rho g r_i^2}{2\mu}\left(\omega + \frac{1}{2}\omega^2 + \frac{1}{3}\omega^3 + \text{---}\right) + \frac{\rho g R^2}{4\mu}\omega(2 - \omega) \qquad \text{(III-5)}$$

where ω denotes the relative position in the film, m/R, as before. For this case, the integration can be carried out more efficiently by expanding the squared term in Equation (III-1) and considering the separate integrations resulting. Equation (III-1) becomes, therefore

$$\mathring{M}_F = \frac{2\pi\rho}{g_c}\int_{r_i}^{R}(V_b^2 - 2vV_b + v^2)\, r\, dr$$

which can also be written as

$$\mathring{M}_F = \frac{2\pi\rho}{g_c}\,\frac{(R^2-r_i^2)}{2}\,V_b^2 - \frac{4\pi\rho V_b}{g_c}\int_{r_i}^{R} vr\, dr + \frac{2\pi\rho}{g_c}\int_{r_i}^{R} v^2 r\, dr \quad \text{(III-6)}$$

The second term on the right-hand side of Equation (III-6) can be simplified by the introduction of the average velocity in the film, V_F, defined in Equation (II-10) to give

$$\mathring{M}_F = \frac{\pi\rho}{g_c}\left[(R^2-r_i^2)\,V_b^2 - 2(R^2-r_i^2)\,V_bV_F + 2\int_{r_i}^{R} v^2 r\, dr\right] \quad \text{(III-7)}$$

Substituting for the film velocity from Equation (II-13) and solving the integral results in the equation

$$\mathring{M}_F = \frac{\pi\rho R^2}{g_c}\zeta(2-\zeta)V_b^2 + \frac{2\pi\rho^2 R^4 g}{g_c\mu}\,Y_1V_b + \frac{\pi\rho^3 R^6 g^2}{g_c\mu^2}\,Y_3 \quad \text{(III-8)}$$

where Y_1 is given by Equation (II-14) and Y_3 by the equation

$$Y_3 = \frac{4}{15}\zeta^5 - \frac{17}{45}\zeta^6 + \frac{13}{105}\zeta^7 + \text{----} \quad \text{(III-9)}$$

B29813